Thèse n° 8329

Numerical investigations of 3D CFTs using conformal bootstrap methods

Présentée le 6 novembre 2020

à la Faculté des sciences de base
Groupe Vichi
Programme doctoral en physique

pour l'obtention du grade de Docteur ès Sciences

par

Marten Jan REEHORST

Acceptée sur proposition du jury

Prof. V. Savona, président du jury
Prof. A. Vichi, directeur de thèse
Dr M. Paulos, rapporteur
Dr S. Chester, rapporteur
Prof. R. Rattazzi, rapporteur

École
polytechnique
fédérale
de Lausanne

2020

Acknowledgements

First let me thank my supervisor Alessandro for giving me this amazing opportunity and guiding me throughout my PhD with great kindness and understanding. I'm also extremely grateful to my main collaborator Emilio for his patience with my questions and for his perpetual and infectious enthusiasm. In this spirit I should also thank Marc for always answering my questions after talks, clarifying any points that I might have missed (as well as for being a great guy in general). I thank Joao for teaching me a lot about CFTs both in his course on the subject and outside of it. I thank Sasha greatly for our often more philosophical and less physics-centered discussions. I will greatly miss our lunch time discussions.

I would also like to thank all of my office mates, lunch partners, and my fellow students (also known as "those of the open space") and the members of "string theory in secret": Aditya, Adrien, Alfredo, Andre, Andrea, Bernardo, Emmanuelle, Francisco, Gabriel, Gil, Ivo, Jan, Jeanne, Joao, Kamran, Kin, Lorenzo, and the other Lorenzo, Miguel, Ning, Sander and Siyu. I hope you do not mind me outing you here ☺ (it is still hidden who is in which group so I think it is okay). We really all became one tight-knit group of friends and it is hard to say goodbye now that we will scatter all over the world. We had some amazing times at conferences visiting São Paulo, Los Angeles, Las Vegas, New York, Toronto, and the Niagara Falls.[1] I hope that at future conferences we will have the chance to meet again. If not I will just have to make more effort to stay in touch. You are well worth the effort. From Geneva I must not forget my great and culturally refined friend Manuel. You showed me places I normally would not have gone to and which having been there I would not have wanted to miss for the world (and in return I took you to the worst music ever performed, sorry for that).

Special thanks go to Andrea and Kin, for saving me from being homeless by sub-renting me their apartments at exactly the right times so that I managed to keep a roof above my head during my PhD. (And to Sander for lending me his car to help me move.)

[1] If someone from the Simons foundation is reading this: We also did some physics, don't worry your money was well spent.

Even greater thanks go to Aditya for introducing me to weight training and volunteering as my personal coach. I thank him and Bhusan for being by gym buddies and keeping me motivated to work-out and stay healthy during my PhD here, but most importantly, if not for Aditya I would not have been at the gym to meet...

Julia, to whom my greatest thanks go. Everything is so much better since I met you.

Finally, let me thank the home front. I thank my high school friends or the "IgDudes", David, Tal, Tycho, Ruben, Marc, Tom and Faan, and all my friends with whom I studied physics. Especially, Faan and Tal, who were in both groups. and have been awesome friends for a long time. The fact that all three of us started physics together must have had at least something to do with our great high school physics teacher Mr. Steenbakkers. For his inspiring classes I am immensely grateful.

I thank Pieter for being the amazing friend he is. And I thank Tom for all our friday night boardgames before I left to Switzerland and for compressing a years worth of friday nights into a few weeks of return visits since then.

And last but not least, I thank my parents and my brother for all their support and for being my best friends. It is cruel how science forces families so far apart but the moment I arrive home on holidays it feels as if I never left.

Foreword

This thesis is based on one published and one forthcoming paper.

- Chapter 1 is based on M. Reehorst, E. Trevisani, and A. Vichi, "Mixed Scalar-Current bootstrap in three dimensions," `arXiv:1911.05747 [hep-th]`
- Chapter 2 is based on M. Reehorst, M. Refinetti, and A. Vichi, "Bootstrapping the ARP^3 model using traceless symmetric $O(N)$ scalars," `arXiv:20xx.xxxxx [hep-th]`

Abstract

Conformal field theories (CFTs) play a very significant role in modern physics, appearing in such diverse fields as particle physics, condensed matter and statistical physics and in quantum gravity both as the string worldsheet theory and through the AdS/CFT correspondence. In recent years major breakthroughs have been made in solving these CFTs through a method called numerical conformal bootstrap. This method uses consistency conditions on the CFT data in order to find and constrain conformal field theories and obtain precise measurements of physical observables. In this thesis we apply the conformal bootstrap to study among others the $O(2)$- and the ARP^3- models in 3D.
In the first chapter we extend the conventional scalar numerical conformal bootstrap to a mixed system of correlators involving a scalar field charged under a global $U(1)$ symmetry and the associated conserved spin-1 current J_μ. The inclusion of a conserved spinning operator is an important advance in the numerical bootstrap program. Using numerical bootstrap techniques we obtain bounds on new observables not accessible in the usual scalar bootstrap. Concentrating on the $O(2)$ model we extract rigorous bounds on the three-point function coefficient of two currents and the unique relevant scalar singlet, as well as those of two currents and the stress tensor. Using these results, and comparing with a quantum Monte Carlo simulation of the $O(2)$ model conductivity, we give estimates of the thermal one-point function of the relevant singlet and the stress tensor. We also obtain new bounds on operators in various sectors.
In the second chapter we investigate the existence of a second-order phase transition in the ARP^3 model. This model has a global $O(4)$ symmetry and a discrete Z_2 gauge symmetry. It was shown by a perturbative renormalization group analysis that its Landau-Ginzburg-Wilson effective description does not have any stable fixed point, thus disallowing a second-order phase transition. However, it was also shown that lattice simulations contradict this, finding strong evidence for the existence of a second-order phase transition. In this chapter we apply conformal bootstrap methods to the correlator of four scalars t transforming in the traceless symmetric representation of $O(4)$ in order to investigate the existence of this second order phase transition. We find various features that stand out in the region predicted by the lattice data. Moreover, under reasonable assumptions a candidate island can be isolated. We also apply a mixed $t-s$ bootstrap setup in which this island persists. In addition we study the kink-landscape for all representations appearing in the $t \times t$ OPE for general N. Among others, we find a new family of kinks in the upper-bound on the dimension of the first scalar operator in the "Box" and "Hook" representations.
Keywords: Conformal field theory (CFT), Numerical conformal bootstrap, Non-perturbative quantum field theory, O(2) model, APR^3 model, spinning correlators, Mixed Scalar-Current bootstrap.

Zusammenfassung

Konforme Feldtheorien (CFTs) spielen in der modernen Physik eine sehr wichtige Rolle und finden in diversen Gebieten Anwendung, beispielsweise in der Teilchenphysik, Physik der kondensierten Materie und der statistischen Physik und in der Quantengravitation sowohl als String Worldsheet Theory als auch mit der AdS/CFT-Korrespondenz. In den letzten Jahren wurden mittels der numerischen konformen Bootstrap-Methode grosse Durchbrüche erzielt. Diese Methode wendet Konsistenzbedingungen auf CFT-Daten an um konforme Feldtheorien zu finden, einzuschränken und genaue Messungen von physikalischen Observablen zu erhalten. In dieser Dissertation wenden wir die konforme Bootstrap an um unter anderem die $O(2)$- und ARP^3-Modelle zu untersuchen.

Im ersten Kapitel erweitern wir die konventionelle skalare numerische konforme Bootstrap auf ein gemischtes System von Korrelatoren an, das ein skalares Feld, geladen unter einer globalen $U(1)$-Symmetrie, und den dazugehörigen konservierten Spin-1-Strom J_μ beinhaltet. Das Einbeziehen eines konservierten Spinoperators ist ein wichtiger Fortschritt im numerischen Bootstrap-Programm. Indem wir numerische Bootstrap-Techniken einsetzen, erhalten wir Beschränkungen von neuen Observablen, die mit der normalen skalaren Bootstrap nicht zugänglich sind. Auf das $O(2)$-Modell fokussierend extrahieren wir strenge Beschränkungen für den Drei-Punkte-Funktionskoeffizienten von zwei Stömen und dem einzigartigen skalaren Singlet sowie diejenigen von zwei Strömungen und dem Energie-Impuls Tensor. Mittels dieser Resultate und im Vergleich mit einer Quanten-Monte-Carlo-Simulation der Leitfähigkeit des $O(2)$.Modells schätzen wir die thermale Ein-Punkt-Funktion des relevanten Singlets und des Energie-Impuls-Tensor. Ebenfalls erhalten wir neue Beschränkungen von Operatoren in verschiedenen Sektoren.

Im zweiten Kapitel untersuchen wir die Existenz eines Phasenübergangs zweiter Ordnung im ARP^3-Modell. Dieses Modell hat eine globale $O(4)$-Symmetrie und eine diskrete Z_2-Gauge-Symmetrie. Eine perturbative Renormierungsgruppenanalyse hat gezeigt, dass seine effektive Beschreibung nach Landau-Ginzburg-Wilson keinen stabilen Fixpunkt hat und somit keinen Phasenübergang zweiter Ordnung zulässt. Es wurde jedoch auch gezeigt, dass Gittersimulationen dieser Erkenntnis widersprechen, indem sie starke Beweise für

die Existenz eines Phasenübergangs zweiter Ordnung fanden. In diesem Kapitel wenden wir konforme Bootstrap-Methoden auf den Korrelator von vier t-Skalaren an, die sich in die «traceless symmetric» Darstellung von $O(4)$ transformieren, um die Existenz dieses Phasenübergangs zweiter Ordnung zu untersuchen. Wir finden verschiedene Merkmale, die in der durch die Gitterdaten vorhergesagten Region hervorstechen. Darüber hinaus kann unter vernünftigen Annahmen eine Insel isoliert werden. Wir wenden auch eine gemischte $t - s$-Bootstrap-Anordnung an, in der diese Insel fortbesteht. Darüber hinaus untersuchen wir die Knicklandschaft für alle Darstellungen, die in der $t \times t$ OPE für allgemeine N erscheinen. Unter anderem finden eine neue Familie von Knicken in der oberen Beschränkung auf die Dimension des ersten Skalaroperators in den «Box» und «Hook»-Darstellungen.

Contents

Acknowledgements **i**

Foreword **iii**

Abstract **v**

Introduction **1**

1 Mixed Scalar-Current bootstrap in three dimensions. **11**
1.1 Introduction and summary of results 11
1.1.1 New data for the $O(2)$ model 13
1.1.2 Conductivity at finite temperature 17
1.2 Setup 19
1.2.1 3pt functions 21
1.2.2 Crossing equations 22
1.2.3 Conformal Blocks 25
1.2.4 Sum rules 28
1.3 Results 32
1.3.1 Bounds on operator dimensions 32
1.3.2 Bounds on central charges 37
1.4 Conclusions 40

2 Bootstrapping the ARP^3 model **43**
2.1 Introduction and summary of results 43
2.2 Background 46
2.2.1 RP^{N-1} and ARP^{N-1} model 46
2.2.2 The Landau-Ginzburg-Wilson effective action 47
2.2.3 Lattice evidence 49
2.3 Setup 50
2.3.1 The $t \times t$ OPE 51
2.3.2 4pt functions and the crossing equations 52

2.3.3 Relationships between the traceless symmetric $O(N)$ bootstrap and the $O(N(N+1)/2-1)$ vector bootstrap. 54
2.3.4 Setup of mixed $t-s$ bootstrap 58
2.4 Single correlator results 59
2.4.1 Bounds on operator dimensions and OPE coefficients 60
2.4.2 Isolating the ARP^3 model 66
2.5 Results mixed t-s bootstrap 73
2.6 A systematic study of general N 78
2.7 Conclusions 83

Conclusion and Outlook **85**

A Appendices to chapter 1 **87**
A.1 Conductivity in terms of CFT data 87
A.2 Three point functions 90
A.2.1 Scalar-scalar OPE 90
A.2.2 Current-scalar OPE 90
A.2.3 Current-current OPE 91
A.3 Conformal Blocks 93
A.3.1 $JJ\phi\bar{\phi}$ 93
A.3.2 $J\phi J\bar{\phi}$ 94
A.3.3 $\phi JJ\bar{\phi}$ 94
A.3.4 Conformal block decomposition 95
A.4 Vectors for the bootstrap equations 96

B Appendices to chapter 2 **99**
B.1 Spectra at maximal OPE values 99

Bibliography **106**

Introduction

Quantum field theory (QFT) has been successfully used to describe particle physics and condensed matter systems. The Standard Model is one of the most accurate physical theories we know. Using perturbation theory particle interactions can be predicted to astounding precision. Yet, there is much left to be explored. Most studies in QFT are restricted to a perturbative approach dealing with asymptotic series. These expansion are known to break down when the involved coupling constants become strong. Many interesting physical phenomena are described by such strongly coupled systems. For example, it is impossible to study confinement in Quantum Chromo Dynamics (QCD) perturbatively, due to a growing coupling constant at low energies. Similarly many interesting condensed matter systems such as the Ising and O(2) model are described by strongly coupled quantum field theories and cannot be solved perturbatively. That is why it is important to develop methods to solve quantum field theories non-perturbatively. While lattice computations can sometimes provide the non-perturbative answers we seek they do not give a complete answer due to finite size effects. Thus, it is essential to develop other non-perturbative approaches to solving quantum field theories.

While it is very difficult to solve QFTs non-perturbatively there are some instances where much progress can be made by studying consistency conditions. An especially promising approach is available for conformal field theories (CFTs). These theories are highly constrained due to additional symmetry requirements. As a consequence CFTs can be defined by a set of numbers called the CFT data. Moreover, this CFT data has to obey non-trivial consistency conditions in the form of sum rules. The study of these consistency conditions is called the conformal bootstrap. In this thesis we study these consistency conditions for two systems of physical interest using analytical and numerical methods.

While CFTs are highly constrained they are also highly non-trivial, interesting and universally present. At low energies QFTs will in general flow to a scale invariant fixed point. The symmetry of the theory at such a fixed point is usually enhanced to full conformal symmetry. As a consequence the theory at the fixed point is described by a

CFT.[2] If the QFT is UV-complete the high energy limit of the QFT is also expected to be described by a CFT and the theory at any energy can be understood as a deformation of the UV-CFT by a relevant operator. This evolution from UV to IR is described by the Renormalization Group (RG).

Similarly, condensed matter systems undergoing a second order phase transition are also understood to be described by scale invariant fixed points of renormalization group flows. Notable examples of such critical points are liquid-vapor transitions, transitions between ferromagnetism and paramagnetism for various types of magnets and the superfluid transition of ^{4}He. At these critical points the correlation length, which is normally given by the tiny interaction length of the microscopic interaction, diverges and various observables show power law behavior whose exponents are called critical exponents. Moreover, many such phase transitions turn out to be described by the same critical exponents. Critical points exhibiting the same critical exponents are said to be in the same universality class. The fact that different critical points are described by the same critical exponents can be understood from an RG point of view. Scale invariance at the transition imposes strong constraints on the effective description and forces the suppression of so called *irrelevant* couplings that are sensitive to the microscopic degrees of freedom of the system. As a consequence only the symmetry at the RG fixed point matters in determining the universality class of a critical point and all phase transitions with the same symmetries are described by the same critical exponents.

Thus, the transition between liquid and vapor is described by the same critical exponents as the transition in easy-axis magnets[3]. The easy-plane ferromagnetic-to-paramagnetic transition of for example $GdAlO_3$ has the same critical exponents as the superfluid transition in ^{4}He. And again the Curie transitions in isotropic magnets such as Fe or Ni also have the same critical exponents. Due to their Z_2, $O(2)$ and $O(3)$ symmetry these transitions are respectively described by the fixed point of the Ising model, the O(2) model and the O(3) model, regardless of the details of the microscopic realization. These were examples of euclidean statistical physics descriptions of systems at finite temperature. Additional the same CFTs can describe quantum phase transitions at zero temperature when wick rotated. For example the quantum critical point of thin-film

[2] In $d = 2$ dimensions the enhancement to full conformal symmetry is proven to occur for any unitary Poincaré-invariant theory with a scale current and a discrete spectrum in the scaling dimension as long as the scale invariance is unbroken. For other dimensions there is no non-perturbative proof but the enhancement is expected to occur under the same assumptions. The additional assumptions are essential since there are counter examples of scale invariant theories without conformal invariance. However, for any interesting physical theory the enhancement is expected to occur [3].

[3] Easy axis magnets are magnets with one energetically favored axis for the microscopic spins to be aligned with. As an effect the spin is effectively constrained to point either up or down in the direction of the easy-axis. Dysprosium ethyl sulfate (DyES) forms such a magnet for example. If instead a plane is energetically favored, forcing the spins to lie on a circle, this is called an easy-plane magnet.

superconductors is described by the Lorentzian O(2) model.

Finally, CFTs appear in quantum gravity both directly as the theory describing a string worldsheet and indirectly through the AdS/CFT correspondence.

The conformal bootstrap. Central to the conformal bootstrap are two simple ideas. Firstly, a conformal field theory is completely described by an (infinite) set of numbers called the CFT data. And secondly this CFT data obeys complicated consistency relations which are hypothesized to constrain the OPE data to families of isolated points in the OPE data parameter space corresponding to CFTs with different symmetries.[4]

In this thesis we will mostly consider Euclidean signature CFTs, thus we will study QFTs with $SO(d+1,1)$ symmetry. This symmetry group includes translations, rotations, dilations (i.e. scale transformations) and special conformal transformations. These CFTs can be analytically continued to Lorentzian QFTs by Wick rotation.[5]

The main objects in a QFT are correlation functions of local operators. These operators transform under a finite dimensional representation of the (euclidean) Lorentz group. Additionally, they are taken to be diagonal under the dilation operator meaning that $[D, \mathcal{O}(0)] = \Delta_O \mathcal{O}(0)$. The eigenvalue Δ is called the (conformal) dimension of $\mathcal{O}$. The operators can be classified into primary operators and descendants. The translation and special conformal transformation operators P^μ and K^μ respectively act as raising and lowering operators changing the conformal dimension by ± 1. Primary operators are the lowest dimensional states, such that $[K_\mu, \mathcal{O}(0)] = 0$. In unitary CFTs primary operators are guaranteed to have a dimension above a certain spin dependent positive value. This lower bound is refered to as the unitarity bound. Descendants are built from primary operators by acting with the raising operators P_μ. Primaries act as the building blocks of all operators and unless specified otherwise any operator $\mathcal{O}$ in the rest of the thesis is assumed to be a primary operator.

The simplest correlation functions is the one point correlator $\langle \mathcal{O}(\mathbf{x}) \rangle$. This function has to be independent of $\mathbf{x}$ due to for example translational invariance. Additional scale invariance implies there is no scale that this one point correlator can depend on. Thus, we conclude $\langle \mathcal{O} \rangle = 0$. Two point functions can be non-zero but are completely determined by conformal invariance (up to an arbitrary normalization constant). For

[4] Sometimes there can be connected lines (or higher dimensional planes) of consistent CFTs such as for example the generalized free theory (GFT) line which exists for all Δ above the unitarity bound (where Δ is the dimension of the fundamental operator of the GFT.

[5] This thesis focuses on reflection positive CFTs. When Wick rotated to Lorentzian signature these CFTs will be unitary. Note that statistical descriptions of statistical physics systems do not necessarily have to have this symmetry. Hence non-unitary CFTs are also of interest. However, the main bootstrap methods rely heavily on reflection positivity and do not extend to these CFTs.

three point functions the x_i dependence can be fixed completely by conformal invariance but a non-trivial constant usually denoted $\lambda_{\mathcal{O}_1\mathcal{O}_2\mathcal{O}_3}$ is left undetermined. This constant depends on the type of operators appearing in the three point function. The four point correlator can only be fixed up to a function $g(u, v)$ of two conformally invariant cross ratios build from x_1, x_2, x_3 and x_4 and here one might fear that for higher-point functions things only get worse as there will be more and more of such invariants.

However, CFTs come equipped with an additional powerful tool called the *Operator Product Expansion* (OPE). The OPE relates the product of two operators to an (infinite) sum over single operators. The coefficient appearing in front of the single operators in this sum depends the operator appearing in the sum and on the two operators in the initial product. In fact the constant is given by the coefficient of the three point function of those three operators. That is why we call the constants $\lambda_{\mathcal{O}_1\mathcal{O}_2\mathcal{O}_3}$ OPE coefficients. The OPE follows from the fact that in a CFT local operators acting on the vacuum provide a complete set of states, a fact called the *operator-state correspondence*.

The OPE can be used to relate n-point functions to a sum over $(n-1)$-point functions. As a consequence all correlators can in principle be expressed in terms of three point correlators. Therefore, the OPE constants $\lambda_{\mathcal{O}_1\mathcal{O}_2\mathcal{O}_3}$ in principle determine all correlation functions of the CFT. Therefore this data is called the CFT data.[6]

Moreover, by applying the OPE in different orders to for example a four point correlator one can retrieve consistency conditions on the constants $\lambda_{\mathcal{O}_1\mathcal{O}_2\mathcal{O}_3}$.[7] The resulting constraints are called the crossing equations. They are highly non-trivial to solve and are expected to fully determine the CFT given some minor other input on the symmetries of the CFT and for example the number of relevant operators.

The crossing equation. The conformal bootstrap equations are given by applying the OPE inside a four-point function in two different ways or equivalently by inserting a complete set of states in the middle of the four point function for two different orderings of the four operators.[8] In order to insert a complete set of states we first define a projection operator onto the conformal multiplet of a primary operator $\mathcal{O}_{\Delta,l}$ by $\mathcal{P}_{\Delta,l} = \sum_{\alpha,\beta=\mathcal{O},P\mathcal{O},PP\mathcal{O}\cdots} \frac{|\alpha\rangle\langle\beta|}{\langle\alpha|\beta\rangle}$. Here the sum over α and β runs over all descendants of the primary operator $\mathcal{O}$. The identity can then be written as $\mathbf{1} = \sum_{\Delta,l} \mathcal{P}_{\Delta,l}$. For example applied to the four-point function of 4 identical scalars, i.e. $\mathcal{O}_{1,2,3,4} = \phi$, applying the

[6] Usually one considers the OPE data to consist of the spectrum, i.e. the local operators with non-zero two point functions, plus the OPE constants relating these operators, i.e. the OPE constants $\lambda_{\mathcal{O}_1\mathcal{O}_2\mathcal{O}_3}$. One could interpret the latter data as contained in the OPE coefficients $\lambda_{O_1O_2,\mathbf{1}}$.

[7] One can show that if and only if all four point functions obey the resulting consistency conditions the OPE is associative. So no new constraints can be found by examining higher point functions.

[8] Operators in a euclidean correlation functions commute.

projector for two different operator orderings gives the relation

$$\sum_{\Delta,l} \langle\phi(x_1)\phi(x_2)|\,\mathcal{P}_{\Delta,l}\,|\phi(x_3)\phi(x_4)\rangle = \sum_{\Delta,l} \lambda_{12\mathcal{O}}\lambda_{\mathcal{O}^\dagger 34} G^{1234}_{\Delta,l}(x_1,x_2,x_3,x_4)$$
$$= \sum_{\Delta,l} \langle\phi(x_3)\phi(x_2)|\,\mathcal{P}_{\Delta,l}\,|\phi(x_1)\phi(x_4)\rangle = \sum_{\Delta,l} \lambda_{32\mathcal{O}}\lambda_{\mathcal{O}^\dagger 14} G^{3214}_{\Delta,l}(x_3,x_2,x_1,x_4)\,. \tag{1}$$

The function $G^{1234}_{\Delta,l}$ is called the conformal partial wave. It is related to a function called the conformal block through $G^{1234}_{\mathcal{O}}(x_1,x_2,x_3,x_4) = K_4(x_1,x_2,x_3,x_4)g^{1234}_{\mathcal{O}}(u,v)$ where K_4 is a kinematic factor chosen by convention so that the remainder depends only on the conformal cross ratios u and v.[9] The conformal block g depends on the operators appearing in the four-point function, often called the *external* operators, and on the operator $\mathcal{O}$ appearing in the sum, i.e. the *exchanged* operator. In the case of scalar operators the conformal block only depends on the external operators through the quantities $\Delta_{12} = \Delta_1 - \Delta_2$ and $\Delta_{34} = \Delta_3 - \Delta_4$ (or on Δ_{32} and Δ_{14} in the exchanged channel). In the case of spinning external operators G also depends on the spin of the external operators. Spinning three- and four-point functions can have multiple allowed tensor structures. In this case the different three-point structures are summed over and every different four-point tensor structure will give its own crossing equation since different tensor structures cannot cancel each other. We can write this more general case as

$$k(u,v)\sum_{\mathcal{O},p,q} \lambda^{(p)}_{12\mathcal{O}}\lambda^{(q)}_{34\mathcal{O}} g^{(p,q)\,1234}_{\mathcal{O},s}(u,v) = k(v,u)\sum_{\mathcal{O},p,q,s'} \lambda^{(p)}_{32\mathcal{O}}\lambda^{(q)}_{14\mathcal{O}} M^{ss'} g^{(p,q)\,3214}_{\mathcal{O},s'}(v,u) \tag{2}$$

Here the indices p,q run over the different allowed three-point functions while s labels the different four-point tensor structures. The crossing equation can relate combinations of different tensor structures and hence a matrix $M^{ss'}$ appears.

Conformal blocks and how to compute them. By inserting a complete set of states we found that the contribution to the four-point function of one (primal) operator is controlled by the conformal block for that operator. If, after inserting the projector $\mathcal{P}_{\Delta,l}$ in the four-point function, we also insert the quadratic Casimir operator of the conformal group we can find a differential equation that the conformal block must obey. Acting to the left on $\mathcal{P}_{\Delta,l}$ the conformal Casimir simply gives the eigenvalue $C_{\Delta,l}$. Acting to the right on the operators $\mathcal{O}_3$ and $\mathcal{O}_4$ it acts as a differential operator resulting in differential equation of the form

$$\mathcal{D}g_{\Delta,l} = C_{\Delta,l}g_{\Delta,l} \tag{3}$$

where $\mathcal{D}$ is a second order differential operator. In even dimensions this differential

[9] Some of the literature does not make a distinction between conformal partial waves and conformal blocks and uses these names interchangeably.

equation can be solved exactly for scalars but in 3D alternative methods need to be used. We will now give a brief overview of one of the main methods to compute the conformal block. This method uses recursion relations to relate the conformal blocks $g_{\Delta,l}$ to other conformal blocks $g_{\Delta',l'}$ (of lower order in a small parameter ρ). One advantage of this method is that it is most easily extended to the computation of spinning conformal blocks as required for the numerical bootstrap setup described in chapter 1.

For Δ above the unitarity bound the matrix $\langle\alpha|\beta\rangle$ appearing in the projector above is positive definite and invertible. However, below the unitarity bound there are special values Δ_A^* where $\langle\alpha|\beta\rangle = 0$ for certain descendants. This means that the conformal block has to have a pole at $\Delta = \Delta_A^*$.[10] It turns out that the residue at this pole is proportional to another conformal block, $g_{\Delta,l} \sim \frac{R_A}{\Delta_A^*} g_{\Delta_A,l_A}$. Here Δ_A and l_A are the dimension and spin of the first null (zero norm) descendant. To write a recursion relation based on this it is useful to write the conformal blocks in *radial coordinates* r and η which are a function of the conformal cross ratios u and v above [4]. One can then define a regularized conformal block $h_{\Delta,l}$ through $g_{\Delta,l}(r,\eta) = (4r)^{\Delta} h_{\Delta,l}(r,\eta)$ and find a recursion relation of the form

$$h_{\Delta,\ell}(r,\eta) = h_{\infty,\ell}(r,\eta) + \sum_A \frac{R_A}{\Delta - \Delta_A^*} (4r)^{n_A}\, h_{\Delta_A^*+n_A,\ell_A}(r,\eta)\,. \tag{4}$$

The conventional numerical bootstrap approach expands the crossing equations around the so called self dual point where $r = 3 - 2\sqrt{2} \approx 0.1716 \ll 1$. Thus the equation above can be used as a recursion relation to compute $h_{\Delta,l}$ from different conformal blocks $h_{\Delta_A^*+n_A,\ell_A}$ at a lower order in r. The Δ-independent term $h_{\infty,\ell}(r,\eta)$ can be found by solving the Casimir equation at large Δ. The position of the poles Δ_A^* can be found by studying explicitly the norm for the various descendants which we schemetically denoted as $P\mathcal{O}, PP\mathcal{O}, \cdots$. The residue R_A is given by three parts. One part is controlled by the left three point function $\langle\mathcal{O}_1\mathcal{O}_2\mathcal{O}\rangle$ while another is controlled by the right three point function $\langle\mathcal{O}\mathcal{O}_3\mathcal{O}_4\rangle$. The remaining part can be found from the rate at which $\langle\mathcal{O}_{\Delta,l}|\mathcal{O}_{\Delta,l}\rangle$ becomes null as one takes the limit $\Delta \to \Delta_A^*$. For scalars these ingredients were found in [5] while the spinning case was studied in [6]. In the case of spinning operators the indices p, q of the three point tensor structures appear again and the recursion relation will mix the three point tensor indices p and q. On the other hand the recursion relation is diagonal in the four-point indices s.

Numerical conformal bootstrap The main idea of the numerical conformal bootstrap is to admit defeat to solving the full crossing equations. Instead one should attempt to bound CFT data by truncating the equations and showing the inconsistency of an assumption on the spectrum. Take the simplest example of crossing of four identical

[10] In 3D it only has single poles. In 4D it also has double poles.

scalar operators ϕ. In this case the crossing equation reads

$$\sum_{\mathcal{O}} \lambda^2_{\phi\phi\mathcal{O}} F_{\Delta,l}(u,v) = 0 \qquad \text{with} \qquad F_{\Delta,l}(u,v) = G_{\Delta,l}(u,v) - G_{\Delta,l}(v,u) \tag{5}$$

If one could find a linear functional α that is positive on say the unit operator contribution, i.e. $\alpha[F_{0,0}] > 0$, and non-negative for all other Δ and l allowed by unitarity then any non-zero OPE coefficient $\lambda_{\phi\phi\mathcal{O}}$ would lead to a contradiction since the positive contribution from the identity operator would not be canceled by any other operator.[11] The existence of such a functional would proof that no non-trivial CFT exists. Of course such a functional cannot be found. However, a functional can be found such that it is positive for all Δ greater than some critical value Δ_s^*. The existence of such a functional proves that the $\phi \times \phi$ OPE has to exchange an operator s with $\Delta_s < \Delta_s^*$. The search for such a functional α is usually done numerically. The canonical approach considers functionals of the form $\alpha[F] = \sum_{n,m} \alpha_{n,m} \partial_z^n \partial_z^m F|_{z=\bar{z}=1/2}$ with $n, m \in Z$ and $n + m < \Lambda$ where Λ is some cut-off on the number of derivatives that are included. The bigger the search space for the functional (larger Λ) the more parameter space can be excluded. Initial studies, such as the breakthrough papers [7–11], discretized and truncated the (Δ, l) space to approximate the continuous non-negativity constraint to a finite set of linear constraints (linear in $\lambda_{\phi\phi\mathcal{O}}$).[12] α can then be found through linear programming. The discretization of Δ can be avoided by writing the problem as a polynomial inequality [12]. Such a polynomial inequality can then be written as a semi-definite problem which can be solved by semi-definite programming.[13] In practice the semi-definite problems that appear in the conformal bootstrap are found to require high precision arithmetic. SDPB is a dedicated high precision semi-definite problem solver for the type of semi-definite problems that appear in the conformal bootstrap [13]. A new version was recently released and was used for many of the computations in this thesis [14].

Semi-definite programming also allows the extension of the conformal bootstrap to *mixed* bootstrap setups studying multiple correlation functions at once. One of the biggest achievements of the numerical conformal bootstrap program was the isolation of a small precision island corresponding to the Ising CFT [5, 15], see figure 1 . With this island the conformal bootstrap gives the most accurate measurement of the Ising critical exponents related to Δ_σ and Δ_ϵ.

The new frontier: spinning correlators Until recently most numerical bootstrap

[11] We are allowed to move the linear functional inside the OPE sum due to the convergence properties of the OPE.

[12] The large Δ and l behavior is such that it is generally safe to make such a truncation.

[13] A semi-definite problem is a convex optimization problem with nice convergence properties, although not as nice as linear programs. Any linear program can be written as a semi-definite program but the reverse statement is not true.

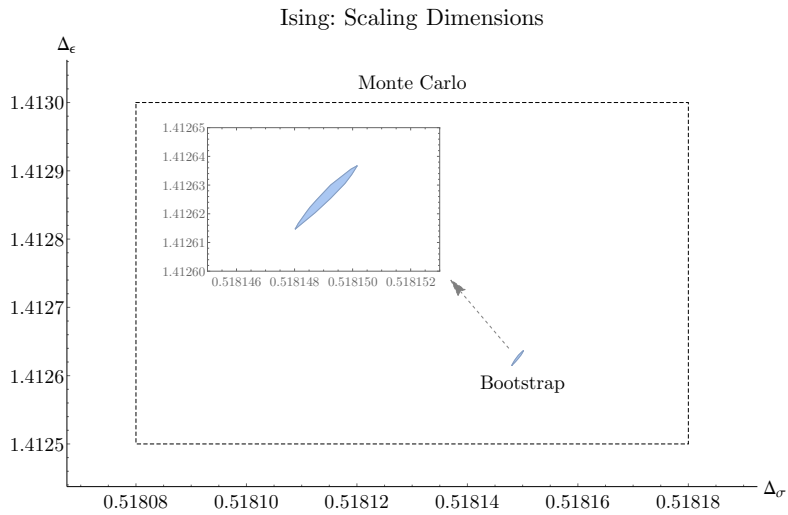

Figure 1: Allowed space in the $(\Delta_\sigma, \Delta_\epsilon)$ plane and a comparison with a Monte Carlo prediction for the same quantities. The conformal bootstrap island gives a far more accurate prediction of the quantities Δ_σ and Δ_ϵ. This figure was borrowed from [15].

studies examined the crossing equations only involving external scalar operators. In recent years this has been expanded to spinning correlators [16–19, 1, 20]. This is an important new frontier. Spinning operators can give access to new sectors and allows the conformal bootstrap to be applied to new theories. Additionally, there are some spinning operators that are of special importance. A conserved stress tensor is present in all local CFTs. Similarly, a conserved current exists for all CFTs with a continuous global symmetry. There is an intimate relation between the existence of such a conserved operator and the symmetries of the CFT. Moreover, the inclusion of correlators of conserved operators in the numerical conformal bootstrap offers a major advantage over other operators: The dimension of the conserved operator is fixed and known. The fact that each new external operator adds another parameter that has to be scanned over is a major obstacle to the multi-correlator bootstrap. However, the crossing equations of conserved operators can be added without increasing the dimensionality of this search space. Still, there is a cost. Correlation functions of spinning operators allow for many tensor structures and many bootstrap equations. This can be very constraining. However, more equations also mean heavier numerics. In addition it becomes more expensive and complicated to set up the appropriate semi-definite programming problem due to the many different crossing equations involved and the different required conformal blocks. An important goal of the work presented in chapter one of this thesis is the assessment of the value of a mixed scalar-current bootstrap.

Further recommended reading This introduction aimed to give context to the re-

search presented in the main chapters of this thesis. However, including a full in-depth treatment of CFT physics required to understand all the details in this thesis is of course an impossible task. Instead I include references for some further advised reading below:

- For a more complete introduction to the conformal bootstrap: [21, 22].
- For an overview of 3D conformal bootstrap results (on results until 2018): [23].
- For the embedding space treatment of spinning operators: [24, 25].
- On spinning conformal blocks: [6, 26, 27].
- On the renormalization group and the connection to statistical physics systems: [28].

1 Mixed Scalar-Current bootstrap in three dimensions.

Based on research done in collaboration with Emilio Trevisani and Alessandro Vichi [1]. *I, the candidate, performed and analyzed the numerical computations presented in this paper and made major contributions to all steps of the research including: the study of and comparison against the relevant literature, the analytic computations leading to the numerical setup, and the writing of the paper itself.*

1.1 Introduction and summary of results

Three dimensional Conformal Field Theories (CFTs) display a rich variety and range of applications. While some of them were introduced a long time ago in order to describe long known phase transitions in condensed matter and statistical models, in recent years the zoo of renormalization group (RG) fixed points has vastly grown.

The numerical conformal bootstrap represents a powerful tool to shed some light on the intricate world of three dimensional CFTs. After its revival a decade ago [7–11], it has been successfully used to extract the most precise prediction of critical exponents in key examples [5, 29, 30, 13, 15, 31, 32]. Moreover, interesting studies also displayed hints of novel (and yet unclassified) CFTs [33, 34]. Many other great results have been achieved in three dimensions [35, 16, 36–40, 17, 41, 19, 42–46]. See also [47, 48] for recent reviews on the subject.

When examining the results obtained in the last few years, it appears evident that bootstrap methods in presence of a global symmetry seem to be less powerful when compared to simpler systems like the Ising model or its supersymmetric extension. One possible argument is that, given that the theory is more involved, one simply needs to consider correlators involving more than two scalars. In particular, relevant scalar

operators seem to play a crucial role.

A second explanation could reside in how the presence of a global symmetry is imposed. In past studies, the existence of a global symmetry was injected by declaring that operators entering a correlation function transform according to irreducible representations of the global symmetry group. In addition, selection rules were imposed on the operator product expansion (OPE) of these operators. A complementary approach was also initiated in [18], where the presence of a global symmetry was enforced by studying the correlation function of the associated conserved spin-1 current. The latter method is definitively preferable, but comes at the expense of considering spinning operators and thus complicating the analysis. As a plus side, however, it does not introduce any new parameter to scan over, since conserved currents have fixed dimensions. In this work we push this approach one step further, and explore the constraints arising from the mixed system of correlation functions involving one conserved current, associated to a $U(1)$ global symmetry, together with a scalar field charged under it.
One should be careful with the latter statement: without further assumptions, including a conserved current in the bootstrap does not give us the right to identify it with the generator of the global symmetry under which the scalar is charged. A trivial counter examples is the tensor product of a generalized free scalar field ϕ and a generalized free vector field J_μ. In order to impose that the external scalar and current couple non trivially, one should force the correct global symmetry Ward identity, namely that the three point function $\langle \phi \bar{\phi} J_\mu \rangle$ is non vanishing.[1] In this work we use this assumption in our studies of the $O(2)$ model. We plan to systematically make use of this assumption in more general future explorations.

Among the obvious targets of our investigation one can list the $O(2)$ vector model, the Gross Neveu Yukawa model with $N = 2$ fermions, and QED_3, both fermionic or bosonic, where one identifies the global symmetry with the topological $U(1)_T$. Although in principle our set up could be used to analyze any system possessing a $U(1)$ symmetry, we found that our numerical bounds are subject to the same limitations as the single scalar correlator analysis, namely they lose constraining power as the dimension of the scalar grows. For this reason we mostly focus on the $O(2)$ model where the charge-1 scalar has dimension close to the free value. We also explored more general bounds and did not find other evidences of CFTs saturating them.

[1] In the numerical bootstrap framework this is equivalent to impose a finite current central charge C_J, see section 1.2.1.

1.1.1 New data for the $O(2)$ model

In this section we collect the most important constraints obtained in the present work. The interested reader can find all the technical details and proper definitions in the next sections. Additional and more general plots can be found in section 1.3.

As mentioned in the previous section, we mostly focused on the $O(2)$ model. In this case we identify our scalar ϕ with the order parameter of the Landau Ginzburg description of the phase transition, while J_μ is the current associated to the global $O(2)$ symmetry. According to recent bootstrap results [15], this model is confined to live on a narrow island in the plane (Δ_ϕ, Δ_S), where S here is the unique neutral relevant scalar operator. Previous bootstrap studies also constrained the dimension of the unique relevant traceless symmetric operator t_{ij}, the central charge C_T and the current central charge C_J[2] [35, 30]. A few OPE coefficients have also been determined in [15], such as $\lambda_{\phi\bar{\phi}S}$ and λ_{SSS}.

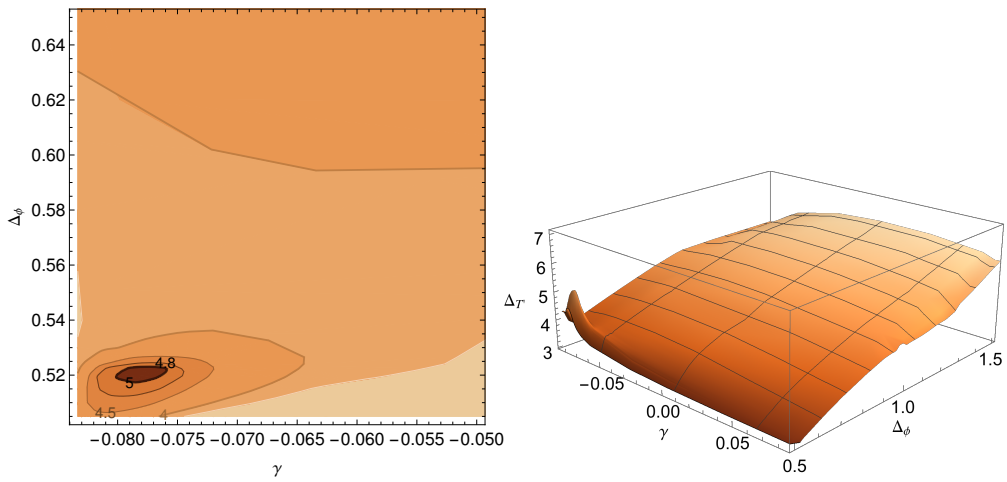

(a) (b)

Figure 1.1: On the left: allowed region in the plane (Δ_ϕ, γ) assuming that the first spin-2, parity-even and neutral traceless symmetric tensor T' after the conserved stress energy tensor has dimension $\Delta_{T'} \geq 3.8, 4, 4.5, 4.8, 5$. As the gap increases the allowed region shrinks to an island. On the right: bound on $\Delta_{T'}$ as a function of γ and Δ_S. The bounds have been obtained at $\Lambda = 13$.

When bootstrapping a mixed system of scalars, one can impose gaps in various scalar sectors and exploit the existence of few relevant operators to create islands in parameter

[2]These are defined respectively as the normalization of the two-point function of the stress tensor $T_{\mu\nu}$ and the $U(1)$ current J_μ.

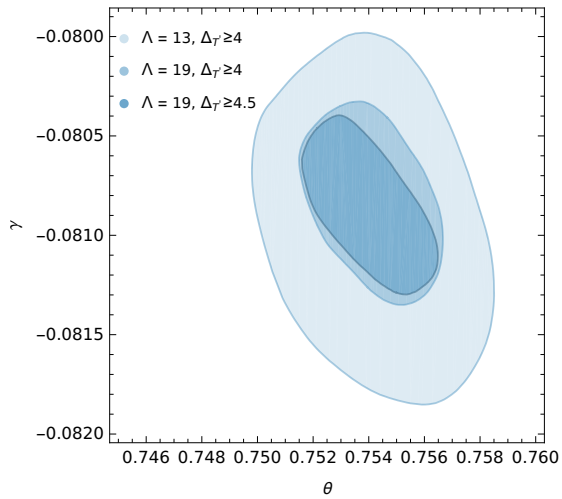

Figure 1.2: Allowed region in the plane (γ, θ) assuming the known O(2) constraints shown in Table 1.1 and $\Delta_{T'} \geq 4, 4.5$. The lighter region has been computed at $\Lambda = 13$. The two smaller regions instead have been computed at $\Lambda = 19$.

space. In our setup, however, the same strategy does not work.[3] Our strategy will then be to identify a new set of assumptions that allow to create an island and use them to extract constraints on CFT-data that have never been bound before, such as the parameter γ and the OPE coefficients λ_{JJS}. While the latter is self explanatory, the former is related to the three point function of two currents and the stress tensor —see section 1.2.1. As discussed in [49, 50], the conformal collider bounds require the parameter γ to range between $[-1/12, 1/12]$, with the extremes corresponding to free theories. Numerical evidences of these bounds were also found by [18]. The value of this parameter in the $O(2)$ model was not known, although strong numerical evidences supported a negative value, which was also confirmed by [18] under somewhat strong assumptions on the spectrum of the theory.[4]

In our explorations we found that a discriminant characteristic of the $O(2)$ model is the presence of a rather large gap between the stress tensor and the next spin-2 neutral operator, let us call it T'. This property translates in a sharp peak in the bound on $\Delta_{T'}$ as a function of Δ_ϕ and γ, as shown in Fig. 1.1b. Intuitively this happens because fake solutions of crossing or non-local theories do not require a stress tensor but usually possess a spin-2 operator close to the unitarity bound; hence the bound on T' is effectively

[3]Because of Ward identities, the charge-1 sector does not contain scalars, besides ϕ itself. Gaps in the other scalar sectors are not sufficient to create islands.

[4]In particular we checked that the assumption that all parity-odd operators have twist $\tau = \Delta - \ell \geq 2.5$ is inconsistent for the $O(2)$ model. The milder assumption $\tau \geq 2$ is still consistent.

a bound on the first spin-2 operator and only for local theories (which have a conserved stress tensor) it becomes a bound on the second spin-2 operator. This property was also exploited in [42] to create isolated regions in single correlator bootstrap.
In Fig. 1.1a we show the allowed region in the plane (Δ_ϕ, γ) with increasing gaps on T'. By raising the gap $\Delta_{T'}$, the allowed region shrinks to a very small island, with a Δ_ϕ value centered around the expected value of the $O(2)$ model. By making the conservative assumption $\Delta_{T'} \geq 4$, we are able to create an isolated region, with the parameter γ confined close to the lower extreme of its interval.

The above analysis shows that, in order to isolate the $O(2)$ model, we can impose a mild gap between the stress tensor operator and the next operator in the same sector. Independent evidence for this can be found by considering the mixed correlator bootstrap of scalars as in [15] and extracting the spectrum while moving inside the island. In what follows we then use two assumptions to isolate the $O(2)$ model, one more conservative and one more realistic: $\Delta_{T'} \geq 4, 4.5$. A refined analysis [51] of the $O(2)$ model involving three external scalar operators, ϕ, S and the unique relevant charge two scalar t, has found $\Delta_{T'} \geq 4.6$, which is consistent with both our assumptions.

Since in this section we are focusing on the $O(2)$ model, in addition to the gap on T' we will also input information from previous bootstrap analysis and use this assumptions to determine bounds on new quantities.

Let us begin by γ and the OPE coefficient λ_{JJS}. We remind that, due to our framework, the unique relevant neutral scalar S appears in two OPEs, schematically:

$$\begin{aligned} J \times J &\sim 1 + \lambda_{JJS} S + \dots \,, \\ \phi \times \bar{\phi} &\sim 1 + \lambda_{\phi\bar{\phi}S} S + \dots \,. \end{aligned} \tag{1.1}$$

Let us define the ratio of OPE coefficients,

$$\tan\theta = \frac{\lambda_{JJS}}{\lambda_{\phi\bar{\phi}S}} \,. \tag{1.2}$$

We can then inspect what values of γ and the angle θ are consistent with the $O(2)$ model information we know. Fig. 1.2 shows the allowed region in the (γ, θ) plane once we input the best determination for Δ_ϕ and Δ_S from [15] as well as other known O(2) constraints shown in Table 1.1.[5] Notice that in Fig. 1.2 and in the following plots we fixed the external dimension to a precise value. Given the small size of the allowed range for Δ_ϕ [15, 51], moving this value would not alter the figure in a noticeable way.

[5] We demand positivity for a scan over the allowed intervals for Δ_S and Δ_t. Instead for Δ_ϕ we pick a central value in the allowed island.

O(2) assumptions
$\Delta_\phi = 0.5191$
$\Delta_S \in [1.509, 1.514]$
$\Delta_{S'} > 3$
$\Delta_t \in [1.204, 1.215]$
$\Delta_{t'} > 3$
$\Delta_{0,-}^{Q=0} > 3$
$C_J < 0.9066\, C_{J^{\text{free}}}$

Table 1.1: List of assumptions used in our analysis. The bound for Δ_S is taken from [15]. The bound for Δ_t and C_J are taken from [30]. S' and t' are respectively the first operators appearing after S and t. Evidences for the gap on $\Delta_{0,-}^{Q=0}$ were presented in [18].

Using the value determined in [15] for $\lambda_{\phi\bar{\phi}S}$ and (1.2) we then conclude (for $\Delta_{T'} \geq 4$):

$$\begin{aligned} &\gamma = -0.0808(5), \\ &|\lambda_{JJS}| = 0.645(4)\,. \end{aligned} \tag{1.3}$$

Similarly, we can extract upper and lower bounds on the central charge C_T. These are shown in Fig. 1.3 and allow us to conclude:

$$\frac{C_T}{C_T^{\text{free}}} = 0.9442(6)\,. \tag{1.4}$$

Finally, using the same set of assumptions, we can extract upper bounds on low lying operators. We stress that these are bona fide upper bounds and are not obtained by the extremal functional method. As an example we show in Fig. 1.4 the upper bounds on the first neutral parity-odd scalar as a function of γ for fixed Δ_ϕ. Again changing the value of Δ_ϕ within its allowed range does not affect the results in a noticeable way. Notice that passing from $\Lambda = 13$ to $\Lambda = 19$ makes the bound stronger by a 5%, suggesting that the bound is still not converged.

We repeated a similar analysis in other channels and we obtained the bounds summarized in Table 1.2.

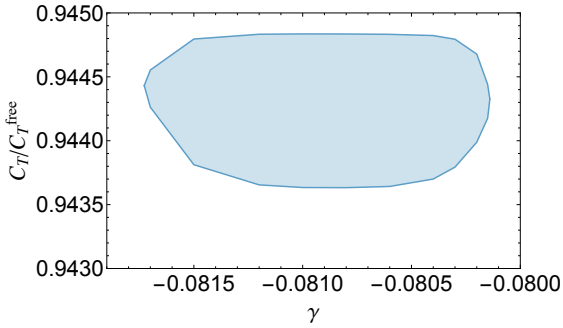

Figure 1.3: Upper and lower bound on the central charge C_T normalized to the free value assuming the constraints shown in Table 1.1 and $\Delta_{T'} \geq 4.5$. The bounds have been computed at $\Lambda = 13$.

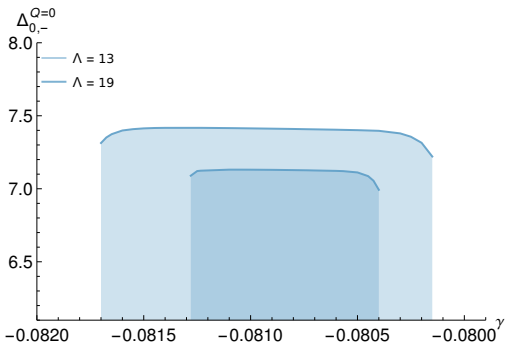

Figure 1.4: Bound on the the dimension of the first neutral parity-odd scalar assuming the known $O(2)$ constraints shown in Table 1.1 and $\Delta_{T'} \geq 4.5$. The bounds terminate because γ is confined in an interval, see Fig. 1.2.

ℓ	P	Q	$\Lambda = 13$	$\Lambda = 19$
0	$-$	0	7.45	7.13
1	$-$	1	10.14	8.59
2	$-$	1	4.47	4.47
1	$+$	1	2.96	2.95

Table 1.2: Upper bounds on operators in the $O(2)$ models.

1.1.2 Conductivity at finite temperature

CFTs also play an important role in the description of certain quantum critical points. It was observed in [52] that transport properties of systems near a quantum critical point

can be expressed in terms of CFT-data. There, the conductivity of a global symmetry current in a (2+1) CFT non-zero temperature was computed in terms of the OPE $J \times J$ and compared with a quantum Monte Carlo simulation (QMC) of the $O(2)$-model in the limit of high frequencies, $w \gg T$.
The imaginary frequency conductivity is related to the thermal expectation value of the current two point function by the expression

$$\frac{\sigma(iw)}{\sigma_Q} = -\frac{1}{|w|}\langle \widetilde{J}_{\mu=2}(-w)\widetilde{J}_{\nu=2}(w)\rangle_T + (\text{contact terms})\,, \tag{1.5}$$

where $\sigma_Q = e^2/\hbar$ is the conductance quantum unit and $\widetilde{J}_\mu(w)$ denotes the Fourier transform of the current $J_\mu(x)$.[6]
When using the OPE, the left-hand side receives contributions to all operators that acquire a thermal expectation value.[7] The leading term comes from the identity exchange and corresponds to a constant value, usually called σ_∞, identified with the conductivity at $T = 0$. Next, for each primary operator $\mathcal{O}$ entering the $J \times J$ OPE, the conductivity receives a contribution scaling as $(T/w)^{\Delta_\mathcal{O}}$. As pointed out in [52], in the $O(N)$ model, the leading term in the expansion is the unique $O(N)$ singlet relevant scalar, followed by the stress tensor and then irrelevant operators.

In order to compare our bootstrap prediction with the quantum Monte Carlo simulation for the $O(2)$ model, we first need to express the conductivity defined in (1.5) in terms of the CFT-data. After a brief calculation[8], summarized in appendix A.1, we obtain:

$$\begin{aligned}\frac{\sigma(iw)}{\sigma_Q} &= \frac{C_J}{32} + \frac{C_J\lambda_{JJS}}{4\pi}\frac{\Gamma(\Delta_S+1)\sin\left(\frac{\pi\Delta_S}{2}\right)}{2-\Delta_S}\Upsilon^{-1}\left(\frac{T}{w}\right)^{\Delta_S} + 72\frac{\gamma C_J}{C_T}H_{xx}\left(\frac{T}{w}\right)^3\dots \\ &= \sigma_\infty + b_1\left(\frac{T}{w}\right)^{\Delta_S} + b_2\left(\frac{T}{w}\right)^3 + \dots\,,\end{aligned} \tag{1.6}$$

where Δ_S is the dimension of the relevant singlet in the $O(2)$ model, Υ^{-1} measures the normalized thermal expectation value of S, and H_{xx} is the thermal one-point function of the stress tensor xx component, see appendix A.1 for a precise definition. The parameter λ_{JJS} is the OPE coefficient determined in (1.3). The central charges C_J and C_T measure the normalization of the conserved current J_μ and the stress tensor $T_{\mu\nu}$. Our conventions are such that in the theory of a single complex scalar one has

$$C_J^{\text{free}} = 2\,, \qquad C_T^{\text{free}} = 3\,. \tag{1.7}$$

[6]The conductivity is defined only on Matsubara frequencies $w_n = 2\pi nT$, but can be analytically continued to intermediate values.
[7]Only primary operators acquire a thermal expectation value.
[8]See also [53] for a similar expression.

By fitting the quantum Monte Carlo data, [52] obtained the values $\sigma_\infty^{QMC} = 0.5662(5)$, $b_1^{QMC} = 1.43(5)$, $b_2^{QMC} = -0.4(1)$, $\Delta_S^{QMC} = 1.526(65)$. In addition, they independently determined $\Upsilon = 1.18(13)$, by fitting different observables, namely the one- and two-point function of the operator S. Using (1.6) and the bounds on C_J obtained in [30], we can test the consistency of the results:

$$\begin{aligned} \text{Bootstrap + QMC conductivity fit:} \quad & \Upsilon = 1.257(60)\,, \\ \text{QMC } \Upsilon \text{ direct fit:} \quad & \Upsilon = 1.18(13)\,. \end{aligned}$$

We see that the two determinations of the parameter Υ are in agreement within their errors. In particular the one using the bootstrap results for λ_{JJS} and Δ_S is more accurate.[9]

Plugging (1.3) and (1.4) in expression (1.6) we could also extract the value of the stress tensor thermal one-point function. Unfortunately the fit of the conductivity performed in [52] is marginally sensitive to the sub-leading terms and the value determined for b_2 has a large uncertainty.[10] Nevertheless, we can estimate:

$$\text{Bootstrap + QMC conductivity fit:} \qquad H_{xx} = 0.105(30)\,.$$

It would be nice to use the analytic bootstrap at finite temperature [55–57] to compute the values of Υ and H_{xx} and compare them with the predictions given in this work.

1.2 Setup

In this section we explain our setup. We first discuss which are the possible operators exchanged in the OPEs and we enumerate their associated OPE coefficients. In subsection 1.2.2 we explain how to write the crossing equations of the mixed J-ϕ sector (the two sectors with only currents or only scalars were already studied in the literature, *e.g.* [35, 18]). In subsection 1.2.3 we sketch which are the relevant conformal blocks and how we computed them. Finally in subsection 1.2.4 we summarize the full set of bootstrap equations in the form of sum rules.

Before entering the details of the setup, let us introduce the embedding space formalism [25], which will be useful to classify conformal invariant tensor structures. The idea

[9] Notice however that the value extracted for σ_∞^{QMC} from the fit of the conductivity is quite off compared to latest bootstrap and Monte Carlo determinations, which could be caused by systematic errors estimated of order 5-10% in [54]. The value of Δ_S^{QMC} has instead larger uncertainties.

[10] Notice also that the next correction would come from the second neutral scalar S', which has dimension slightly above 3, and should therefore be treated on equal footing as the stress tensor.

is to uplift each coordinate to a null cone in $\mathbb{R}^{d+1,1}$, namely $x \in \mathbb{R}^d \to P \in \mathbb{R}^{d+1,1}$ such that $P^2 = 0$. This is very convenient since the conformal group $SO(d+1,1)$ acts linearly on $\mathbb{R}^{d+1,1}$ thus trivializing the problem of finding conformal invariants —in fact the scalar product $P_1 \cdot P_2$ of two embedding points is conformal invariant. In order to define correlation functions in embedding space we uplift primary operators. We shall focus on primary operators $\mathcal{O}(x,z) = z_{\mu_1} \cdots z_{\mu_\ell} \mathcal{O}^{\mu_1 \cdots \mu_\ell}(x)$ in a traceless and symmetric representation of $SO(d)$, which are conveniently contracted with null polarization vectors z^μ. Each operator $\mathcal{O}(x,z)$ with dimension Δ and spin ℓ is associated to a field $\mathcal{O}(P,Z)$, which satisfies the condition

$$\mathcal{O}(\lambda P, \alpha Z + \beta P) = \lambda^{-\Delta} \alpha^\ell \mathcal{O}(P,Z)\,, \tag{1.8}$$

where $Z \in \mathbb{R}^{d+1,1}$ is an uplifted polarization vector. In the following we often classify conformal invariant tensor structures by using the embedding space building blocks introduced in [25],

$$\begin{aligned} H_{ij} &\equiv \frac{(Z_i \cdot Z_j)(P_i \cdot P_j) - (Z_i \cdot P_j)(Z_j \cdot P_i)}{(P_i \cdot P_j)}\,, \\ V_{i,jk} &\equiv \frac{(Z_i \cdot P_j)(P_i \cdot P_k) - (Z_i \cdot P_k)(P_i \cdot P_j)}{\sqrt{-2(P_i \cdot P_j)(P_i \cdot P_k)(P_j \cdot P_k)}}\,. \end{aligned} \tag{1.9}$$

For example the two-point function of a primary operator $\mathcal{O}$ with dimension Δ and spin ℓ is defined as follows

$$\langle \mathcal{O}(P_1, Z_1) \mathcal{O}(P_2, Z_2) \rangle = \frac{H_{12}^\ell}{P_{12}^\Delta}\,, \tag{1.10}$$

where $P_{ij} \equiv -2 P_i \cdot P_j$. The central charges of a theory are defined from the two point functions of canonically normalized currents and stress tensors,

$$\langle J(P_1, Z_1) J(P_2, Z_2) \rangle = \frac{C_J}{(4\pi)^2} \frac{H_{12}}{P_{12}^{d-1}}\,, \qquad \langle T(P_1, Z_1) T(P_2, Z_2) \rangle = \frac{C_J}{(4\pi)^2} \frac{H_{12}^2}{P_{12}^d}\,. \tag{1.11}$$

However we keep these operators to be unit normalized according to (1.10). Therefore in our conventions J and T are rescaled as follows

$$J \to J(4\pi)/\sqrt{C_J}\,, \qquad T \to T(4\pi)/\sqrt{C_T}\,. \tag{1.12}$$

1.2.1 3pt functions

One of the features that makes the scalar-current bootstrap richer and more involved is the presence of various different OPEs:

$$J \times J, \qquad J \times \phi, \qquad \phi \times \phi, \qquad \bar{\phi} \times \phi \ . \tag{1.13}$$

Imposing the equality of operators in $J \times J$ and $\phi \times \phi$ and asking for conservation of the currents we can enumerate the allowed OPE tensor structures as indicated in Table 1.3. The operators are written in the form $\mathcal{O}^{Q}_{\ell p}$, where ℓ is the $SO(3)$ spin, p is the parity and

	$JJ\mathcal{O}^{Q=0}_{\ell+}$	$JJ\mathcal{O}^{Q=0}_{\ell-}$	$J\phi\mathcal{O}^{Q=1}_{\ell+}$	$J\phi\mathcal{O}^{Q=1}_{\ell-}$	$\phi\bar{\phi}\mathcal{O}^{Q=0}_{\ell+}$	$\phi\phi\mathcal{O}^{Q=2}_{\ell+}$
$\ell = 0$	1	1	1	0	1	1
$\ell = 1$	0	0	1	1	1	0
$\ell > 0$, even	2	1	1	1	1	1
$\ell > 1$, odd	0	1	1	1	1	0

Table 1.3: Summary of the number of allowed tensor structures for each three point function in our setup. The labels $\ell, \pm, Q$ respectively correspond to spin, parity and $U(1)$ charge of the exchanged operator.

Q is the charge under the $U(1)$ global symmetry. In the following we may drop some of these labels for the sake of brevity.

For most of the three-point functions considered in table 1.3 there exists a unique tensor structure. We will refer to the associated OPE coefficient as λ, *i.e.*

$$\lambda_{JJ\mathcal{O}_{\ell=0+}} \ , \qquad \lambda_{JJ\mathcal{O}_-} \ , \qquad \lambda_{J\phi\mathcal{O}_\pm} \ , \qquad \lambda_{\phi\phi\mathcal{O}_+} \ , \qquad \lambda_{\phi\bar{\phi}\mathcal{O}_+} \ . \tag{1.14}$$

Conversely there are two distinct OPE coefficients in the three-point functions of two currents and a parity even operator $\mathcal{O}^{Q=0}_{\ell+}$ with even $\ell \neq 0$ which we will define as

$$\lambda^{(1)}_{JJ\mathcal{O}_+} \ , \qquad \lambda^{(2)}_{JJ\mathcal{O}_+} \ . \tag{1.15}$$

The explicit basis used to define OPE coefficients will not play an important role for the understanding of the results. For this reason we decided to keep this definition implicit in the main text and collect all the conventions in appendix A.2.

Next we use Ward identities to relate some OPE coefficients to the central charges C_J and C_T of equation (1.11). Using the Ward identities for J, we fix the OPE $\lambda_{\phi\bar{\phi}J}$ in

terms of C_J. For concreteness, in our normalization this relation takes the form[11]

$$\lambda_{\phi\bar{\phi}J} = \frac{4\pi}{\sqrt{C_J}} \ . \tag{1.16}$$

From the Ward identities of T the OPE coefficients $\lambda_{\phi\bar{\phi}T}$ can be fixed in terms of C_T and Δ_ϕ. Similarly the OPE coefficients $\lambda^{(1)}_{JJT}, \lambda^{(2)}_{JJT}$ are fixed in terms of C_T and an extra parameter that we call γ. In our normalization:

$$\lambda_{\phi\bar{\phi}T} = \frac{\sqrt{3}}{2}\Delta_\phi\sqrt{\frac{C_{T_{\text{free}}}}{C_T}} \ , \tag{1.17}$$

$$\lambda^{(1)}_{JJT} = \frac{\sqrt{3}}{8}(1-12\gamma)\sqrt{\frac{C_{T_{\text{free}}}}{C_T}} \ , \tag{1.18}$$

$$\lambda^{(2)}_{JJT} = \frac{\sqrt{3}}{4}(5-12\gamma)\sqrt{\frac{C_{T_{\text{free}}}}{C_T}} \ , \tag{1.19}$$

where $C_{T_{\text{free}}} \equiv 3$ is the central charge of a free complex scalar. The coefficient γ is further constrained by the conformal collider bounds [49] to lie in the following interval

$$-\frac{1}{12} \leq \gamma \leq \frac{1}{12} \ . \tag{1.20}$$

The two extremes correspond to complex free scalar ($\gamma = -\frac{1}{12}$) and free fermion theory ($\gamma = \frac{1}{12}$).

1.2.2 Crossing equations

In this section we want to obtain all the crossing equations relevant for our setup. Fortunately a big part of this goal is already solved in previous papers. For the scalar correlators the situation is the standard one discussed for example in [35]. For the case of four currents we exactly use the same setup detailed in [18]. What is left to discuss is the case of mixed correlators of two scalars and two conserved currents. In the rest of the section we focus on detailing this case.

Tensor structures

We start by considering four point functions of two scalars ϕ_i and two (so far non conserved) vectors J_i. In order to classify the different tensor structures in their four point functions it is convenient to write the correlation functions in embedding space

[11] We always assume that the external scalar has charge $Q = 1$ under the global $U(1)$.

[25],

$$\begin{aligned}
\langle J_1(P_1,Z_1)\phi_1(P_2)J_2(P_3,Z_3)\phi_2(P_4)\rangle &\equiv \mathcal{K}(P_i)\textstyle\sum_{s=1}^5 f_s(u,v)Q_s^{(f)}(\{P_i,Z_i\}) \ , \quad (1.21)\\
\langle J_1(P_1,Z_1)J_2(P_2,Z_2)\phi_1(P_3)\phi_2(P_4)\rangle &\equiv \mathcal{K}(P_i)\textstyle\sum_{s=1}^5 g_s(u,v)Q_s^{(g)}(\{P_i,Z_i\}) \ , \quad (1.22)\\
\langle \phi_1(P_1)J_1(P_2,Z_2)J_2(P_3,Z_3)\phi_2(P_4)\rangle &\equiv \mathcal{K}(P_i)\textstyle\sum_{s=1}^5 h_s(u,v)Q_s^{(h)}(\{P_i,Z_i\}) \ , \quad (1.23)
\end{aligned}$$

where $u \equiv P_{12}P_{34}/(P_{13}P_{24})$ and $v \equiv P_{23}P_{14}/(P_{13}P_{24})$ are the usual conformal cross ratios. The function $\mathcal{K}$ is a fixed kinematical factor

$$\mathcal{K}(P_i) \equiv \kappa(v)\frac{\left(\frac{P_{24}}{P_{14}}\right)^{\frac{\Delta_1-\Delta_2}{2}}\left(\frac{P_{14}}{P_{13}}\right)^{\frac{\Delta_3-\Delta_4}{2}}}{(P_{12})^{\frac{\Delta_1+\Delta_2}{2}}(P_{34})^{\frac{\Delta_3+\Delta_4}{2}}} \ , \qquad \kappa(v) \equiv v^{-\frac{\Delta_2+\Delta_3}{2}} \ . \tag{1.24}$$

The factor $\kappa(v)$ is introduced to get nicer definitions for the crossing equations. The tensor structures Q_s are the s-th component of the vectors $\vec{Q}$ defined below

$$\begin{aligned}
\vec{Q}^{(f)} &= \{H_{13}, V_{1,23}V_{3,21}, V_{1,23}V_{3,41}, V_{1,43}V_{3,21}, V_{1,43}V_{3,41}\} \ ,\\
\vec{Q}^{(g)} &= \{H_{12}, V_{1,23}V_{2,14}, V_{1,23}V_{2,34}, V_{1,43}V_{2,14}, V_{1,43}V_{2,34}\} \ ,\\
\vec{Q}^{(h)} &= \{H_{23}, V_{2,14}V_{3,21}, V_{2,14}V_{3,41}, V_{2,34}V_{3,21}, V_{2,34}V_{3,41}\} \ ,
\end{aligned} \tag{1.25}$$

where the structures H_{ij} and $V_{i,jk}$ are the building blocks of [25] defined in (1.9). So far the structures Q_s are fixed only by scaling. Extra constraints will be imposed in the following by requiring that the two currents J_i are equal and conserved and by imposing that $\Delta_{\phi_1} = \Delta_{\phi_2}$.

Crossing equations

Now that the tensor structures are classified, we are ready to write the crossing equations. Crossing equations are obtained by demanding the invariance of the four point functions under the permutations $1 \leftrightarrow 3$ (*i.e.* of the operators inserted at point P_1 and P_3). This implies relations between different functions f_s and relates the functions g_s and h_s. The resulting equations can be diagonalized by introducing the following change of basis,

$$f_s \equiv \tfrac{1}{\sqrt{2}}\sum_{s'=1}^{5}(M_f)_{ss'}\hat{f}_{s'} \ , \qquad g_s \equiv \tfrac{1}{\sqrt{2}}\sum_{s'=1}^{5}(M_g)_{ss'}\hat{g}_{s'} \ , \qquad h_s \equiv \tfrac{1}{\sqrt{2}}\sum_{s'=1}^{5}(M_h)_{ss'}\hat{h}_{s'} \ , \tag{1.26}$$

where $M_{f,g,h}$ are 5×5 matrices defined as follows

$$M_f \equiv \begin{pmatrix} 0 & 0 & 0 & \sqrt{2} & 0 \\ 0 & 1 & 0 & 0 & -1 \\ 1 & 0 & 1 & 0 & 0 \\ 1 & 0 & -1 & 0 & 0 \\ 0 & 1 & 0 & 0 & 1 \end{pmatrix}, \quad M_g \equiv \begin{pmatrix} 0 & 0 & 0 & \sqrt{2} & 0 \\ 0 & 1 & -1 & 0 & 0 \\ 1 & 0 & 0 & 0 & 1 \\ 1 & 0 & 0 & 0 & -1 \\ 0 & 1 & 1 & 0 & 0 \end{pmatrix}, \quad M_h \equiv \begin{pmatrix} 0 & 0 & 0 & \sqrt{2} & 0 \\ 1 & 0 & 0 & 0 & -1 \\ 0 & 1 & 1 & 0 & 0 \\ 0 & 1 & -1 & 0 & 0 \\ 1 & 0 & 0 & 0 & 1 \end{pmatrix}. \tag{1.27}$$

With these definitions the permutation $1 \leftrightarrow 3$ in (1.21) and (1.22) results in the following set of crossing equations

$$\begin{aligned} \hat{f}_s(u,v) &= \hat{f}_s(v,u) \ , \quad s = 1,2,4,5 \ , \qquad \hat{f}_3(u,v) = -\hat{f}_3(v,u) \ , \\ \hat{g}_s(u,v) &= \hat{h}_s(v,u) \ , \quad s = 1,2,3,4 \ , \qquad \hat{g}_5(u,v) = -\hat{h}_5(v,u) \ . \end{aligned} \tag{1.28}$$

Equality

When the two vectors and the two scalars are equal (*i.e.* $J_i = J$, $\phi_i = \mathcal{O}$) we can use extra crossing relations (for example a $J\mathcal{O}J\mathcal{O}$ is invariant under $(1,2) \leftrightarrow (3,4)$) which constrain the functions $\hat{f}, \hat{g}, \hat{h}$,

$$\hat{f}_5(u,v) = 0 \ , \qquad \hat{g}_5(u,v) = 0 \ , \qquad \hat{h}_5(u,v) = 0 \ . \tag{1.29}$$

However, we are interested in the case of different scalar operators with the same scaling dimension $\Delta_{\phi_1} = \Delta_{\phi_2}$. In this case we are not allowed to use the crossing relation above, however (1.29) still holds. Indeed we could show that for $\Delta_{\phi_1} = \Delta_{\phi_2}$ the conformal blocks which decompose the functions $\hat{f}_5, \hat{g}_5, \hat{h}_5$ exactly vanish. Thus, the functions must vanish too.

Conservation

Conservation of the two operators J_i gives four independent partial differential equations (of the first order) for the functions $\hat{f}_s$ (similarly for $\hat{g}_s$ and $\hat{h}_s$),

$$\begin{aligned} &\sum_{s=1}^{5} [(M_u^{(f)})_{s's}\partial_u + (M_v^{(f)})_{s's}\partial_v + (M_0^{(f)})_{s's}]\hat{f}_s(u,v) = 0 \ , \qquad s' = 1,2,3,4, \\ &\sum_{s=1}^{5} [(M_u^{(g)})_{s's}\partial_u + (M_v^{(g)})_{s's}\partial_v + (M_0^{(g)})_{s's}]\hat{g}_s(u,v) = 0 \ , \qquad s' = 1,2,3,4, \\ &\sum_{s=1}^{5} [(M_u^{(h)})_{s's}\partial_u + (M_v^{(h)})_{s's}\partial_v + (M_0^{(h)})_{s's}]\hat{h}_s(u,v) = 0 \ , \qquad s' = 1,2,3,4, \end{aligned} \tag{1.30}$$

where M_u, M_v, M_0 are 4×5 matrices which depend on u, v.

Two of the four differential equations in (1.30) (for example $s' = 3, 4$) involve only the fifth functions $\hat{f}_5$ (similarly for $\hat{g}_5$ and $\hat{h}_5$). These two equations are therefore not important in our setup since, as we argued above, the functions $\hat{f}_5, \hat{g}_5, \hat{h}_5$ must vanish when $J_1 = J_2$ and $\Delta_{\phi_1} = \Delta_{\phi_2}$.[12]

The remaining two differential equations, $s' = 1, 2$, involve non zero functions. For the case $J_1\phi_1 J_2\phi_2$ one can use them to evolve the crossing equations of $\hat{f}_3(u, v) = -\hat{f}_3(v, u)$ and $\hat{f}_4(u, v) = \hat{f}_4(v, u)$ from the line $u = v$ to the plane. The crossing equation for $\hat{f}_4$ is trivially satisfied on the line therefore we do not need to impose extra equations. On the other hand to ensure crossing symmetry for $\hat{f}_3$ we need to impose the extra condition $\hat{f}_3(u, u) = 0$. For the case of $JJ\phi\bar{\phi}$ the conservation equations can be used to evolve the equations $\hat{g}_3(u, v) = \hat{h}_3(v, u)$ and $\hat{g}_4(u, v) = \hat{h}_4(v, u)$ from the line $u = v$ to the full plane. One can in fact explicitly check that the evolution equations for $\hat{g}_3(u, v)$ and $\hat{g}_4(u, v)$ are exactly equal to the ones of $\hat{h}_3(v, u)$ and $\hat{h}_4(v, u)$. In summary the final set of crossing equations for two conserved equal currents and two scalars with equal dimensions are

$$\hat{f}_s(u, v) = \hat{f}_s(v, u) \ , \quad \hat{g}_s(u, v) = \hat{h}_s(v, u) \ , \qquad (s = 1, 2) \tag{1.34}$$

with the following constraint on the line

$$\hat{f}_3(u, u) = 0 \ , \quad \hat{g}_3(u, u) = \hat{h}_3(u, u) \ , \quad \hat{g}_4(u, u) = \hat{h}_4(u, u) \ . \tag{1.35}$$

1.2.3 Conformal Blocks

In the previous section we explained how to write the crossing equations. The basic idea of the bootstrap is to require the compatibility of the crossing equations with the conformal block decomposition. In this section we explain which are the relevant conformal blocks for our setup.

Let us consider a four point functions $\langle \mathcal{O}_1 \mathcal{O}_2 \mathcal{O}_3 \mathcal{O}_4 \rangle$ of operators $\mathcal{O}_i$ with dimensions Δ_i

[12] As a curiosity we would like to report that, when the conformal dimensions of the two scalars is Δ_ϕ and the one of the currents is Δ_J, we could solve these two differential equations, finding

$$\hat{f}_5(u, v) = c_1 \left(1 - 2u + (u - v)^2 - 2v\right)^{-\frac{\Delta_J}{2}} (uv)^{\frac{\Delta_\phi}{2} + \frac{\Delta_J}{2}} \ , \tag{1.31}$$

$$\hat{g}_5(u, v) = c_2 \, u^{\Delta_J + \frac{1}{2}} v^{\frac{\Delta_\phi}{2} + \frac{\Delta_J}{2}} \left(1 - 2u + (u - v)^2 - 2v\right)^{-\frac{\Delta_J}{2}} \ , \tag{1.32}$$

$$\hat{h}_5(u, v) = c_3 \, u^{\frac{\Delta_\phi}{2} + \frac{\Delta_J}{2}} v^{\Delta_J + \frac{1}{2}} \left(1 - 2u + (u - v)^2 - 2v\right)^{-\frac{\Delta_J}{2}} \ , \tag{1.33}$$

where c_i are constants of integration. Compatibility with the conformal blocks decomposition requires $c_i = 0$.

and spin ℓ_i. By taking the OPE $\mathcal{O}_1 \times \mathcal{O}_2$ and $\mathcal{O}_3 \times \mathcal{O}_4$ we obtain the following conformal block decomposition

$$\langle \mathcal{O}_1 \mathcal{O}_2 \mathcal{O}_3 \mathcal{O}_4 \rangle = \mathcal{K} \sum_{p,q} \lambda^{(p)}_{\mathcal{O}_1 \mathcal{O}_2 \mathcal{O}} \lambda^{(q)}_{\mathcal{O}_3 \mathcal{O}_4 \mathcal{O}} \sum_s g^{(p,q)\,\mathcal{O}_1\mathcal{O}_2\mathcal{O}_3\mathcal{O}_4}_{\mathcal{O},s}(u,v) Q_s \,, \tag{1.36}$$

where $\mathcal{K}$ is the prefactor defined in (1.24), Q_s are the four-point function conformal invariant tensor structures (E.g. (1.25)) and $\lambda^{(p)}, \lambda^{(q)}$ are the left and right OPE coefficients. The conformal blocks $g^{(p,q)\,\mathcal{O}_1\mathcal{O}_2\mathcal{O}_3\mathcal{O}_4}_{\mathcal{O},s}(u,v)$ are functions of the cross ratios u and v, built out of the insertions of the four operators. They depend on the representation of the exchanged operator $\mathcal{O}$ which is labelled by Δ, ℓ and $\pm$. The dependence on the external operators $\mathcal{O}_i$ is twofold. Firstly, they depend on their conformal dimension Δ_i, through the combinations Δ_{12} and Δ_{34}, where $\Delta_{ij} \equiv \Delta_i - \Delta_j$. Most importantly they depend on the spins ℓ_i of $\mathcal{O}_i$ which are responsible for the presence of different tensor structures both for the OPE and for the four point function. This affects the possible values of the conformal block labels p, q and s.

There are different strategies to compute conformal blocks. In this paper we mostly used a recurrence relation [35, 6] which builds the blocks as a power series in the radial coordinates $r \equiv |\rho|, \eta \equiv (\rho + \bar{\rho})/(2|\rho|)$ of [4], where

$$\rho = \frac{z}{(1+\sqrt{1-z})^2} \,, \qquad \bar{\rho} = \frac{\bar{z}}{(1+\sqrt{1-\bar{z}})^2} \,, \tag{1.37}$$

and $u = z\bar{z}$ and $v = (1-z)(1-\bar{z})$. The recurrence relation is defined by studying the analytic structure of the conformal blocks as functions of Δ. It takes the form

$$h^{(p,q)\,\mathcal{O}_1\mathcal{O}_2\mathcal{O}_3\mathcal{O}_4}_{\Delta\ell,s}(r,\eta) = h^{(p,q)\,\mathcal{O}_1\mathcal{O}_2\mathcal{O}_3\mathcal{O}_4}_{\infty\ell,s}(r,\eta) + \sum_A (4r)^{n_A} \frac{(R_A)_{pp'qq'}}{\Delta - \Delta^\star_A} h^{(p,q)\,\mathcal{O}_1\mathcal{O}_2\mathcal{O}_3\mathcal{O}_4}_{\Delta_A\ell_A,s}(r,\eta) \,, \tag{1.38}$$

where $h^{(p,q)}_{\Delta\ell,s}(r,\eta) \equiv (4r)^{-\Delta} g^{(p,q)}_{\Delta\ell,s}(r,\eta)$. There are a few ingredients that enter this formula: h_∞, R_A and the labels $\Delta^\star_A, \Delta_A, \ell_A, n_A$. The latter are known from representation theory for any conformal block in generic dimensions, while h_∞, R_A can be computed by some standard computations [6, 26, 58]. Moreover, recently the paper [59] appeared with a closed form solution for h_∞ and R_A for any conformal block in $d = 3$. This will be a very useful tool to implement the conformal bootstrap in more complicated situations involving mixed correlators with spinning operators.

For our setup we need to compute five different kinds of conformal blocks

$$g^{\phi\phi\phi\phi}_{\mathcal{O}}(u,v) \,, \qquad g^{J\phi J\phi}_{\mathcal{O},s}(u,v) \,, \qquad g^{\phi JJ\phi}_{\mathcal{O},s}(u,v) \,, \qquad g^{(p)\,JJ\phi\phi}_{\mathcal{O},s}(u,v) \,, \qquad g^{(p,q)\,JJJJ}_{\mathcal{O},s}(u,v) \,, \tag{1.39}$$

where ϕ here stands for any scalar operator of dimension Δ_ϕ. In the following we discuss how we computed these conformal blocks and some of their features.

$\phi\phi\phi\phi$: The scalar block is a single function of the cross ratios which we computed, as customary, by means of the recurrence relation (1.38).

$J\phi J\phi$: The mixed blocks $g_{\mathcal{O},s}^{J\phi J\phi}(u,v)$ were computed in [26] using the recurrence relation (1.38). We used the ancillary file that was included in the publication. Notice that in [26] the blocks are defined for generic spacetime dimension d and also for generic non conserved vectors J_1, J_2 and different scalars ϕ_1, ϕ_2. The package generates $g_{\mathcal{O},s}^{(p,q)\,J\phi J\phi}(u,v)$ for $s = 1, \dots 5$ and for $\mathcal{O}$ belonging both to traceless symmetric representation of spin ℓ (in this case $p, q = 1, 2$) and to the mixed symmetric representation $(\ell, 1)$ of $SO(d)$ (in this case $p, q = 1$). For our setup we need to consider $\phi_1 = \phi_2$ and $J_1 = J_2$ conserved in dimension $d = 3$ —their normalization is discussed in appendix A.3.2. This implies that we do not need to compute the 5 structures labelled by s but only the three combinations useful to decompose (1.34) and (1.35) (one of these combinations is computed only in the $u = v$ line). Finally, we stress that the $(\ell, 1)$ representation of $SO(d)$ is identified as a parity odd spin ℓ representation of $SO(3)$.

$\phi JJ\phi$: The blocks $g_{\mathcal{O},s}^{\phi JJ\phi}(u,v)$ have the same exact features as $g_{\mathcal{O},s}^{J\phi J\phi}(u,v)$. Indeed they can be computed from the latter by using permutation of the operators $1 \leftrightarrow 2$ as explained in appendix A.3.3. In particular one can compute the blocks $g_{\mathcal{O},s}^{\phi JJ\phi}(u,v)$ at some order in the r expansion by knowing the blocks $g_{\mathcal{O},s}^{J\phi J\phi}(u,v)$ at the same order (provided that the complete dependence in the variable η is known at that order). However we decided to compute these blocks by using the differential operators of [24] to test if this algorithm was as effective as the recurrence relation. In our implementations, the recurrence relation was faster.

$JJ\phi\phi$: We computed $g_{\mathcal{O},s}^{\phi JJ\phi}(u,v)$ using the recurrence relation (1.38) as we detail in appendix A.3.1. Our program works in arbitrary dimensions and for generic vector and scalar operators. For a generic setup p and s take values from 1 to 5. In our case, due to conservation, p only runs over 1 and 2 and we only require $s = 1, 2, 3, 4$ (two on the u, v plane plus two at the $u = v$ line) which are enough to expand the crossing equations (1.34) and (1.35).

$JJJJ$: The $g_{\mathcal{O},s}^{(p,q)\,JJJJ}(u,v)$ blocks were computed in [18] using a recurrence relation valid for generic vectors in $d = 3$. Of the 41 values of s, only 11 combinations are useful to expand the crossing equation for conserved equal currents (5 on the full u, v plane, 5 on the $u = v$ line and 1 at the point $u = v = 1/4$). Moreover, for the

conserved blocks, the values of p, q again run only from 1 to 2. In this work we re-used the blocks generated for the paper [18].

Generating the five ingredients is not trivial. The $JJJJ$ blocks are the hardest task which was already done. However, computing the blocks $\phi JJ\phi$ and $J\phi J\phi$ is also very expensive because they both depend on the value of Δ_ϕ. We decided to generate these functions at low derivative order with an explicit dependence on Δ_ϕ. This enabled us to perform some exploratory scans in the dimension of ϕ. We then computed them at higher derivatives for some fixed values of Δ_ϕ compatible with the $O(2)$ model. Finally, the computation of the $JJ\phi\phi$ and $\phi\phi\phi\phi$ blocks is reasonably fast.

1.2.4 Sum rules

The bootstrap equations are obtained by combining the crossing equations of subsection 1.2.2 with the conformal block decomposition of subsection 1.2.3. They take the form of sum rules for some functions $F^{[\pm]}$ which are defined in terms of combinations of conformal blocks,

$$F^{[\pm]\mathcal{O}_1\mathcal{O}_2\mathcal{O}_3\mathcal{O}_4} \equiv \kappa(v) g_{\mathcal{O}}^{\mathcal{O}_1\mathcal{O}_2\mathcal{O}_3\mathcal{O}_4}(u,v) \pm (u \leftrightarrow v) \ , \qquad \kappa(v) \equiv v^{-\frac{\Delta_2+\Delta_3}{2}} \ . \tag{1.40}$$

In what follows we write down the sum rules for all the considered correlators. The goal is to reach a single vectorial bootstrap equation that can be analyzed by means of semidefinite programming.

The scalar sector

Let us start by reviewing how the scalar bootstrap equations arise. By equating the OPE channels (12)(34) = (13)(24) of the correlation function $\langle \phi\bar{\phi}\phi\bar{\phi}\rangle$, we get the following equation

$$\sum_{\mathcal{O}^{Q=0}_{\Delta\,\ell\,+}} (-1)^\ell |\lambda_{\phi\bar{\phi}\mathcal{O}}|^2 F_{\mathcal{O}}^{[-]\phi\bar{\phi}\phi\bar{\phi}}(u,v) = 0 \, . \tag{1.41}$$

The same strategy applied to $\langle \bar{\phi}\phi\phi\bar{\phi}\rangle$ generates two equations

$$\sum_{\mathcal{O}^{Q=0}_{\Delta\,\ell\,+}} |\lambda_{\phi\bar{\phi}\mathcal{O}}|^2 F_{\mathcal{O}}^{[\pm]\bar{\phi}\phi\phi\bar{\phi}}(u,v) \mp \sum_{\mathcal{O}^{Q=2}_{\Delta\,\ell\,+}} |\lambda_{\phi\phi\mathcal{O}}|^2 F_{\mathcal{O}}^{[\pm]\phi\phi\bar{\phi}\bar{\phi}}(u,v) = 0 \, , \tag{1.42}$$

parametrized by the label $\pm$.

The mixed sector

As we explain in subsection 1.2.2, the crossing equations for the mixed correlators take a

simpler form in the hatted basis (1.26). It is therefore convenient to define new functions $F^{[\pm]}$ which are rotated accordingly,

$$\begin{aligned} F^{[\pm]J\phi J\bar{\phi}}_{\mathcal{O},s}(u,v) &\equiv \kappa(v)^{-1}\textstyle\sum_{s'=1}^{5}(M_f^{-1})_{ss'}g^{[J\phi J\bar{\phi}]}_{\mathcal{O},s'}(u,v)\pm(u\leftrightarrow v)\ , \\ F^{(q)[\pm]JJ\phi\bar{\phi}}_{\mathcal{O},s}(u,v) &\equiv \kappa(v)^{-1}\textstyle\sum_{s'=1}^{5}(M_g^{-1})_{ss'}g^{(q)[JJ\phi\bar{\phi}]}_{\mathcal{O},s'}(u,v)\pm(u\leftrightarrow v)\ , \\ F^{[\pm]\phi JJ\bar{\phi}}_{\mathcal{O},s}(u,v) &\equiv \kappa(v)^{-1}\textstyle\sum_{s'=1}^{5}(M_h^{-1})_{ss'}g^{[\phi JJ\bar{\phi}]}_{\mathcal{O},s'}(u,v)\pm(u\leftrightarrow v)\ , \end{aligned} \tag{1.43}$$

In this notation it is easy to write the bootstrap equations. From $\langle J\phi J\bar{\phi}\rangle$ we get two equations on the plane and one on a line

$$\sum_{\mathcal{O}^{Q=1}_{\Delta\,\ell\,\pm}}\sigma_{\mathcal{O}}|\lambda_{J\phi\mathcal{O}}|^2F^{[-]J\phi J\bar{\phi}}_{\mathcal{O},s}(u,v)=0\,,\quad s=1,2\,, \tag{1.44}$$

$$\sum_{\mathcal{O}^{Q=1}_{\Delta\,\ell\,\pm}}\sigma_{\mathcal{O}}|\lambda_{J\phi\mathcal{O}}|^2F^{[+]J\phi J\bar{\phi}}_{\mathcal{O},s}(u,u)=0\ ,\qquad s=3\,. \tag{1.45}$$

Here σ is a sign which depends on the normalization of the three point functions.[13] In our case

$$\sigma_{\mathcal{O}}=\begin{cases}1 & \text{if } \mathcal{O}=\bar{\phi}\\ (-1)^{\ell+p+1} & \text{if } \mathcal{O}\neq\bar{\phi}\end{cases}\ , \tag{1.48}$$

where $p=0,1$ and ℓ are respectively the parity and the spin of the exchanged operator $\mathcal{O}$.

From $\langle\phi JJ\bar{\phi}\rangle$ we get four equations on a plane (labelled by $s=1,2$ and $[\pm]$) and two on the line ($s=3,4$),

$$\sum_{\mathcal{O}^{Q=0}_{\Delta\,\ell\,+}}\sum_{q=1}^{2}\lambda^{(q)}_{JJ\mathcal{O}}\lambda_{\phi\bar{\phi}\mathcal{O}}F^{(q)[\pm]JJ\phi\bar{\phi}}_{\mathcal{O},s}(u,v)\mp\sum_{\mathcal{O}^{Q=1}_{\Delta\,\ell\,\pm}}\sigma_{\mathcal{O}}|\lambda_{J\phi\mathcal{O}}|^2F^{[\pm]\phi JJ\bar{\phi}}_{\mathcal{O},s}(u,v)=0\,,\ s=1,2\,, \tag{1.49}$$

$$\sum_{\mathcal{O}^{Q=0}_{\Delta\,\ell\,+}}\sum_{q=1}^{2}\lambda^{(q)}_{JJ\mathcal{O}}\lambda_{\phi\bar{\phi}\mathcal{O}}F^{(q)[+]JJ\phi\bar{\phi}}_{\mathcal{O},s}(u,u)-\sum_{\mathcal{O}^{Q=1}_{\Delta\,\ell\,\pm}}\sigma_{\mathcal{O}}|\lambda_{J\phi\mathcal{O}}|^2F^{[+]\phi JJ\bar{\phi}}_{\mathcal{O},s}(u,u)=0\,,\ s=3,4\,. \tag{1.50}$$

The current sector

[13] This is due to the fact that we need rewrite the OPE coefficients in a positive combination,

$$\lambda_{\phi J\bar{\phi}}\lambda_{\phi J\bar{\phi}}=\lambda_{J\phi\bar{\phi}}\lambda_{\phi J\bar{\phi}}\ =\ |\lambda_{J\phi\bar{\phi}}|^2\,, \tag{1.46}$$

$$\lambda_{\phi J\mathcal{O}}\lambda_{\bar{\mathcal{O}}J\bar{\phi}}=\lambda_{J\phi\mathcal{O}}\lambda_{\bar{\mathcal{O}}J\bar{\phi}}\ =\ (-1)^{\ell+p+1}|\lambda_{J\phi\mathcal{O}}|^2\qquad(l>0)\,. \tag{1.47}$$

Finally we review the sum rules for $\langle JJJJ\rangle$ as obtained in [18]. In that case conservation and equality of the currents produced a set of 5 crossing equations valid on the plane, 5 on a line and a single one at a point. In terms of opportune functions $F^{[\pm]}$,[14] the equations are casted into the following sum rules

$$\sum_{p=1}^{2}\sum_{q=1}^{2}\sum_{\mathcal{O}^{Q=0}_{\Delta\,\ell\,+}}\lambda^{(p)}_{JJ\mathcal{O}_+}\lambda^{(q)}_{JJ\mathcal{O}_+}F^{[-](p,q)JJJJ}_{\mathcal{O}_+,s}(u,v)+\sum_{\mathcal{O}^{Q=0}_{\Delta\,\ell\,-}}|\lambda_{JJ\mathcal{O}_-}|^2F^{[-]JJJJ}_{\mathcal{O}_-,s}(u,v)=0\,,\quad s=\begin{matrix}13,15,\\16,17\end{matrix}$$

$$\sum_{p=1}^{2}\sum_{q=1}^{2}\sum_{\mathcal{O}^{Q=0}_{\Delta\,\ell\,+}}\lambda^{(p)}_{JJ\mathcal{O}_+}\lambda^{(q)}_{JJ\mathcal{O}_+}F^{[+](p,q)JJJJ}_{\mathcal{O}_+,s}(u,v)+\sum_{\mathcal{O}^{Q=0}_{\Delta\,\ell\,-}}|\lambda_{JJ\mathcal{O}_-}|^2F^{[+]JJJJ}_{\mathcal{O}_-,s}(u,v)=0\,,\qquad s=7$$

$$\sum_{p=1}^{2}\sum_{q=1}^{2}\sum_{\mathcal{O}^{Q=0}_{\Delta\,\ell\,+}}\lambda^{(p)}_{JJ\mathcal{O}_+}\lambda^{(q)}_{JJ\mathcal{O}_+}F^{[+](p,q)JJJJ}_{\mathcal{O}_+,s}(u,u)+\sum_{\mathcal{O}^{Q=0}_{\Delta\,\ell\,-}}|\lambda_{JJ\mathcal{O}_-}|^2F^{[+]JJJJ}_{\mathcal{O}_-,s}(u,u)=0\,,\quad s=\begin{matrix}1,2,4,\\5,6\end{matrix}$$

$$\sum_{p=1}^{2}\sum_{q=1}^{2}\sum_{\mathcal{O}^{Q=0}_{\Delta\,\ell\,+}}\lambda^{(p)}_{JJ\mathcal{O}_+}\lambda^{(q)}_{JJ\mathcal{O}_+}F^{[+](p,q)JJJJ}_{\mathcal{O}_+,s}(\tfrac{1}{4},\tfrac{1}{4})+\sum_{\mathcal{O}^{Q=0}_{\Delta\,\ell\,-}}|\lambda_{JJ\mathcal{O}_-}|^2F^{[+]JJJJ}_{\mathcal{O}_-,s}(\tfrac{1}{4},\tfrac{1}{4})=0\,,\qquad s=3$$

In the equations above we explicitly show the parity of the exchanged operator since the number of OPE coefficients depends on this quantum number.

The bootstrap equation

Since $\lambda^{(p)}_{JJ\mathcal{O}_+}\lambda^{(q)}_{JJ\mathcal{O}_+}$ and $\lambda^{(p)}_{JJ\mathcal{O}}\lambda_{\phi\bar{\phi}\mathcal{O}}$ are not ensured to be positive quantities, it is necessary to rearrange the equations into a single expression that can be studied using the standard

[14] The exact meaning of the functions $F^{[\pm]}$ is defined in [18], where it is used the notation $F^{[+]}\to\tilde{H}$ and $F^{[-]}\to\tilde{F}$.

semidefinite programming techniques,

$$\vec{\lambda}_{\mathbb{1}}^T \vec{V}^{Q=0}_{0,0,+} \vec{\lambda}_{\mathbb{1}} + \sum_{\mathcal{O}^{Q=0}_{\ell=0,+}} \begin{pmatrix} \lambda_{\phi\bar{\phi}\mathcal{O}_+} \\ \\ \lambda^{(1)}_{JJ\mathcal{O}_+} \end{pmatrix}^T \cdot \vec{V}^{Q=0}_{\Delta,0,+} \cdot \begin{pmatrix} \lambda_{\phi\bar{\phi}\mathcal{O}_+} \\ \\ \lambda^{(1)}_{JJ\mathcal{O}_+} \end{pmatrix} + \sum_{\mathcal{O}^{Q=0}_{\ell>0\text{ even},+}} \begin{pmatrix} \lambda_{\phi\bar{\phi}\mathcal{O}_+} \\ \lambda^{(1)}_{JJ\mathcal{O}_+} \\ \lambda^{(2)}_{JJ\mathcal{O}_+} \end{pmatrix}^T \cdot \vec{V}^{Q=0}_{\Delta,\ell,+} \cdot \begin{pmatrix} \lambda_{\phi\bar{\phi}\mathcal{O}_+} \\ \lambda^{(1)}_{JJ\mathcal{O}_+} \\ \lambda^{(2)}_{JJ\mathcal{O}_+} \end{pmatrix}$$
$$+ \sum_{\mathcal{O}^{Q=0}_{\ell\text{ odd},+}} |\lambda_{\phi\bar{\phi}\mathcal{O}}|^2 \vec{V}^{Q=0}_{\Delta,\ell,+} + \sum_{\mathcal{O}^{Q=0}_{\ell\neq 1,-}} |\lambda_{JJ\mathcal{O}_-}|^2 \vec{V}^{Q=0}_{\Delta,\ell,-} + \sum_{\mathcal{O}^{Q=1}_{\ell\geq 1,+}} |\lambda_{J\phi\mathcal{O}}|^2 \vec{V}^{Q=1}_{\Delta,\ell,+} + \sum_{\mathcal{O}^{Q=1}_{\ell\geq 1,-}} |\lambda_{J\phi\mathcal{O}}|^2 \vec{V}^{Q=1}_{\Delta,\ell,-}$$
$$+ \sum_{\mathcal{O}^{Q=2}_{\ell\text{ even},+}} |\lambda_{\phi\phi\mathcal{O}}|^2 \vec{V}^{Q=2}_{\Delta,\ell,+} + |\lambda_{J\phi\bar{\phi}}|^2 \ \vec{V}^{Q=1}_{\Delta_\phi,0,+} = 0\,. \tag{1.51}$$

where $\vec{\lambda}_{\mathbb{1}} = (1,1)$. Here we have separated the case of $\mathcal{O}^{Q=0}_{\ell=0,+}$ from the other $\ell > 0$, since in former case there is no OPE coefficient $\lambda^{(2)}_{JJ\mathcal{O}}$. In appendix A.4 we write explicitly all the vectors $\vec{V}^{Q}_{\Delta,\ell,\pm}$, where Δ is the conformal dimension, ℓ is the spin, $\pm$ is the parity and $Q = 0, 1, 2$ is the charge of the exchanged operator. By construction all the vectors $\vec{V}$ are 23 dimensional. The 23 components of the vector $\vec{V}^{Q=0}_{\Delta,\ell,+}$ are 3×3 matrices for $\ell > 0$, and 2×2 matrices for $\ell = 0$. The components of all the other vectors $\vec{V}$ do not have any matrix structure.

In the next sections we use the following convention to denote the gaps of the exchanged operators

$$\Delta^{Q}_{\ell,\pm} \equiv \text{Gap for operators with spin } \ell\text{, parity } \pm \text{ and charge } Q\ . \tag{1.52}$$

In this notation the bootstrap equations (1.51) depend on the following five infinite families of gaps,

$$\Delta^{Q=0}_{\ell,+}\,, \qquad \Delta^{Q=0}_{\ell,-}\,, \qquad \Delta^{Q=1}_{\ell,+}\,, \qquad \Delta^{Q=1}_{\ell,-}\,, \qquad \Delta^{Q=2}_{\ell,+}\,. \tag{1.53}$$

For brevity we sometimes refer to the gap of important operators by their name, *e.g.* $\Delta_S = \Delta^{Q=0}_{\ell=0,+}$, $\Delta_{\phi^2} = \Delta^{Q=2}_{\ell=0,+}$, $\Delta_T = \Delta^{Q=0}_{\ell=2,+}$, and so on. We assume that the CFT is unitarity, namely that all gaps in (1.51) are consistent with the unitarity bounds,

$$\Delta^{Q}_{\ell=0,\pm} \geq \frac{d}{2} - 1\ , \qquad \Delta^{Q}_{\ell>0,\pm} \geq \ell + d - 2\ . \tag{1.54}$$

If we increase enough some of the gaps $\Delta^{Q}_{\ell,\pm}$, we may find that the equations (1.51) cannot be satisfied. In this case we say that the corresponding CFT is excluded. We can thus think of Δ_ϕ and the gaps (1.53) as the knobs which can turn to generate bounds. Equation (1.51) can also be used to compute upper bounds on OPE coefficients. In the following we show some interesting bounds obtained in this setup. All semi-definite

problems have been solved using SDPB [13] with parameters as in [18].

1.3 Results

1.3.1 Bounds on operator dimensions

Scalar operators

We begin by studying the bound on the first parity-even scalar, neutral under the global $U(1)$ symmetry. We denote its dimension by Δ_S. As shown in Fig. 1.5 the bound coincides with the constraint one would get by bootstrapping only the scalar correlator $\langle\phi\bar{\phi}\phi\bar{\phi}\rangle$, until it reaches the maximal value allowed by the current bound [18]. At that point the bound becomes flat and independent on the external dimension. Although no new interesting features appears, this bound represents a validation of our methods and shows how the different crossing relations interplay.

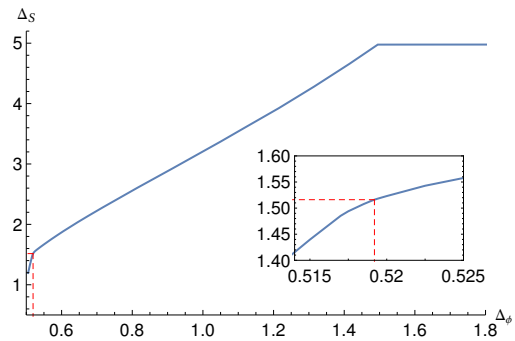

Figure 1.5: Bound on the dimension of the first neutral parity-even scalar operator as a function of Δ_ϕ. For $\Delta_\phi \lesssim 1.5$ the bound is driven by the scalar bound. The plateau for larger values of Δ_ϕ corresponds to the bound from the current bootstrap. The bound displays a kink corresponding to the $O(2)$ model. The bounds have been obtained at $\Lambda = 13$.

Next we consider a bound on the dimension of the first parity-even charge-2 scalar t. We denote its dimension by Δ_t. This operator only appears in the $\phi \times \phi$ OPE, thus it is natural to expect that the bound is completely driven by the scalar crossing equations only. We show this plot in Fig. 1.6, together with the same bound obtained using only scalar correlators at higher Λ.[15] The bound only shows a kink in corresponding to the

[15]Given the numerical complexity of our setup we could not push the mixed correlator analysis to the same value of Λ.

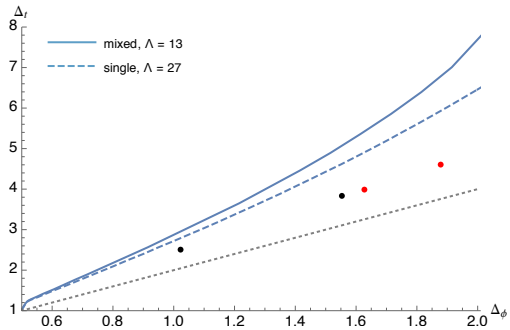

Figure 1.6: Bound on the dimension of the first charge-2 parity-even scalar operator as a function of Δ_ϕ. The bound displays a kink in corresponding to the $O(2)$ model. The continuous line was obtained using the mixed system of bootstrap equations at $\Lambda = 13$; the blue dashed line only uses the scalar correlator at $\Lambda = 27$. The grey dotted line is the generalized free theory line. The red (black) dots correspond to the dimension of the monopoles with charge $q = 1/2$ and $q = 1$ in bosonic (fermionic) QED_3 computed in large-N expansion [61, 60]. Here we show respectively $N = 10, 12$ and $N = 4, 6$.

$O(2)$ model, nevertheless it allows to make contact with another set of CFTs that must obey our exclusion plots.
The infrared fixed point of fermionic and bosonic QED_3 contains a topological global $U(1)$ symmetry: we can then interpret ϕ as a scalar monopole operator with topological charge $q = 1/2$ under this symmetry and identify J_μ with the associated current; then the bound on Δ_t is interpreted as the bound on the smaller monopole with charge $q = 1$. Interestingly the dimension of these operators have been computed in a large N expansion [60], where N is the number of copies of fermions or bosons in the gauge theory. The predictions are shown in Fig. 1.6: although they do not saturate the bound, they seem to get close for small values of N (where however the large-N expansion is not accurate).

The only other sector containing scalars in the mixed system of J and ϕ is the neutral parity-odd one. We do not show its bound here, since it coincides exactly with the one obtained in [18], except that it has a termination point dictated by the maximal value of Δ_S allowed as a function of Δ_ϕ.

Operators with spin

We now move to bounds on operators with spin. We have already pointed out in section 1.2 the advantages of bounding the dimension of $T'_{\mu\nu}$ —the first neutral parity-even spin-2 operator after the stress tensor— to pinpoint the $O(2)$ model. Let us now review this statement by exploring the bound on $\Delta_{T'}$ on a broader range of parameters. In Fig. 1.7

we show its upper bound as a function of the external dimension Δ_ϕ and the parameter $\gamma \in [-1/12, 1/12]$ defined in (1.19).

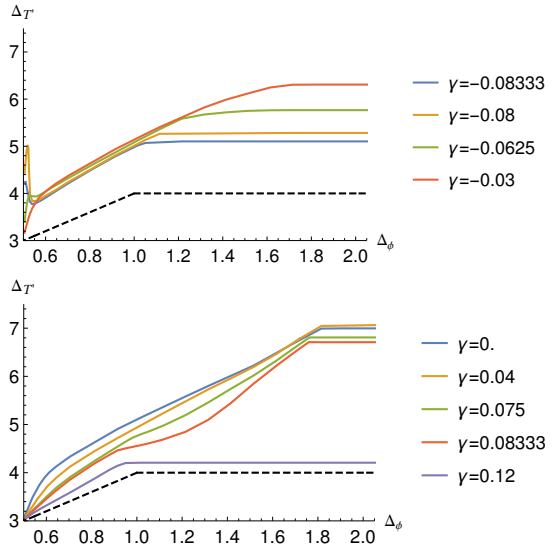

Figure 1.7: Bound on the dimension of the first neutral parity-even spin-2 operator after the stress tensor as a function of Δ_ϕ. Different curves corresponds to different values of the parameter γ defined in (1.19). The dashed curves correspond to the function $\min(4, 2\Delta_\phi + 2)$. The bounds have been obtained at $\Lambda = 13$.

We observe two interesting features at the extremes of the γ interval. Close to the $\gamma \sim -1/12$ the upper bound on $\Delta_{T'}$ develops a sharp peak corresponding to a somewhat large gap in the spin-2 sector. We interpret this gap as the signal of the existence of a local CFT. Non-local theories or fake solutions of the crossing equations do not require a conserved spin-2 primary. As a result for those theories the bound on $\Delta_{T'}$ is actually a bound on the first spin-2 operator. In section 1.1 we exploited this peak to create an island in the (Δ_ϕ, γ) plane and provide the first precise determination of γ for the $O(2)$ model.[16]

In the proximity of the other extreme the bounds shows instead a clear kink around $\Delta_\phi \sim 0.91$. Although it would be nice to interpret this feature as an existing CFT, we are not aware of obvious candidates. The value $\gamma \sim 1/12$ suggests that the putative CFT should admit a description in terms of fermions: in that case the scalar ϕ could be a fermion bilinear with a large anomalous dimension. Another possibility is that ϕ is

[16] One can show the peak persist once additional information about the $O(2)$ model is injected, such as the presence of a single relevant neutral scalar.

a monopole operator of a QED_3-like theory.[17] Unfortunately the parameter γ for the topological current has never been computed. We leave the investigation of this kink for future studies. It is also plausible that this is a reminiscence of the trivial solution in which ϕ is a generalised free field and J is a decoupled conserved current. In this case one has $\Delta_{T'} = \min(4, 2\Delta_\phi + 2)$. This solution is shown by a black dashed curve in Fig. 1.7. We observe indeed that for values of γ outside the conformal collider interval the bounds approaches this solution.

We also notice that all the curves in Fig. 1.7 eventually reach a plateau. We checked that at this point the Δ_ϕ-independent constraints from $\langle JJJJ \rangle$ take over.

So far we have considered bounds on operators that were accessible both using the scalar correlator alone or the four current correlator alone. Let us now move to operators in the $Q = 1$ sector, i.e. appearing in the OPE $J \times \phi$. We recall that, due to conservation, the only scalar allowed in the OPE is ϕ itself. Moving to spin-1 operators, we find parity-even and parity-odd charge-1 vectors.
In Fig. 1.8a we plot the bound on the dimension of the first parity-even vector charged under the global $U(1)$. With no additional assumption the bound displays the characteristic fake-primary effect discussed in [20] due to a contamination from charge-1 spin-2 operators at threshold. By imposing a gap in the latter sector, the fake-primary effect is removed. In addition to the jump, the bound also displays a kink approximatively in correspondence with the $O(2)$ model. However we observed that, injecting additional information, the height of the kink changes substantially.[18] For instance, by imposing the existence of a single relevant spin-1 neutral current, the bound drops as shown in Fig. 1.8b. We checked that imposing extra assumptions does not substantially improve the bound further.[19]

We conclude the section by presenting in Fig. 1.9a and Fig. 1.9b bounds on the first parity-odd charge-1 vector and tensor. Also in this case we must remove the fake primary effect by imposing a finite gap in the spin-2 and spin-3 charge-1 parity-odd sector. In the former case, however, the bound turns out to be heavily dependent on the gap. With a gap smaller that 4.1 the bound seems to diverge when approaching the $O(2)$ model, however increasing the gap to 4.5, changes drastically the shape of the bound. We should point out that further investigations show that a gap in the spin-2 charged parity-odd sector of 4.5 is inconsistent with additional assumptions about the $O(2)$ model.

[17] For instance large-N computation and bootstrap studies suggest that the smallest monopole in fermionic QED_3 with 4 flavours has dimension $\Delta_M \sim 1.034$. The existence of a fixed point at small N is an open question for both bosonic and fermionic QED_3[47, 62]. In principle $U(1)$ Chern-Simons theories with non vanishing κ must also obey our bounds.

[18] It could be that the kink observed without further assumptions corresponds to another CFT.

[19] See also the upper bound presented in Table 1.2 found under additional constraints.

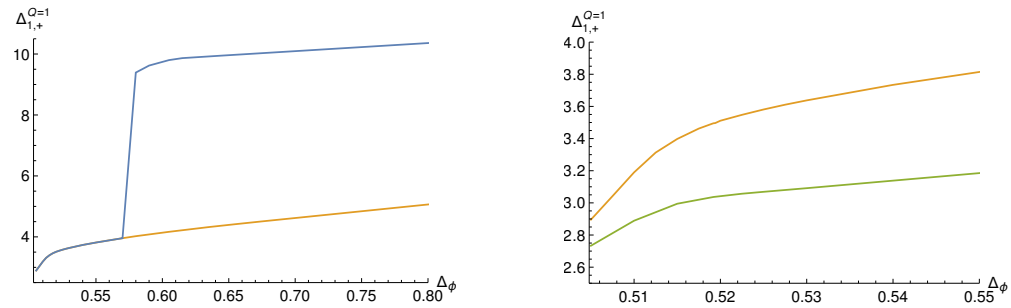

(a) (b)

Figure 1.8: On the left: bound on the dimension of the first charge-1 parity-even spin-1 operator as a function of Δ_ϕ. Assuming a gap of 4 in the charge-1 parity-even spin-2 sector removes the fake primary effect. On the right: same bound with and without the assumption of no relevant neutral vectors besides J. The bounds have been obtained at $\Lambda = 13$.

Notice also that the bound in Fig. 1.9a stops existing as Δ_ϕ approaches 0.96. A similar phenomenon was observed in [63]. Also in our case, the point where the bound stops existing shifts as we increase Λ. We believe this is a numerical artifact which could be cured by imposing ad hoc gaps in the spectrum.

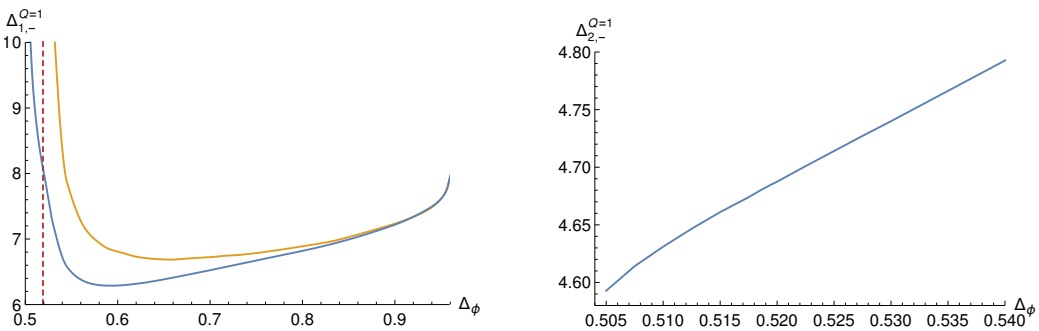

(a) (b)

Figure 1.9: On the left: bound on the dimension of the first charge-1 parity-odd spin-1 operator as a function of Δ_ϕ. The dashed red line corresponds to the value of Δ_ϕ of the $O(2)$ model. The two lines corresponds to different gaps in the charge-1 spin-2 parity-odd sector to remove the fake primary effect. On the right: bound on the dimension of the first charge-1 spin-2 parity-even operator as a function of Δ_ϕ. When the bound reaches 5 it jumps to a much higher value. The bounds have been obtained at $\Lambda = 13$.

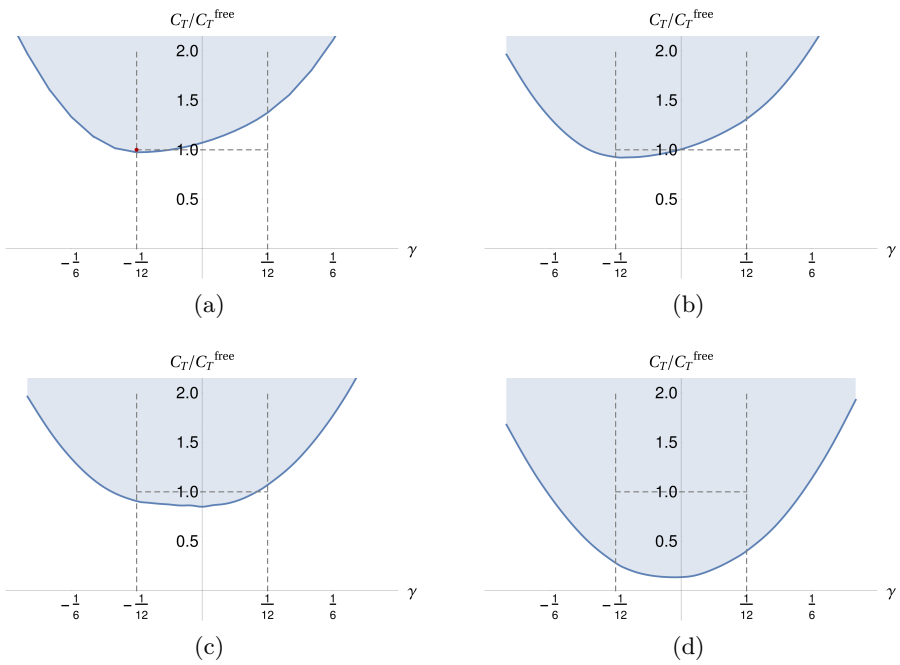

Figure 1.10: Lower bound on the central charge $C_T/C_{T^{\text{free}}}$ as a function of γ for $\Delta_\phi = 0.505, 0.5192, 0.605, 1.05$. The shaded region is allowed. The bounds have been obtained at $\Lambda = 13$.

1.3.2 Bounds on central charges

Among the OPE coefficients appearing in the conformal block decomposition of our correlation functions, the one associated to the exchange of the stress tensor plays a special role. It is indeed related to the central charge C_T by conformal Ward identities. As shown in (1.19), the precise relation involves the parameter γ, which due to the collider bounds is constrained in the interval $[-1/12, 1/12]$. Using the bootstrap, we can then place a lower bound on the central charge as a function of the external dimension Δ_ϕ and the parameter γ. Lower bounds on the central charge for theories with $O(2)$ symmetry have also been computed using the scalar correlator [35] or the current correlator only [18]. In the former case the bound decreases with Δ_ϕ and is always weaker than the free theory value C_T^{free}, with a change of slope in proximity of the $O(2)$ model.[20] In the latter case the bound remains below the free theory value for the allowed range of γ and rapidly increases outside.[21]

[20] The discontinuity appeared to be slightly off in Δ_ϕ.

[21] Assuming a mild gap after the stress tensor make the collider bounds more manifest and the bounds rapidly grows for $|\gamma| > 1/12$.

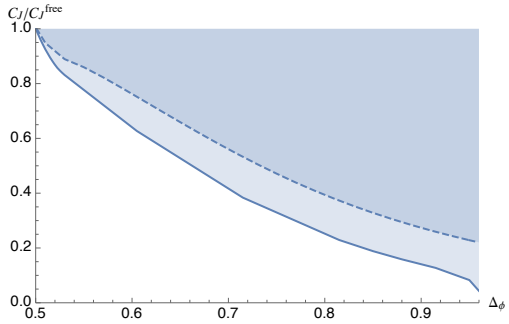

Figure 1.11: Lower bound on C_J as a function of Δ_ϕ. The solid line is computed at $\Lambda = 13$ using the mixed system of J-ϕ correlators, while the dashed line is computed at $\Lambda = 27$ using only the scalar correlator. Both lines show a feature corresponding to the $O(2)$ model.

In Fig. 1.10 we show the results of our analysis. For values of Δ_ϕ close to unitarity, the bound displays a minimum in correspondence with the free scalar theory values of γ and C_T (the red dot in the picture). Increasing Δ_ϕ to 0.5192 the bound gets slightly weaker to accommodate a smaller central charge, as expected in the $O(2)$ model (dashed line in Fig. 1.10b). Interestingly one can already observe that $C_T \leq C_T^{\text{free}}$ requires a negative γ. Increasing further the value of Δ_ϕ makes the bound relax to the bounds obtained using currents alone, Fig. 1.10d.

We conclude this section by studying the constraints imposed on the central charge C_J. Due to Ward identities, this quantity is related to the inverse of the OPE coefficient $\lambda_{\phi\bar{\phi}J}$ according to (1.16). Notice that the latter OPE coefficient appears both in the scalar correlator and in the mixed channel, schematically:

$$\begin{aligned} \phi \times \bar{\phi} &\sim 1 + \lambda_{\phi\bar{\phi}J}\, J + \dots\,, \\ J \times \phi &\sim \lambda_{\phi J\bar{\phi}}\, \phi + \dots\,. \end{aligned} \tag{1.55}$$

There is however an important difference between the above expressions: in the first line the block associated to the exchange of a conserved current is continuously connected to non conserved spin-1 blocks; on the contrary, in the mixed channel, the block associated to the exchange of $\bar{\phi}$ itself plays a special role and is, in fact, isolated. In practice this means that this block cannot be mimicked by an operator arbitrarily close in dimension and one can hope to place also an upper bound on C_J under suitable assumptions. We will come back to this shortly.

Let us begin by exploring lower bounds on C_J. This is shown in Fig. 1.11 as a function of Δ_ϕ. By comparison we also show the bound obtained using the scalar correlator with

higher numerical power. The shape is substantially similar and the only distinguishable feature is in correspondence with the $O(2)$ model, as already observed in [64].[22]

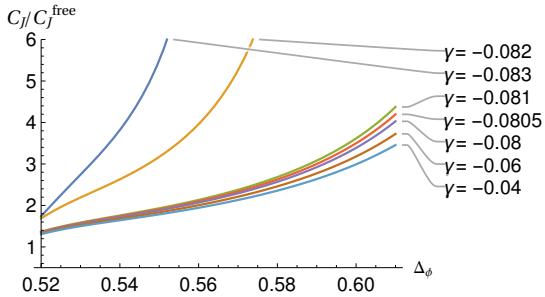

Figure 1.12: Upper bound on C_J normalized to the central charge of a free complex boson as a function of Δ_ϕ at fixed values of the parameter γ assuming $C_T \leq 0.95 C_T^{\text{free}}$. The bounds have been obtained at $\Lambda = 13$.

As mentioned earlier, in a pure scalar bootstrap setup, extracting bounds on C_J would require to isolate the current conformal block by assuming a gap on the next spin-1 operator. In the present framework, however, the isolated nature of the ϕ-conformal block in the mixed channel can be exploited to compute such a bound. Notice that a finite value of C_J implies that the scalar is indeed charged under the external current J. Despite the fact that we would like to focus on those cases, it is perfectly legitimate to have a correlation function of a conserved current associated to a $U(1)$ under which the complex scalar ϕ is neutral.[23] Thus, we do not expect an upper bound to exist without further assumptions.

In our investigations we found that assuming a small value of the central charge C_T forces a finite value of C_J. This is shown in Fig. 1.12, where we computed an upper bound on C_J as a function of Δ_ϕ for several values of γ. This is the first numerical evidence that the existence of a local stress tensor, together with a set of selection rules, implies the presence of conserved current in the scalar OPE.

[22]The fact that the bound decreases for large external dimensions is expected: if one interpret J as a topological $U(1)$ current in QED_3 and ϕ as a monopole operator then one has the asymptotic behavior [60, 65]:

$$\Delta_\phi \simeq 0.265 N_f - 0.0383 + O\left(\frac{1}{N_f}\right), \qquad \frac{C_J}{C_J^{\text{free}}} \simeq \frac{3.2423}{N_f}\left(1 - \frac{0.1423}{N_f} + O\left(\frac{1}{N_f^2}\right)\right), \tag{1.56}$$

where N_f is the number of fermions in the UV theory. Unfortunately our bound is still far from these values.

[23]The simplest case is a tensor product of a generalized free vector field and a generalized free scalar theory. Alternatively one can consider for instance the $O(4)$-vector model identify $\phi \equiv \phi_1 + i\phi_2$ and J as the generator of rotations in the 3-4 direction.

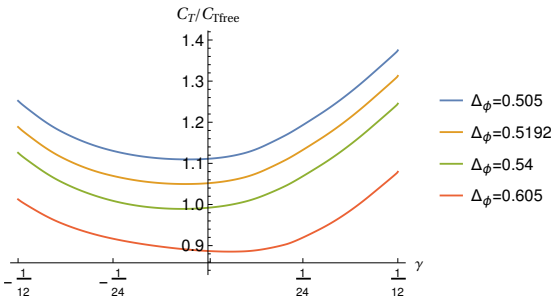

Figure 1.13: Lower bound on the central charge normalized to the central charge of a free complex boson as a function of the parameter γ at fixed values of Δ_ϕ assuming that the scalar ϕ is neutral under the symmetry generated by the current J. The bounds have been obtained at $\Lambda = 13$.

We could go one step further and ask for what values of the central charge such a bound exists. This question can also be recast as a lower bound on C_T, assuming $C_J \to \infty$. Fig. 1.13 answer precisely this question. We observe that if the central charge is below the bound for given γ and Δ_ϕ, the scalar must be charged under the external current J. Intuitively this result can be restated as: in order to have an extended symmetry, one needs enough degrees of freedom. While this statement is obvious in free theories, it interesting to show that it can be extended to interacting CFTs, although at present the bound on C_J only exists for small C_T and Δ_ϕ close to the unitarity bound.[24]

1.4 Conclusions

In this work we studied the impact of considering correlation functions involving a spin-1 conserved current and a scalar operator charged under the associated global $U(1)$. Using numerical bootstrap techniques we have explored the space of constraints. We found that only the $O(2)$ model seems to stand out, appearing as kinks in several operators bounds and as a sharp peak in the bound on the first spin-2 operator after the stress tensor. By using these features we manage to constrain several observables that are not accessible by the scalar bootstrap, such as dimensions of certain operators and three-point functions coefficients involving two currents and a third operator. In particular, we determined with some accuracy the OPE coefficient λ_{JJS}, where S is the unique relevant neutral deformation in the $O(2)$ model. This parameter controls the leading correction to the conductivity σ in the $O(2)$ model at finite temperature and high frequencies. We expressed the dependence of σ in terms of the CFT data and compared it to the QMC simulations of [52] to extract the expectation value of the operator S at finite temperature.

[24]Indeed for larger values Δ_ϕ, the bounds of Fig. 1.13 are on top of the bounds with no assumptions on C_J shown in Fig. 1.10.

Our determination agrees with the direct QMC determination and is more accurate.

We also accurately determined two more quantities, γ and the central charge C_T, appearing in the next-to-leading correction of σ. Their knowledge allowed to extract the thermal expectation value of the stress tensor from the fit of the conductivity. In order to improve the sensitivity to sub-leading corrections, the precision of the QMC simulation should be increased, with particular attention to systematic errors.
Recently a QMC study of the Gross-Neveu model was performed in [66], together with a fit of the conductivity. It would be interesting to repeat our bootstrap analysis and extract the relevant CFT-data to compare with those results.[25] In order to focus on the Gross-Neveu model one should presumably consider external fermions.

Part of the motivation of this work was to establish whether it is worthwhile to include conserved currents in the bootstrap. For certain questions we observed that the presence of the spin-1 current was not determinant. On the other hand, when scanning over parameters such as γ and θ, we observed interesting interplay of the crossing equations. To make a conclusive statement one should consider an even more complicated system and include the neutral scalar S as an external operator. That analysis, in conjunction with new algorithms to cheaply scan over the OPE parameter space [51] could represent the correct approach to deal with CFTs with global symmetries.

[25] We thank William Witczak-Krempa for bringing this work to our attention.

2 Bootstrapping the ARP^3 model using traceless symmetric $O(N)$ scalars.

Based on research done in collaboration with Maria Refinetti and Alessandro Vichi [2]. *I, the candidate, performed and analyzed the numerical computations presented in this chapter and made major contributions to all steps of the research including the study of and comparison against the relevant literature and the analytic computations leading to the numerical setup. The chapter as it appears here was written exclusively by me.*

2.1 Introduction and summary of results

The conformal bootstrap has successfully classified many 3D CFTs (see for example [35, 5, 30, 15, 67]). In most of these cases the bound on the dimension of the first singlet shows a clear kink in the immediate vicinity of the the CFT (an exception is [68]). However, some theories could be living in the interior of these bounds. Such a theory can still be found as long as it lives close to the edge of the allowed region in some other parameter space. Still, creating an island isolating the allowed dimensions of lowest dimensional relevant operators is more challenging for such a theory and requires additional assumptions to be made[1] In this chapter we aim to isolate such a theory, namely the ARP^3 model.

The ARP^3-model has $O(4)$ symmetry as well as a discrete Z_2 gauge symmetry. The effective LGW action assumes a gauge invariant order parameter transforming in the traceless symmetric representation. Previous studies of 3D CFTs with $O(N)$ symmetry

[1] One notable advantage of the singlet channel over the other channels is that the number of relevant singlet can usually easily be found from experimental realizations and/or lattice simulations. For other representation one needs to make an educated guess on the dimension of the second lowest operator in order isolate the lowest operator.

have always assumed the existence of the vector representation ϕ. However, in the LGW description of the ARP^3 model no such operator exists.

Lattice computations have shown evidence for the existence of a fixed point for this model despite the fact that LGW effective action shows no such fixed point[69]. Possible explanations could be that this gauge-invariant order parameter is not capturing the full physics near the phase transition or that the perturbative computation (a five-loop epsilon expansion [69]) of the critical value of N where two fix points merge and above which the CFT becomes complex is inaccurate. This study aims to solve this discrepancy using the conformal bootstrap.

According to lattice Monte Carlo simulations [69] the ARP^3 model has one relevant singlet scalar with a dimension, $\Delta_s = 1.28 \pm 0.13$ and the dimension of the first traceless symmetric operator is found to be $\Delta_t = 0.54 \pm 0.02$. Thus it lives deep in the interior of the one relevant singlet scalar bounds.

Hence, in order to isolate an island in the (Δ_t, Δ_s) plane we are required to make certain assumptions. These assumptions are motivated by features found in the OPE data of non-trivial representations. Most notably we observe a peak in the maximal allowed gap for the dimension of the first spin-2 singlet after the stress tensor ($\Delta_{T'}$) and kinks in the dimension of the first mixed symmetry $\{2, 2\}$, or *Box*, scalar (Δ_b) and the first anti-symmetric vector after the conserved current ($\Delta_{J'}$). All these features appear near the value of Δ_t predicted by the lattice simulations. Additionally, a small gap in the dimension of the first $\{3, 3\}$, or *Hook*, vector allows us to exclude solutions related to the $O(9)$ model.[2]

Under these assumptions we manage to isolate an island in both the (Δ_t, Δ_s) and (Δ_t, Δ_b) planes. The islands are shown in figures 2.1b and 2.1a. The islands are consistent with the lattice bounds.

The traceless symmetric operator t in the ARP^3 model is expected to be Z_2-odd due to the transformation rules of the Landau-Ginzburg-Wilson order parameter. We therefore also study the mixed t-s bootstrap where the external operator t is assumed to be Z_2-odd. This $t - s$ bootstrap setup revealed that the top part of the peak found in $\Delta_{T'}$ was not given by true solutions with one relevant singlet. Moreover, the island in figure 2.1b persists in the mixed setup at $\Lambda = 35$. Unexpectedly the mixed setup did not result in

[2]The $O(9)$ model appears due to an identification between ϕ^a and t^{ij} in the crossing equations for their respective four point functions. Under this identification the $O(9)$ theory appears to have a Hook vector with dimension $\Delta_h = 2$, i.e. at the unitarity bound. No theory with $O(4)$ symmetry is expected to have such an operator. Thus a small gap $\Delta_h > 2.05$ allows the exclusion of theories with $O(9)$ symmetry. This is explained further in section 2.3.3.

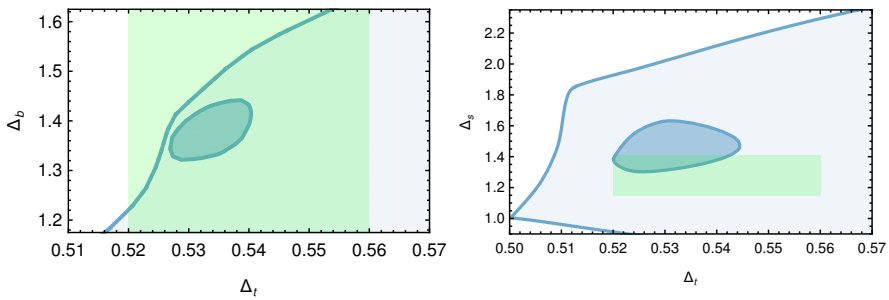

(a) (b)

Figure 2.1: On the right: Allowed region in the $(\Delta_t, \Delta_\mathrm{b})$ plane assuming $\Delta_{T'} > 4.5$, $\Delta_{J'} > 3$, $\Delta_h > 2.05$ and $\Delta_b > 2.8$. The green region shows the prediction for the ARP^3 model from lattice computations. On the right: Corresponding allowed region in the (Δ_t, Δ_s) plane (assuming $\Delta_b > 1.3$ instead of $\Delta_{b'} > 2.8$ to avoid scanning over a 3 dimensional parameter space). The bounds have been obtained at $\Lambda = 35$.

any major improvements to the bound under these assumptions.

The mixed setup does allow access to the Z_2-odd traceless symmetric representations exchanged in the $t \times s$ OPE. This allows us to isolate $\Delta_{t'_O}$ under the assumption that t' is the only relevant Z_2-odd traceless symmetric scalar besides t itself. This bound is shown in figure 2.2. The figure also includes the 3 dimensional allowed island under the same assumptions that allowed us to isolate the island in figure 2.1b. All computations in the mixed setup make use of the OPE scanning algorithm of [67]. As a side effect this allows us to estimate that $\frac{\lambda_{sss}}{\lambda_{tts}} \in (0.025, 2.5)$.[3]

Additionally we performed a systematic study of all lowest dimensional operators in the $t \times t$ OPE. This uncovered two new family of sharp kinks as a function of N in the bound on the first Box ($\{2,2\}$) scalar and Hook ($\{3,1\}$) vector, see figures 2.3a and 2.3b. Possibly these kinks are related to the phenomenon found by [70]. There kinks were found to correspond to a linear combination of 4-pt functions from different CFTs, such as $\langle \mathcal{O}\mathcal{O}\mathcal{O}\mathcal{O} \rangle_{\mathrm{GFT}} - \langle \mathcal{O}\mathcal{O}\mathcal{O}\mathcal{O} \rangle_{\mathrm{Free}}$. However, such a solution would only be available at $\Delta_t = 1$ and not for $\Delta_t < 1$.[4] The location of the kink does not seem to converge to $\Delta_t = 1$ for large N.

Moreover, we find strong evidence for solutions of crossing where the external operator t is Z_2-even (unlike in the ARP^3 model). The bound on the first traceless symmetric operator exchanged in $t \times t$ shows some slight kinks. However, when we assume that $t \times t$

[3]In our normalization $\frac{\lambda_{sss}}{\lambda_{tts}} = 1$ for the free theories at $\Delta_t = 1/2$ and $\Delta_t = 1$.

[4]Similarly a linear combination of two different GFTs such as $\langle \mathcal{O}\mathcal{O}\mathcal{O}\mathcal{O} \rangle_{\text{t-GFT}} - \langle \mathcal{O}\mathcal{O}\mathcal{O}\mathcal{O} \rangle_{\phi\text{-GFT}}$ would only be unitary starting from $\Delta_t \geq 1$.

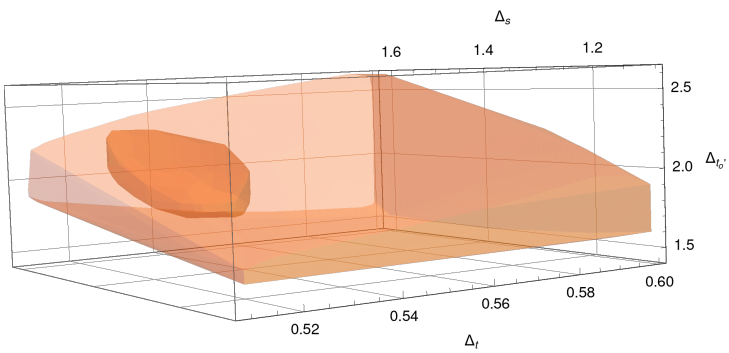

Figure 2.2: In blue: Allowed values for $\Delta_{t'_O}$ for (Δ_t, Δ_s) in the expected ARP^3 region assuming the existence of exactly one relevant singlet and exactly one additional relevant $\mathbb{Z}_2$-odd operator besides t-itself. These bounds have been obtained at $\Lambda = 19$. In orange: Allowed region under the additional assumptions $\Delta_{T'} > 4.5$, $\Delta_{J'} > 3$, $\Delta_h > 2.05$ and $\Delta_b > 1.3$. These bounds have been obtained at $\Lambda = 35$.

exchanges t-itself these kinks become very sharp. This is strong evidence that there is a real Z_2 even CFT living at that kink.[5] These bounds are shown in figures 2.3c and 2.3d. These and some additional kinks are discussed in more detail in section 2.6.

2.2 Background

2.2.1 RP^{N-1} and ARP^{N-1} model

The RP^{N-1} model is defined as a spin system with spins $\mathbf{s_x}$ taking values in the real projective space RP^{N-1}. Equivalently, we can describe the system by considering $\mathbf{s_x}$ to take values from R^N under the restrictions that $s_x \cdot s_x = 1$ and the identification $\mathbf{s_x} \sim -\mathbf{s_x}$, this last can be viewed as a $\mathbb{Z}_2$ gauge symmetry. The hamiltonian can be written as

$$H_{RP^{N-1}} = J \sum_{\langle \mathbf{x},\mathbf{y} \rangle} |\mathbf{s_x} \cdot \mathbf{s_y}|^2 \tag{2.1}$$

where $\langle \mathbf{x}, \mathbf{y} \rangle$ indicates a that the sum runs over pairs of nearest neighbors. For negative J the system is ferromagnetic while for positive J it is anti-ferromagnetic. In this chapter we will study the existence of a fixed point for the case of positive J for $N = 4$, i.e. the ARP^3-model. For this model there is lattice data available that suggest the existence of a fixed point with a traceless symmetric operator of dimension $\Delta_t = 0.54(2)$ and one relevant singlet with dimensions $\Delta_s = 1.28(13)$[71]. The existence of this fixed point is

[5]The t-GFT with the traceless symmetric operator as its fundamental field does not exchange t in the $t \times t$ OPE.

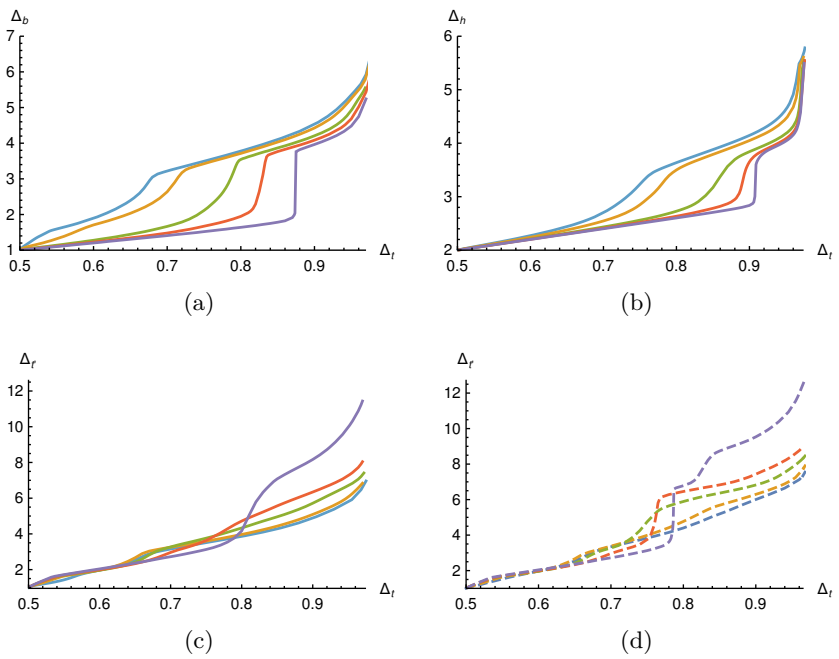

Figure 2.3: Bounds on the dimension of the first Box scalar (a), the first hook vector (b), the first traceless symmetric operator (c) and the first additional traceless symmetric operator assuming the exchange of t-itself (d). The blue, orange, green, red, purple and brown lines correspond to respectively $N = 4, 5, 10, 20, 100, 1000$. (a) and (b) show a family of kinks for all N. However, the locations (Δ_t) of the two families do not coincide. In (c) various families of kinks are visible: One corresponding to the $O(N')$ model, one in the region $0.55 < \Delta_{t'} < 0.6$, one in the region $0.6 < \Delta_{t'} < 0.75$ (this one disappears at $N = 100$), and a last one in the region $0.75 < \Delta_{t'} < 1$. The last family of kinks becomes much sharper and more pronounced under the assumption that t-itself is exchanged (d), especially for $N = 20, 100$. All bounds have been obtained at $\Lambda = 27$.

unexpected since the Landau-Ginzburg-Wilson approach of the same order parameter does not show stable fixed points.[6].

2.2.2 The Landau-Ginzburg-Wilson effective action

The Landau-Ginzburg-Wilson approach dictates that one identifies an order parameter that describes the fluctuations near criticality. The order parameter is chosen such that it vanishes in the disordered phase and is non-zero in the ordered phase. Thus, it is

[6]One unstable fixed point is given by the free Gaussian theory and another by the O(9) model. In addition there are two fixed points that merge at $N = N_c$ and turn complex for $N > N_c$. According to a five-loop epsilon expansions $N_c \approx 3.6$ [71].

expected to be small near criticality. The continuum limit of the order parameter results in a field transforming in the same representation as the order parameter. The stable critical point of the effective field theory describing this field describes the system near criticality.

Ferromagnetic Case: the energy is minimized by aligning the directions of the spins. Thus, at low energy the system breaks $O(N)$ symmetry by aligning in a preferred direction. This configuration preserves translational invariance. In the standard LGW approach one looks for a gauge invariant order parameter that is non-zero in the ordered phase and vanishes in the disordered phase. This order variable will built from the *site variable*,

$$P_x^{ab} = s_x^a s_x^b - \delta^{ab}/N \tag{2.2}$$

We then define the order parameter as its sum over lattice sites

$$M^{ab} = \sum_x P_x^{ab} \,. \tag{2.3}$$

We see that in the ordered phase the contributions to M^{ab} are cumulative, due to the prefered direction, resulting in a non-zero matrix. At high temperature, in the isotropic phase, contributions will cancel so that $\lim_{T->\infty} M^{ab} \to 0$. This order parameter transform as the traceless symmetric representation of $O(4)$. [7]

Taking the continuum limit one can define a local order parameter field Φ^{ab} in the traceless symmetric $O(N)$ representation. Since the order parameter was constructed from a gauge invariant quantity there are no further restriction due to gauge symmetry and we consider the effective hamiltonian:

$$\mathcal{H} = \mathrm{Tr}(\partial_\mu \Phi)^2 + rTr\Phi^2 + w_0\,\mathrm{Tr}(\Phi)^3 + u_0(\mathrm{Tr}(\Phi)^2)^2 + \frac{v_0}{4}\,\mathrm{Tr}\,\Phi^4 \tag{2.4}$$

For low N there are additional relations relating the various terms or equating them to 0.

Anti-ferromagnetic case: Here energy is instead minimized by taking $\mathbf{s_x} \cdot \mathbf{s_y} = \mathbf{0}$ for neighboring sites. Thus, in the ordered phase every spin is orthogonal to its nearest neighbor. Unlike anti-correlation in the usual ferromagnetic case here the two lattices are orthogonal. Orthogonality does not fix the configuration uniquely unlike correlation or anti-correlation. Thus, it is not immediately clear what the symmetries of the ordered state are and what order parameter has a non-zero expectation value in the ordered

[7] Gauge invariance forbids a linear order parameter s_x^a so the next simplest order parameter is quadratic. The vanishing of the order parameter in the disordered phase forces the subtraction of the trace resulting in the traceless symmetric representation.

phase. No comment is made on this in [71]. For the similar case of CP^N models this issue is examined in the [72]. In its appendix it was shown for $N = 3$ that the most degenerate ground state configurations are aligned in the odd or even sub-lattice. Other configurations are allowed but are less degenerate. The argument easily extends to the RP^2 case. However, the argument does not easily extend to larger N because orthogonality becomes much less constraining for larger N. Nevertheless, we expect the same is true here for the ARP^3 model and that the appropriate order parameter is constructed from a staggered site variable:

$$A_x^{ab} = p_x P_x^{ab} \tag{2.5}$$

where $p_x = \exp\left[i\pi \sum_{k=1}^{3} x_k\right]$, i.e. the parity of the lattice site. Summing over the staggered site variable the order parameter is given by

$$M^{ab} = \sum_{\mathbf{x}} A_{\mathbf{x}}^{ab} \tag{2.6}$$

The extra factor of p_x effectively changes the sign of A^{ab} on one of the sub-lattices so that terms add up constructively in the ordered phase. In the disordered phase the staggering has no effect and the order parameter still vanishes.

Summing over all sites we see that under a translation of the spins $s_i \to s_{i+1}$ the order parameter changes as

$$M^{ab} = \sum_x p_x P_x^{ab} \to \sum_x p_x P_{x+1}^{ab} = \sum_x p_{x-1} P_x^{ab} = -M^{ab} \tag{2.7}$$

where we relabeled the spins in the penultimate step[8]. This means that the order parameter is Z_2 odd under this additional symmetry (which is a symmetry of the Hamiltonian). This forbids the cubic term in the effective LGW hamiltonian for the ARP^3 model:

$$\mathcal{H} = \mathrm{Tr}(\partial_\mu \Phi)^2 + rTr\Phi^2 + u_0(\mathrm{Tr}(\Phi)^2)^2 + \frac{v_0}{4}\,\mathrm{Tr}\,\Phi^4 \tag{2.8}$$

2.2.3 Lattice evidence

In finite size scaling one uses the fact that certain RG invariant quantities R are proportional to a universal function $f_R(X)$ where $X = (\beta - \beta_c)L^{1/\nu}$ with ν the correlation

[8]Taking the continuum limit with periodic boundary conditions.

length exponent, L the lattice size, and R the thermodynamic quantity. Scanning over values of β there will be some value $\beta = \beta_c$ for which at any lattice size the RG invariant is given by $R(\beta_c) = f_R(0)$. Plotting $R(\beta, L)$ will show a crossing points where lines $R(\beta)|_L$ of different L meet. From this one can read of β_c.

This is true up to corrections of the form $t^{-y_{irr}/y_t} u_{irr}$. Here t is the reduced temperature, y_{irr} is the RG eigenvalue of the first irrelevant term (and thus negative) and y_t is the eigenvalue of the first irrelevant singlet. u_{irr} is a non-universal constant that depends on the exact UV model that was used. In the case of an irrelevant untuned singlet the total exponent is positive and the extra contribution goes to 0 exactly at $\beta = \beta_c$.

However, if there is an un-tuned relevant singlet the correction goes as $t^{-y_{\text{untuned}}/y_t} u_{irr}$. In this case the total exponent would be negative and this in-analyticity would give a major correction to the universal behavior determined by the CFT, i.e. lines of different L in the finite-size-rescaling would not meet.

In [71] the RG invariant $R_\xi = \frac{\xi}{L}$, where ξ is the correlation length, is studied using finite-size-rescaling. It is observed that lines of different L indeed meet at a critical temperature $\beta_c = 6.779(2)$. Moreover, the critical exponent $\nu = 0.59(5)$ was extracted[9]. Additionally the behavior of the susceptibility around the fixed point is studied in order to extract the critical exponent $\eta = 0.08(4)$. Finally, a study of the Binder parameter shows sizable corrections due to scaling possibly indicating an un-tuned singlet with a dimension that is close to relevant. However, the data was insufficient to give a reliable estimate on the corresponding critical exponent.

This results in the following estimates for the CFT data:

$$\Delta_s = 1.28 \pm 0.13\,,\ \Delta_t = 0.54 \pm 0.02\,,\ \Delta_{s'} > 3 \tag{2.9}$$

2.3 Setup

In this section we explain the bootstrap setup of the $\langle tttt \rangle$ correlator and its extension to the mixed $t - s$ bootstrap. We first discuss the operators that can be exchanged in the $t \times t$ OPE. We then explain how to write the crossing equations and the resulting sum rules for the single $\langle tttt \rangle$ correlator. Next we discuss a map relating the traceless symmetric bootstrap of $O(N)$ to the vector bootstrap of $O(N')$ with $N' = N(N+1)/2-1$. Finally we present the extension to the mixed $t - s$ bootstrap.

[9] The error is due to different methods of fitting the data. The statistical error is much smaller.

2.3.1 The $t \times t$ OPE

We can write the $t \times t$ OPE as

$$t_{\square\square} \times t_{\square\square} = \sum_{\Delta,l} \lambda^{S}_{\Delta,l} S + \lambda^{T^2}_{\Delta,l} T^2_{\square\square} + \lambda^{T^4}_{\Delta,l} T^4_{\square\square\square\square} + \lambda^{A^2}_{\Delta,l} A^2_{\begin{smallmatrix}\square\\\square\end{smallmatrix}}$$
$$+ \lambda^{H}_{\Delta,l} H_{\begin{smallmatrix}\square\square\square\\\square\end{smallmatrix}} + + \lambda^{B}_{\Delta,l} B_{\begin{smallmatrix}\square\square\\\square\square\end{smallmatrix}} \tag{2.10}$$

Here S, T^2, T^4, A^2 refer respectively to the singlet, traceless symmetric, four-index symmetric and the anti-symmetric representations. H refers to the mixed symmetry $\{3,1\}$ representation which we will call the Hook representation, while B refers to the $\{2,2\}$ representation or Box representation. In the rest of the chapter we will leave out the young tableau notation and refer to a dimension Δ and spin l operator as $R_{\Delta,l}$, where $R \in \{S, T^2, T^4, A^2, H, B\}$.[10]

Important special cases of operators are the first anti-symmetric vector, i.e. the conserved current $J = A^2_{2,1}$, the first spin-two singlet, i.e. the stress tensor $T = S_{3,2}$. The first anti-symmetric vector after the current will be denoted J' and the first spin-2 singlet after the stress tensor T'. Furthermore, we will refer to the first singlet scalar as s and the external traceless symmetric scalar as t. Again higher dimensional operators will be referred to by adding primes. For example s' refers to the second lowest dimensional singlet operator. t' will denote the first traceless symmetric operator other than t-itself. Further on when describing the t-s mixed setup the external operator t will be assumed to be odd under an additional Z_2 symmetry. When necessary Z_2-even traceless symmetric operators, i.e. those appearing in the $t \times t$ OPE, will be differentiated from Z_2-odd operators, i.e. those appearing in the $t \times s$ OPE by the additional labels E or O. Similarly the first scalar in the Box representation and the first vector in the Hook representation will be denote by b and h respectively.

Under exchange of x_1 and x_2 the spatial part of the three point function $\langle t(x_1) t_2(x_2) O_3(x_3) \rangle$ goes to $(-1)^L$ times itself. Thus, for even spin the global tensor structure must be symmetric under the exchange of the indices of the first and second operator and for odd spin anti-symmetric. The $\{S, T^2, T^4, B\}$ representations only allow a symmetric structure while the A and H representations only allow an anti-symmetric tensor structure. Thus, the first set of representations will be exchanged for even spin and the second set for odd spin.

[10] One can find which irreps are exchanged in the $t \times t$ OPE by checking that $\square\square \otimes \square\square \otimes R$ contains a singlet, meaning that the OPE coefficients $\lambda_{tt\mathcal{O}_R}$ is allowed to be non-zero by symmetry. Equivalently, one can simply decompose $\square\square \otimes \square\square$. All irreps appearing in that decomposition must contain a singlet in the $\square\square \otimes \square\square \otimes R$ decomposition.

Two OPE coefficients are of special interest. Ward identities relate the OPE coefficients of stress tensor T and the conserved current J respectively to the central charges C_J and C_T:

$$\frac{C_{J_{\text{free}}}}{C_J} = \lambda_{ttJ}^2 \tag{2.11}$$

$$\frac{C_{T_{\text{free}}}}{C_T} = \frac{\lambda_{ttT}^2}{\Delta_t^2} = \frac{\lambda_{ssT}^2}{\Delta_s^2} \tag{2.12}$$

Our approach to finding all allowed O(N) tensor structures for the 3pt and 4pt functions is to write the most general tensor structure obeying the appropriate permutation symmetries using the indexless notation described in [25] to keep track of symmetrized indices. The young tableaux describing the $O(N)$ irreps illustrate how indices corresponding to blocks appearing in the same row are symmetrized while blocks appearing in the same column are anti-symmetrized. The symmetrization of any row can automatically be enforced by contracting all indices corresponding to the same row with the same polarization vector Z. Similarly, indices corresponding to the next row are contracted with U and so on (in this thesis no irreps with more than two rows appear). One then only needs to enforce the anti-symmetry and tracelessness by hand. For tensor with symmetrized indices this notation in terms of polarization vectors is much more compact and useful than using the full index structure.

For example, imposing tracelessness and permutation symmetry we find the allowed tensor structure for $\langle tt\mathcal{O}_B\rangle$,

$$\langle tt\mathcal{O}_B\rangle = \lambda_{ttB}\left(U_3\cdot Z_1 Z_2\cdot Z_3 - U_3\cdot Z_2 Z_1\cdot Z_3\right)^2 . \tag{2.13}$$

All other 3pt tensor structures can be found in the same way. By contracting the indices of an exchanged operator in two 3pt functions, i.e. $\langle ttO^{\alpha\cdots}\rangle\langle O_{\alpha\ldots}tt\rangle$, we can find the invariant subspace of a 4pt function corresponding to the exchange of that irrep allowind the decomposition of the 4pt-function into the contributions from different irreps.[11]

2.3.2 4pt functions and the crossing equations

The crossing equations are obtained in the standard way by equating the s-channel and t-channel decompositions of the 4pt-function. The 4pt-function $\langle tttt\rangle$ has six independent

[11] The sign of the projector gets fixed by imposing reflection positivity on the correlators in mirror symmetric configurations, see for example section III.E.1 in [47].

tensor structures each providing a crossing equation of the form

$$\sum_{R,\mathcal{O}_R} \lambda_{12\mathcal{O}_R}\lambda_{34\mathcal{O}_R} \frac{g^{\Delta_{12},\Delta_{34}}_{\Delta_{\mathcal{O}_R},\ell_{\mathcal{O}_R}}(z,\bar{z})}{(z\bar{z})^{\frac{\Delta_1+\Delta_2}{2}}} = \sum_{R',\mathcal{O}'_{R'}} \lambda_{32\mathcal{O}'}\lambda_{14\mathcal{O}'_{R'}} \frac{g^{\Delta_{32},\Delta_{14}}_{\Delta_{\mathcal{O}'_{R'}},\ell_{\mathcal{O}'_{R'}}}(1-z,1-\bar{z})}{((1-z)(1-\bar{z}))^{\frac{\Delta_3+\Delta_2}{2}}} . \tag{2.14}$$

Here z and $\bar{z}$ are the standard crossing ratios and g is the scalar conformal block. For the single correlator (of identical operators) both R and R' run over $\{S, T^2, T^4, A^2, H, B\}$ and $\Delta_{ij} = 0\,\forall\, i,j$.

The final crossing equations for $\langle tttt\rangle$ can be written as

$$\begin{aligned}\sum_{\mathcal{O}}\lambda^2_{\mathcal{O}}V_{S,\Delta,\ell} + \sum_{\mathcal{O}}\lambda^2_{\mathcal{O}}V_{T^2,\Delta,\ell} + \sum_{\mathcal{O}}\lambda^2_{\mathcal{O}}V_{T^4,\Delta,\ell} + \\ \sum_{\mathcal{O}}\lambda^2_{\mathcal{O}}V_{B,\Delta,\ell} + \sum_{\mathcal{O}}\lambda^2_{\mathcal{O}}V_{A,\Delta,\ell} + \sum_{\mathcal{O}}\lambda^2_{\mathcal{O}}V_{H,\Delta,\ell} = 0_{1\times 6},\end{aligned}$$

where $V_{R,\Delta,\ell}$ is a 6 dimensional vector describing the contribution of a primary operator $\mathcal{O}$ of dimension Δ, spin ℓ, and representation R. The vector $V_{R,\Delta,\ell}$ is expressed in terms of the usual F's and H's

$$\begin{aligned}H =& u^{\frac{1}{2}(\Delta_2+\Delta_3)} g^{\Delta_{12},\Delta_{34}}_{\Delta,\ell}(v,u) + v^{\frac{1}{2}(\Delta_2+\Delta_3)} g^{\Delta_{12},\Delta_{34}}_{\Delta,\ell}(u,v),\\ F =& v^{\frac{1}{2}(\Delta_2+\Delta_3)} g^{\Delta_{12},\Delta_{34}}_{\Delta,\ell}(u,v) - u^{\frac{1}{2}(\Delta_2+\Delta_3)} g^{\Delta_{12},\Delta_{34}}_{\Delta,\ell}(v,u)\end{aligned} \tag{2.15}$$

Here $g^{\Delta_{12},\Delta_{34}}$ is the scalar conformal block normalized as entry 1 of Table I in [47]. In this section the only correlation under consideration is $\langle tttt\rangle$ and this simplifies to

$$\begin{aligned}H =& u^{\Delta_t} g_{\Delta,\ell}(v,u) + v^{\Delta_t} g_{\Delta,\ell}(u,v),\\ F =& v^{\Delta_t} g_{\Delta,\ell}(u,v) - u^{\Delta_t} g_{\Delta,\ell}(v,u)\end{aligned} \tag{2.16}$$

The crossing equations can also be represented by a 6 by 6 matrix. Its explicit form is[12]

$$M_{\langle tttt\rangle,O(N)} = \begin{pmatrix} F & 0 & 0 & 0 & \frac{1}{2}F(n+4)(n-1) & -Fn \\ 0 & F & 0 & 0 & \frac{1}{2}F(n-2) & -\frac{Fn}{2} \\ 0 & 0 & -F & 0 & \frac{1}{2}F(n+4) & -\frac{1}{2}F(n+2) \\ 0 & 0 & 0 & F & -3F & 2F \\ H & 0 & -\frac{2H(n-1)}{n} & -\frac{H(n+4)(n+6)(n-1)}{12n} & -\frac{H(n+4)(n-2)(n-1)}{4n} & -\frac{H(n+2)(n-3)(n-2)}{6n} \\ 0 & H & -\frac{H(n+4)(n-2)}{n(n+2)} & -\frac{H(n+6)(n-2)}{3n} & \frac{H(n+4)(n-2)}{n(n+2)} & \frac{H(n+4)(n-3)}{3n} \end{pmatrix} \tag{2.17}$$

Here rows correspond to the six different equations and columns correspond to the vectors $\{V_S, V_{T^2}, V_A, V_{T^4}, V_H, V_B\}$ in equation 2.15. The bootstrap problem consists of finding a positive linear functional α such that

$$\begin{cases} \alpha(V_{\mathbb{I}}) = 1 \\ \alpha(V_R) \geq 0 \qquad \forall R \in \{S, T^2, T^4, A^2, H, B\}, \quad \forall \Delta_{R,\Delta,\ell} > \Delta^*_{R,\Delta,\ell} \end{cases} \tag{2.18}$$

If such a functional exists it excludes a spectrum with $\Delta_{R,\Delta,\ell} > \Delta^*_{R,\ell}$. $\Delta^*_{R,\Delta,\ell}$ is usually taken to be the unitarity bound except when we try to find the maximal allowed gap for a certain operator or when we have reason to assume a gap above the unitarity bound for a theory that we are trying to isolate.

In practice the crossing equations are truncated by taking derivatives around the crossing symmetric point $z = \bar{z} = 1/2$ and the maximal number of derivatives is denoted by Λ. These truncated crossing equations are used as input in the arbitrary precision semi-definite programming solver SDPB (version 2) [13, 14]. The computations were managed using Simpleboot [73].

In addition to finding the feasible set of $\Delta_{R,\Delta,\ell}$ we can also find lower and upper bounds on squared OPE coefficients λ^2_{ttO} by picking the corresponding vector V_λ to define the normalization of α, i.e. $\alpha(V_\lambda) = \pm 1$ and maximizing the objective $\alpha(V_{\mathbb{I}})$.[13]

2.3.3 Relationships between the traceless symmetric $O(N)$ bootstrap and the $O(N(N+1)/2-1)$ vector bootstrap.

When bootstrapping the system of equations for a $O(N)$ traceless symmetric operator the bounds on the dimension of the first singlet scalar are actually dominated by solutions

[12] The exact form depends on the normalization of the OPE coefficients. We are free to rescale columns by any positive factor and absorb this into the OPE coefficients. We are of course also free to rescale rows, i.e. equations, by any factor.

[13] Normalizing $\alpha(V_\lambda) = 1$ will give us an upper bound while $\alpha(V_\lambda) = -1$ will give a lower bound on the OPE coefficient.

related to $O(N')$ symmetry where $N' = N(N+1)/2 - 1$. The reason is that crossing equations for an $O(N')$ vector are related to those of an $O(N)$ traceless symmetric operator by an identification where the vector ϕ^a gets rewritten as ϕ^{ij} where $a \in \{0, ..., N'\}$ and $i, j \in \{0, ..., N\}$. The $\phi \times \phi$ OPE exchanges operators in the singlet (S), traceless symmetric (T) and antisymmetric (A) representations.[14] Any solution to the $O(N')$ vector bootstrap equations also solves the $O(N)$ traceless symmetric bootstrap equation (giving a solution with $\Delta_{T^2} = \Delta_{T^4} = \Delta_B = \Delta_T$ and $\Delta_{A^2} = \Delta_H = \Delta_A$).

Seen from the dual problem, one can show that there exist a positive linear map T from any functional that is positive on the vectors $\{V_S, V_T, V_A\}$ to a positive functional on the vectors $\{V_S, V_{T^2}, V_{T^4}, V_{A^2}, V_H, V_B\}$. The resulting functional has the following (guaranteed) domain of positivity depending on the positivity properties of the original functional:

$$SO(N') : \alpha_v \to SO(N) : \beta_t \qquad\qquad SO(N) : \beta_t \to SO(N') : \alpha_v$$

$$\Delta_R^* \geq \begin{cases} \Delta_S^* & R = S \\ \Delta_T^* & R \in \{T^2, T^4, B\} \\ \Delta_A^* & R \in \{A, H\} \end{cases} \qquad \Delta_R^* \geq \begin{cases} \Delta_S^* & R = S \\ \max(\Delta_{T^2}^*, \Delta_{T^4}^*, \Delta_B^*) & R = T \\ \max(\Delta_A^*, \Delta_H^*) & R = A \end{cases} \tag{2.19}$$

Here Δ_R^* indicates the minimum of the domain of positivity, i.e. $\alpha(V_R) > 0 \, \forall \, \Delta \in [\Delta_R^*, \infty)$.

A similar argument was recently made for the correspondence between the crossing equations of the $SU(N) \times SU(N)$ bi-fundamental and that of an $O(2N)$ vector in [74].

Theorem: *Given a set of functionals α_a with $a \in \{1, ..., 3\}$ which are positive on respectively the three crossing equations of the $O(N)$-vector system, a set of positive functionals β_i on the six bootstrap equations of the $O(N)$ traceless symmetric irrep can be found using positive linear map T such that $\beta_j = \alpha_i T_{ij}$.*

Proof: The O(N)-vector equations can be written as

$$\sum_O \lambda_O^2 V_{S,\Delta,\ell} + \sum_O \lambda_O^2 V_{T,\Delta,\ell} + \sum_O \lambda_O^2 V_{A,\Delta,\ell} = 0_{1\times 6}, \tag{2.20}$$

[14] In this section T stands for the traceless symmetric representation appearing in the $\phi \times \phi$ OPE. We leave out the superscript in order to differentiate it from the traceless symmetric operators appearing in the $t \times t$ OPE. The same holds for the usage of A versus A^2.

or in matrix form as

$$M_{\langle vvvv\rangle,SO(N')} = \begin{pmatrix} 0 & F & -F \\ F & \left(1-\frac{1}{N'}\right)F & F \\ H & -\left(\frac{1}{N'}+1\right)H & -H \end{pmatrix} = 0, \tag{2.21}$$

where the rows correspond to the three different equations and the columns correspond to the vectors V_S, V_T and V_A.

The problem of positive semi-definiteness of the bootstrap equation (after taking out the term corresponding to the unit operator) can be written as finding α_i such that

$$(\alpha_S\ \alpha_T\ \alpha_A) \equiv (\alpha_1\ \alpha_2\ \alpha_3)\cdot M_{\langle vvvv\rangle,SO(N')} \geq 0, \quad \forall \Delta_{R,\ell} > \Delta^*_{R,\ell} \tag{2.22}$$

We will show the existence of T_{ij} such that $\beta_j = \alpha_i T_{ij}$ and

$$(\alpha_S\ \alpha_{T^2}\ \alpha_{T^4}\ \alpha_{A^2}\ \alpha_H\ \alpha_B) \equiv (\beta_1\ \beta_2\ \beta_3\ \beta_4\ \beta_5\ \beta_6)\cdot M_{\langle tttt\rangle,SO(N)} \geq 0, \quad \forall \Delta_{R',\ell} > \Delta^*_{R',\ell} \tag{2.23}$$

Decomposing the the irrep contributions $\{V_S, V_T, V_A\}$, according to the contributions to $\{V_S, V_{T^2}, V_{T^4}, V_A, V_H, V_{Box}\}$, one finds the following branching rules[15]:

$$\langle vvvv\rangle \text{ of } SO(N') \qquad\qquad \langle tttt\rangle \text{ of } SO(N)$$

$$S \longleftrightarrow V_S, \tag{2.24}$$

$$T \longleftrightarrow V_{T^2} + V_{T^4} + V_B, \tag{2.25}$$

$$A \longleftrightarrow V_A + V_H. \tag{2.26}$$

This motivates us to restrict our search to a map T such that

$$(\beta_S\ \beta_{T^2}\ \beta_{T^4}\ \beta_{A^2}\ \beta_H\ \beta_B) = (\alpha_S\ x_1\alpha_T\ x_2\alpha_T\ x_4\alpha_A\ x_5\alpha_A\ x_3\alpha_T)\,. \tag{2.27}$$

In other words we assume that the map T relates the vectors $\beta_{R'}$ to α_R through $\beta_{R'} = \alpha_R \tilde{T}^R{}_{R'}$ with

$$\tilde{T} = \begin{pmatrix} 1 & 0 & 0 & 0 & 0 & 0 \\ 0 & x_1 & 0 & x_2 & 0 & x_3 \\ 0 & 0 & x_4 & 0 & x_5 & 0 \end{pmatrix}. \tag{2.28}$$

For this ansatz to hold the related linear transformation T between α_i's and β_i's has to be of the form

$$T = \tilde{T}\cdot M^{-1}_{\langle tttt\rangle,O(N)} \tag{2.29}$$

[15] It is essential that $N' = \frac{N(N+1)-2}{2}$ for other N' the branching of T would also contain a singlet.

By imposing that the F and H equations do not mix we can fix the values x_i and find a unique map T (up to an overall constant). The x_i in this map are given by[16]

$$\vec{x} = \frac{1}{n+n^2-4}\left(\frac{\left((n+n^2)-2\right)^2}{n^2+n+2} \quad \frac{n(n+1)(n+2)(n+6)(n-1)^2}{12\left(n^2+n+2\right)} \right.$$
$$\left. \frac{n(n+1)(n+2)^2(n-3)(n-1)}{6\left(n^2+n+2\right)} \quad n(n-1) \quad \frac{1}{4}(n+1)(n+4)(n-2)(n-1)\right) \tag{2.31}$$

The important thing to note is that these x_i are positive for $n > 3$. Thus, any functional $\vec{\alpha}$ such that $(\alpha_S \ \alpha_T \ \alpha_A) \succcurlyeq 0$ guarantees that $(\beta_S \ \beta_{T^2} \ \beta_{T^4} \ \beta_{A^2} \ \beta_H \ \beta_B) \succcurlyeq 0$ since these are given by a positive coefficient times α_S, α_T or α_A. To be precise β_S is guaranteed to be positive for $\Delta > \Delta_S$ while β_{T^2}, β_{T^4} and β_B are guaranteed to be positive for $\Delta > \Delta_T$ and β_{A^2} and β_H for $\Delta > \Delta_A$. (Positivity on this domain is guaranteed, but the functional can be positive on a bigger domain.)

Similarly an inverse map T' can be found which provides a functional that is positive on $\{V_S, V_T, V_A\}$ from functionals positive on $\{V_S, V_{T^2}, V_{T^4}, V_A, V_H, V_{Box}\}$. In this case we look for a T' such that

$$(\alpha_S \ \alpha_T \ \alpha_A) = (\beta_S \quad x_1\beta_{T^2} + x_2\beta_{T^4} + x_3\beta_B \quad x_4\beta_{A^2} + x_5\beta_H)\,. \tag{2.32}$$

Again we find a unique solution for T' and the parameters x_i

$$x_i = \frac{4}{(n+n^2)-2} \quad i = 1,2,3,4,5. \tag{2.33}$$

Here we see that $\alpha_S \succcurlyeq 0$ is guaranteed when $\beta \succcurlyeq 0$, $\alpha_T \succcurlyeq 0$ is guaranteed to be positive on the domain where each of β_{T^2}, β_{T^4} and β_B are positive, i.e. $\Delta \geq \max(\Delta^*_{T^2}, \Delta^*_{T^4}, \Delta^*_B)$ and $\alpha_A \succcurlyeq 0$ is guaranteed to be positive if $\Delta \geq \min(\Delta^*_{A^2}, \Delta^*_H)$. The functional may be positive on a bigger domain. Thus, the (guaranteed) domains of positivity under the mappings T and T' are as described in equation 2.19.

This means that the bootstrap equations of the $O(N)$ traceless symmetric scalar will gives the same bounds as the bootstrap of the vector equations of $O(N')$ as long as we

[16]The explicit form of T in our normalization is given by

$$T = \begin{pmatrix} 0 & \frac{\left((n+n^2)-2\right)^2}{\left(n^2+n+2\right)\left((n+n^2)-4\right)} & \frac{n(n-1)}{(n+n^2)-4} & \frac{n(n+1)(n+2)(n+6)(n-1)^2}{12\left(n^2+n+2\right)\left((n+n^2)-4\right)} & 0 & 0 \\ 1 & \frac{\left(12-8n+2n^3+n^4\right)-7n^2}{\left(n^2+n+2\right)\left((n+n^2)-4\right)} & -\frac{n(n-1)}{(n+n^2)-4} & \frac{n(n+1)(n+3)(n+6)(n-2)(n-1)}{12\left(n^2+n+2\right)\left((n+n^2)-4\right)} & 0 & 0 \\ 0 & 0 & 0 & 0 & 1 & \frac{(2-n)-n^2}{(n+n^2)-4} \end{pmatrix}. \tag{2.30}$$

assume positivity of the form $\Delta_{A^*} = \Delta_{H^*}$ and $\Delta_{T^{2*}} = \Delta_{T^{4*}} = \Delta_{B^*}$. However, stronger bounds can be found in the traceless symmetric bootstrap when we impose a different domain of positivity, i.e. different Δ_{O^*} for these operators.

2.3.4 Setup of mixed $t - s$ bootstrap

The operator t is expected to be Z_2-odd under a discrete (ungauged) $\mathbb{Z}_2$ symmetry. Indeed we saw that the order parameter appearing in the Landau-Ginzburg-Wilson effective theory and the lattice simulations is odd under the exchange of the parity-odd and parity-even lattice sites[17].Therefore one should consider the mixed bootstrap of a Z_2-odd traceless symmetric operator t_O. In that case the full system of crossing equations is given by the crossing equations of the correlators $\langle ttss\rangle$ and $\langle stts\rangle$, $\langle tsts\rangle$, and $\langle ssss\rangle$. Crossing equations involving three t_O-operators trivially vanish because $t_O \times s$ can only exchange $\mathbb{Z}_2$ odd operators while $t \times t$ can only exchange $\mathbb{Z}_2$ even operators. All new correlators are constrained to exchange only a single irrep: $s \times s$ can only exchange neutral operators while $t \times s$ can only exchange operators in the T^2 irrep. The $t \times s$ OPE does not have the permutation symmetry that the $t \times t$ OPE had and thus allows the exchange of both odd and ever spin traceless symmetric operators.

Note that when we do not impose a gap forbidding the exchange of the external operator t in $t \times t$ results in this section also hold for $\mathbb{Z}_2$-even t.

Restricting to the crossing equations for Z_2-odd t_O there are four additional crossing equations, two between $\langle sstt\rangle$ and $\langle tsst\rangle$, one from $\langle tsts\rangle$ and one from $\langle ssss\rangle$. The crossing equations can now be written as

$$\sum_{\mathcal{O}}(\lambda_{tt\mathcal{O}} \quad \lambda_{ss\mathcal{O}})V_{S,\Delta,\ell}\begin{pmatrix}\lambda_{tt\mathcal{O}}\\ \lambda_{ss\mathcal{O}}\end{pmatrix} + \sum_{\mathcal{O}}\lambda^2_{tt\mathcal{O}^+}V_{T^2,+,\Delta,\ell} + \sum_{\mathcal{O}^+}\lambda^2_{ts\mathcal{O}^-}V_{T^2,-,\Delta,\ell} + \sum_{\mathcal{O}}\lambda^2_{\mathcal{O}}V_{T^4,\Delta,\ell} +$$
$$\sum_{\mathcal{O}}\lambda^2_{tt\mathcal{O}}V_{B,\Delta,\ell} + \sum_{\mathcal{O}}\lambda^2_{tt\mathcal{O}}V_{A,\Delta,\ell} + \sum_{\mathcal{O}}\lambda^2_{tt\mathcal{O}}V_{H,\Delta,\ell} + (\lambda_{tts} \quad \lambda_{sss})V_{\text{ext.}}\begin{pmatrix}\lambda_{tts}\\ \lambda_{sss}\end{pmatrix} = 0_{1\times 10},$$

Here we have chosen to separate out the contributions proportional to the OPE coefficients of the external vector into a separate vector $V_{ext.}$. Since the A, T^4, H and B representations cannot be exchanged in the new correlators the vectors V_A, V_{T^4}, V_H, V_B remain unaffected (apart from padding them with an appropriate number of zeros at the end). The entries of V_S become matrices since there are now contributions proportional to λ^2_{ttS}, $\lambda_{ttS}\lambda_{ssS}$ and λ^2_{ssS}. Furthermore, we split the traceless symmetric contribution into a Z_2 even part coming from the $t \times t$ OPE and a Z_2 odd part coming from $t \times s$ OPE.

[17]This exchange is a translation by one lattice site and is thus a symmetry of the Hamiltonian

The Z_2 even part remains identical to the vector V_{T^2} in equation 2.17. The $t \times s$ OPE exchanges traceless symmetric operators of both odd and even spin. The new vectors V_S, $V_{T^2,O}$ and $V_{\text{ext.}}$ are given by

$$V_S = \begin{pmatrix} \frac{1}{2}\left((n+n^2)-2\right)\mathcal{F}_{11}{}^{\Delta_{tt}\Delta_{tt}} \\ \mathbf{0} \\ \mathbf{0} \\ \mathbf{0} \\ \frac{1}{2}\left((n+n^2)-2\right)\mathcal{H}_{11}{}^{\Delta_{tt}\Delta_{tt}} \\ \mathbf{0} \\ \mathbf{0} \\ -\frac{1}{2}\mathcal{H}_{12}{}^{\Delta_{ss}\Delta_{ss}} \\ \frac{1}{2}\mathcal{F}_{12}{}^{\Delta_{ss}\Delta_{ss}} \\ \mathcal{F}_{22}{}^{\Delta_{ss}\Delta_{ss}} \end{pmatrix}, V_{\text{ext.}} = \begin{pmatrix} \frac{1}{2}\left((n+n^2)-2\right)\mathcal{F}_{11}{}^{\Delta_{tt}\Delta_{tt}} \\ \mathbf{0} \\ \mathbf{0} \\ \mathbf{0} \\ \frac{1}{2}\left((n+n^2)-2\right)\mathcal{H}_{11}{}^{\Delta_{tt}\Delta_{tt}} \\ \mathbf{0} \\ \mathcal{F}_{11}{}^{\Delta_{ts}\Delta_{ts}} \\ \mathcal{H}_{11}{}^{\Delta_{ts}\Delta_{ts}} - \frac{1}{2}\mathcal{H}_{12}{}^{\Delta_{ss}\Delta_{ss}} \\ \mathcal{F}_{11}{}^{\Delta_{ts}\Delta_{ts}} + \frac{1}{2}\mathcal{F}_{12}{}^{\Delta_{ss}\Delta_{ss}} \\ \mathcal{F}_{22}{}^{\Delta_{ss}\Delta_{ss}} \end{pmatrix}, V_{T^2,O} = \begin{pmatrix} 0 \\ 0 \\ 0 \\ 0 \\ 0 \\ 0 \\ \mathcal{F}^{\Delta_{ts}\Delta_{ts}} \\ (-1)^L\mathcal{H}^{\Delta_{ts}\Delta_{ts}} \\ (-1)^L\mathcal{F}^{\Delta_{ts}\Delta_{ts}} \\ 0 \end{pmatrix} \tag{2.34}$$

where we defined the matrices

$$\begin{aligned} (\mathcal{F}_{ij}^{\Delta_1,\Delta_2})_{mn} &= \begin{cases} F^{\Delta_1,\Delta_2} & (i=n \wedge j=m) \vee (i=m \wedge j=n) \\ 0 & \text{else} \end{cases} \\ (\mathcal{F}_{ij}^{\Delta_1,\Delta_2})_{mn} &= \begin{cases} H^{\Delta_1,\Delta_2} & (i=n \wedge j=m) \vee (i=m \wedge j=n) \\ 0 & \text{else.} \end{cases} \end{aligned} \tag{2.35}$$

Finally, let us comment that the mixed $t-s$ setup does not break the map between the $O(N')$ vector bootstrap and the $O(N)$ traceless symmetric bootstrap and the same positivity relations in equation 2.19 still hold.

2.4 Single correlator results

We will first discuss the bounds on operator-dimensions in the region where the ARP^3 is expected to live, followed by a similar discussion about bounds on the OPE coefficients λ_{ttT}, λ_{ttJ} and λ_{ttt}. Next we will focus on isolating the ARP^3 model using a set of reasonable assumptions.

Our goal is to isolate an island in the OPE data corresponding to the ARP^3 model (or alternatively to exclude the existence of a plausible theory in the region predicted by lattice computations). Lattice computations find a fixed point with a traceless symmetric scalar with a dimension $\Delta_t = 0.54 \pm 0.02$ and exactly one relevant singlet with dimension 1.28 ± 0.13 [71].

Unlike the Ising and $O(N)$ models for which precision islands have been previously obtained [35, 5, 30, 15, 67] the ARP^3 does not live close to the kink of the singlet bound. Instead it lives well within the allowed region, see figure 2.4. As a consequence the theory is not easily isolated without making appropriate assumptions on the spectrum. However, we will see that bounds on other representations will have features such as kinks and bumps indicating the presence of a theory living close to those extrema. These features will motivate some reasonable assumptions under which isolated islands can be found in the OPE data among others in the (Δ_t, Δ_s) plane.

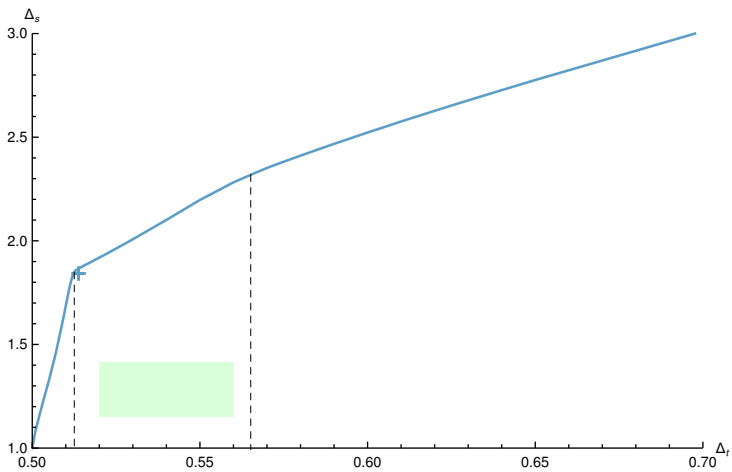

Figure 2.4: Bound on the dimension of the first singlet scalar. The black dashed lines indicate the positions of two kinks. The blue cross indicates the position of the O(9) model (as seen from the traceless symmetric bootstrap under the identification $v^a \to v^{ij}$) [68]. The green region shows the prediction for the ARP^3 model from lattice computations. The bounds have been obtained at $\Lambda = 27$.

2.4.1 Bounds on operator dimensions and OPE coefficients

Physical theories often stand out due to the presence of a large gap above known conserved operators [1, 42]. If we demand positivity on the stress tensor T and maximize the gap $\Delta_{T'}$ until the next spin-2 neutral operator we find a sharp peak as is shown in figure 2.5 (these bounds match those of the $O(N')$ vector bootstrap under the same assumption). The peak coincides with the lattice expectations for the location of the ARP^3 model. On the other hand a high value of $\Delta_{T'}$ is also expected close by due to the O(9) model at $\Delta_t \approx 0.519$.

Similarly the bound on $\Delta_{J'}$, the dimension of the first spin-1 anti-symmetric vector after the conserved current, shows a clear feature within the region of interest. The kink in figure 2.6 hints at the existence of a theory with a high gap $\Delta_{J'}$ in the region

$0.52 < \Delta_t < 0.535$.

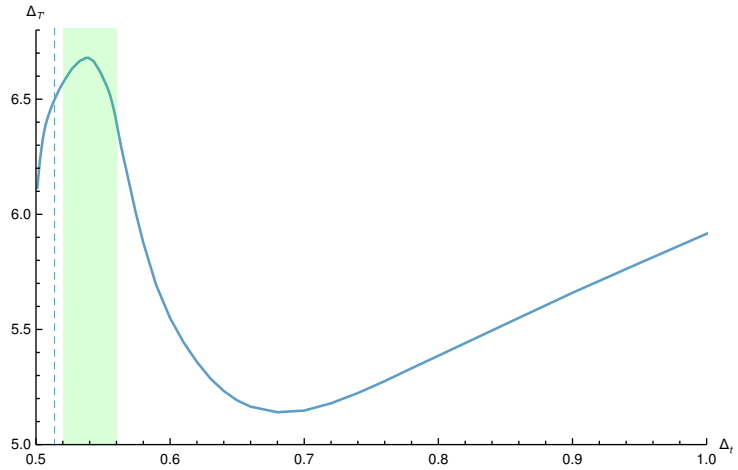

Figure 2.5: Bound on the dimension of the first spin-2 singlet after the stress tensor. The blue dashed line indicates the large N estimate of Δ_ϕ for the $O(9)$ model. The green region shows the prediction for the ARP^3 model from lattice computations. The bounds have been obtained at $\Lambda = 27$.

Next we consider a bound on Δ_{b} , the dimension of the first scalar Box operator. This bound shows two kinks within the expected lattice region. This is shown in figure 2.7.

In the ARP^3 model the lowest dimensional traceless symmetric operator t is expected to be $\mathbb{Z}_2$-odd thus forbidding the exchange of t itself in the $t \times t$ OPE. Thus, we should ask what the maximal allowed gap $\Delta_{t'}$ is. On the other hand, theories without a symmetry forbidding this exchange are expected to exchange t itself as the first traceless symmetric operator. In that case we can assume the exchange of t itself and bound the next traceless symmetric operator t' by demanding positivity on $\Delta_t \cup [\Delta^*_{t'}, \infty)$. Both bounds are shown in figure 2.8. The first bound shows no special features in the region of interest. The second shows two kinks in the ARP^3 region. Also in the ARP^3 region the second bound is higher than the bound without this assumption. The two lines rejoin at a third kink outside the expected ARP^3 region (before separating again).

Finally for the sake of completion we show the bounds on the four-index symmetric scalar and the first Hook vector in figures 2.9a and 2.9b respectively. Neither of these bounds show any clear feature in the ARP^3 region.

We can also find lower and upper bounds on the OPE coefficients squared. An upper bound can be found for the OPE of any operator while a lower bounds can only be found if the operator is disconnected from other similar operators by a gap. We are mainly interested in the separable OPEs of the conserved operators T and J. As usual the

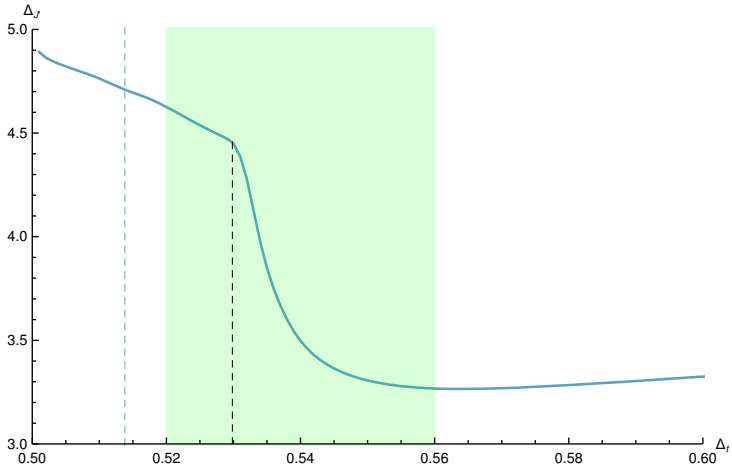

Figure 2.6: Bound on the dimension of the first spin-1 antisymmetric vector after the conserved current. The blue dashed line indicates the large N estimate of Δ_ϕ for the $O(9)$ model. The green region shows the prediction for the ARP^3 model from lattice computations. We see a clear kink within this region indicated by a black dashed line. In addition various small kinks or wobbles appear in the region $0.51 < \Delta_t < 0.52$ though not in correspondence with large N estimate of the location of the $O(9)$ model The bounds have been obtained at $\Lambda = 27$.

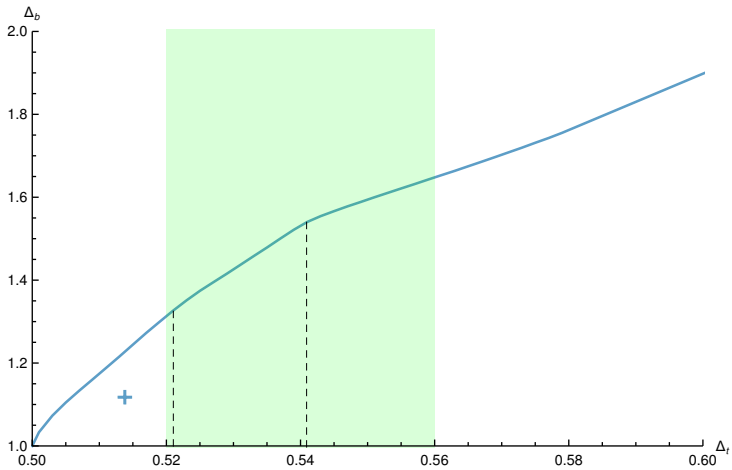

Figure 2.7: Bound on the dimension of the first scalar Box operator. The blue cross indicates the position of the O(9) model. The green region shows the prediction for the ARP^3 model from lattice computations. There are two kinks in this region indicated here by black dashed lines. The bounds have been obtained at $\Lambda = 27$. .

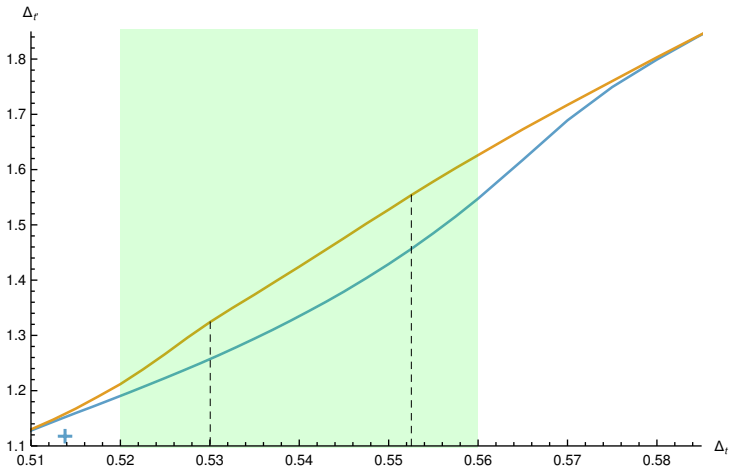

Figure 2.8: The blue line shows the bound on the dimension of the first traceless symmetric operator exchanged in the $t \times t$ OPE. The orange line shows the bound on the dimension of the first additional traceless symmetric operator t' when assuming the exchange of t itself. The green region shows the prediction for the ARP^3 model from lattice computations. In the ARP^3 region allowing the exchange of t itself lifts (weakens) the bound. This higher bound shows two kinks indicated by black dashed lines. The two lines join again at a third kink outside the expected ARP^3 region. The bounds have been obtained at $\Lambda = 27$.

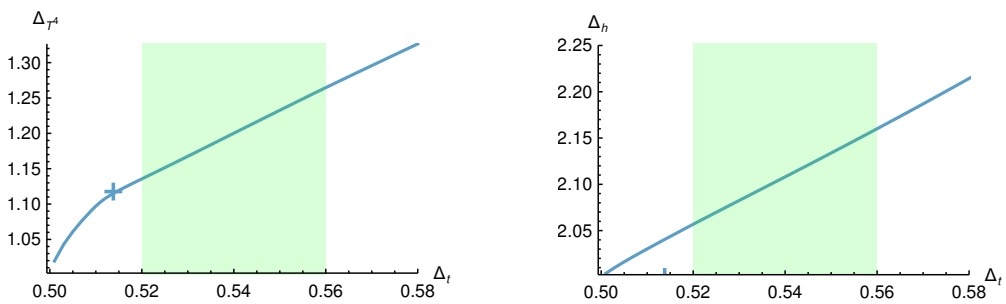

(a) (b)

Figure 2.9: On the left: Bound on the dimension of the first four-index symmetric tensor. The blue cross indicates the large N estimate of the position of the $O(9)$ model. Note that the estimate is excluded by these bounds, indicating an error due to higher order corrections and/or non-perturbative effects. On the right: The same plot but for the bound on the dimension of the first Hook vector. The green region shows the prediction for the ARP^3 model from lattice computations. Neither figure shows any features in this region. The bounds have been obtained at $\Lambda = 27$.

bounds on both of these OPE coefficients gets weaker for larger values of the external dimension. The λ_{ttT} bound shows no clear features but the λ_{ttJ} shows a kink around $\Delta_T = 0.535$. The value of the OPE found depends on the normalization of the conformal blocks (or equivalently the choice of normalization of the three and two point function) and thus it is often preferable to present the normalization invariant quantities of central charges divided by the value of the central charge in the free theory using the same normalizations. The resulting lower bounds on $C_T/C_{T_{\text{free}}}$ and $C_J/C_{J_{\text{free}}}$ are shown in figures 2.10a 2.10b.

Kinks are more clear in the OPE coefficient itself than in its reciprocal thus we also show the upper bound on λ_{ttT} and λ_{ttT} in figure 2.11. In addition that figure includes the upper bound on the λ_{ttt} OPE coefficient. The extremal spectra, obtained using the extremal functional method (EFM) [75]) at these maximal OPE values are included in appendix B.1.

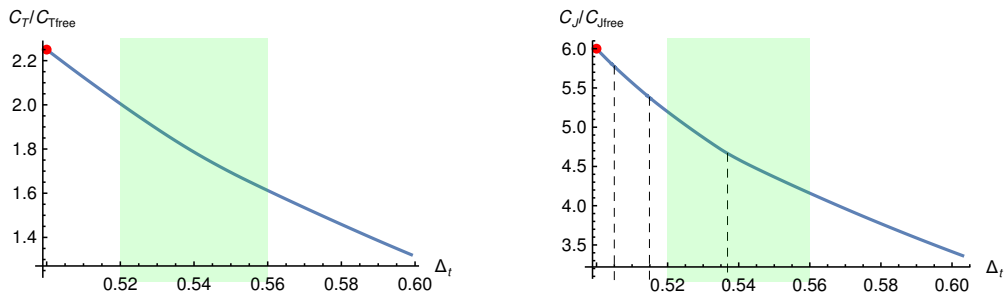

(a) (b)

Figure 2.10: (a): Lower bound on C_T in units of $C^{N=4}_{T_{\text{free}}}$. (b) Lower bound on C_J in units of $C^{N=4}_{J_{\text{free}}}$. The Dashed lines indicate the locations of kinks in the upper bound on λ_{ttJ}. The red dots indicate the central charge values in the $N = 9$ free vector boson theory. All bounds have been obtained at $\Lambda = 27$.

In the next section we will try isolating island in the (Δ_t, Δ_s) and (Δ_t, Δ_b) planes using various assumptions. But before we increase the dimensionality of the parameter space of our search it is smart to see how various assumptions influence the bisection bounds above.

For example, the Box operator shows one very strong kink in the regions allowed by the lattice bounds. However, by repeating that bound under the assumptions $\Delta_{T'} > 5.5$ and $\Delta'_J > 3$, we can see that simultaneously having both a high values near the top of the peak seen in figure 2.5 and high value near the plateau in figure 2.6 is incompatible with Δ_{b} taking a value close to this kink. This is shown in figure 2.12a. This is the first indication that perhaps the assumptions $\Delta_{T'} > 5.5$ and $\Delta_{J'} > 3$ are too strong. We will

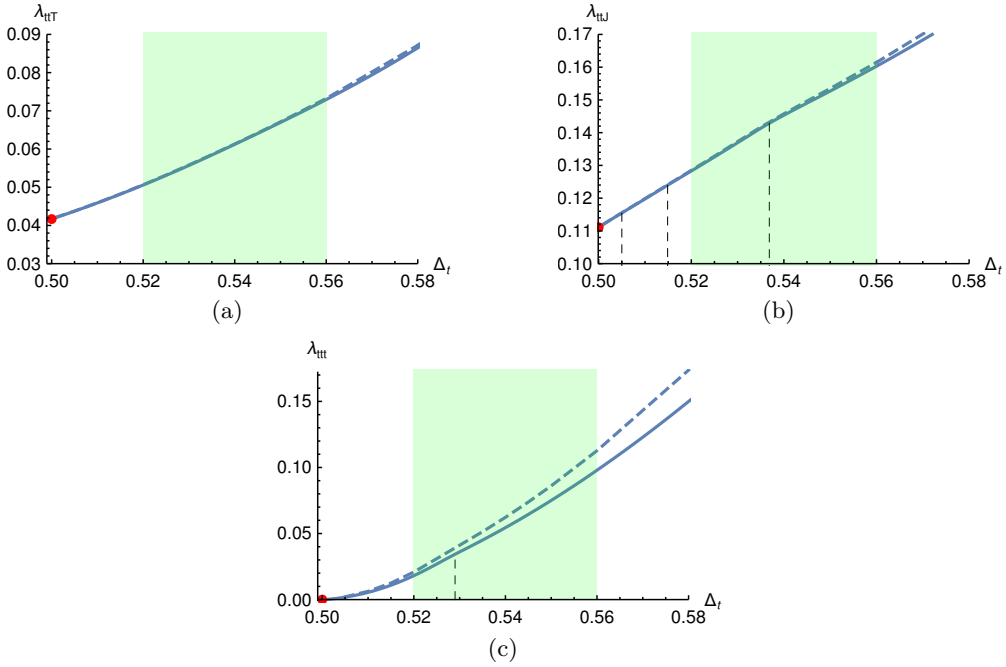

Figure 2.11: (a): Upper bound on λ_{ttT}. This bound shows no special features; (b) Upper bound on λ_{ttJ}. There are kinks at $\Delta_t \approx 0.505, 0.515$ and 0.53685; (c) Upper bound on λ_{ttt} there is one kink at $\Delta_t \approx 0.529$. The red dots indicate the OPE values in the $N = 9$ free vector boson theory. All bounds have been obtained at $\Lambda = 27$.

see more evidence for this later on. We can also consider how assumptions on $\Delta_{T'}$, Δ_h and Δ_{b} influence the maximal allowed gap $\Delta_{J'}$. An example of this is shown in figure 2.12b. This can be useful to already find the allowed Δ_t range under those assumptions in order to better locate any possible island in the larger spaces (Δ_t, Δ_s) and $(\Delta_t, \Delta_{\mathrm{b}})$.

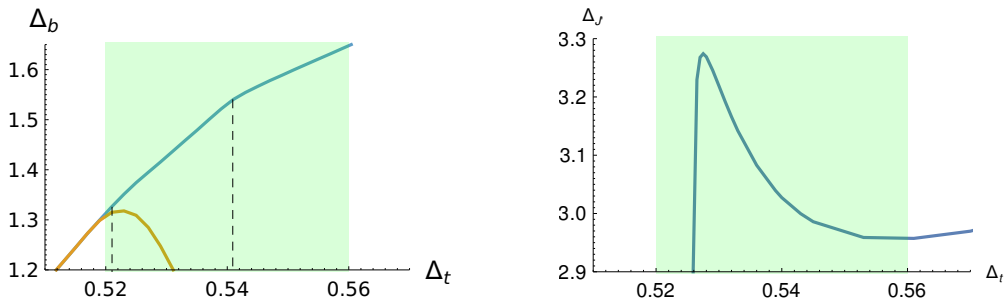

(a) (b)

Figure 2.12: On the left: Bound on the dimension of the first scalar Box operator. The blue line shows the bound under no assumptions while the orange line is found under the assumptions $\Delta_{T'} > 5.5$ and $\Delta_{J'} > 3$. The orange line shows a maximum close to the position of the first kink of the blue line. The green region shows the prediction for the ARP^3 model from lattice computations. This bound has been obtained at $\Lambda = 35$. On the right: The bound on the first anti-symmetric spin-1 operator after the conserved current assuming $\Delta_{T'} > 4.5$, $\Delta_{J'} > 3$, $\Delta_h > 3$ and $\Delta_{\mathrm{b}} > 1.37$. This bound has been obtained at $\Lambda = 35$.

2.4.2 Isolating the ARP^3 model

In order to isolate the ARP^3 theory we will have to make certain assumptions. The simplest assumption to add is the isolation of the first singlet by assuming $\Delta_{s'} > 3$. This assumptions has strong evidence from the lattice simulations. However, we will see this is not enough to isolate the ARP^3 theory. In addition we can make some reasonable assumptions based on the fact that real theories usually have well isolated conserved operators. This motivates us to make assumptions on the gaps $\Delta_{T'}$ and $\Delta_{J'}$. Additionally, it is very useful to consider the effect of a small gap on the dimension of the first hook vector Δ_h to remove solutions related to symmetries with $O(N')$ symmetry. The map from the bootstrap of the $O(N')$-vector to the bootstrap of the traceless symmetric of $O(N')$ decomposes the conserved current of $O(N')$ into both the conserved current of $O(N)$ and a conserved operator in the Hook representation. Since no O(N) symmetric theory is expected to have such a conserved current it should be safe to assume a small gap Δ_h for the dimension of this operator. This will help weed out solutions with $O(N')$ symmetry instead of $O(N)$ symmetry.

A one relevant singlet island

We now attempt to find an island in the (Δ_t,Δ_s) plane. The region allowed under the assumption of the existence of exactly one relevant singlet is shown in figure 2.13a. The main features are controlled by the O(9) free theory and the O(9) model. In addition there is a small appendix around $\Delta_s = \Delta_t = 0.58$. Upon investigation at higher lambda this feature moves and becomes more of an isolated peninsula. This is shown in figure 2.13b. The feature seems to be unrelated to the ARP^3 model or any theory with one relevant singlet, as the mixed $t - s$ bootstrap described in the next section will exclude the whole region $\Delta_s < 1$ under the same assumptions of the existence of exactly one relevant singlet. Thus, either it corresponds to a theory with multiple relevant singlet scalars or, perhaps more likely, it is just some coincidental feature[18].

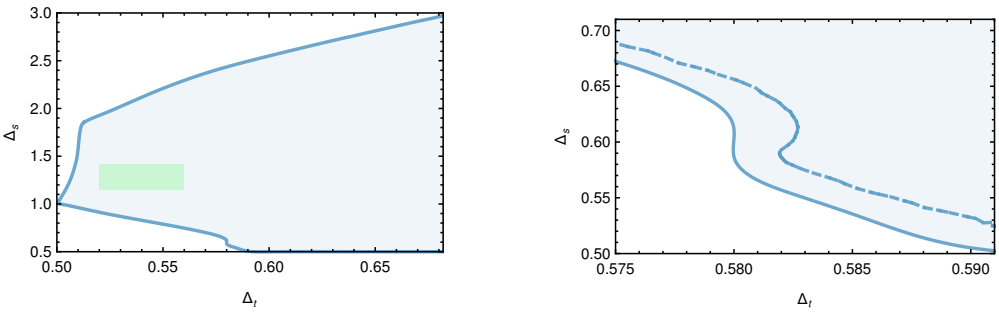

(a) (b)

Figure 2.13: On the left: Allowed region in the (Δ_t, Δ_t) plane assuming the existence of exactly one relevant singlet. The green region shows the prediction for the ARP^3 model from lattice computations. Three features stand out. The free theory can be found at the sharp corner of the peninsula near the unitarity bound. Another corner is controlled by the O(9) model. Lastly a small appendix can be seen around $\Delta_s = \Delta_t = 0.58$. The bounds have been obtained at $\Lambda = 19$. On the right: Zoom of the small appendix on the bottom. As Λ is increased the appendix moves to the right. The bounds have been obtained at $\Lambda = 19$ (solid) and $\Lambda = 27$ (dashed).

In figure 2.5 we saw a strong peak in the allowed value of $\Delta_{T'}$ indicating the existence of an interesting solution to crossing. In figure 2.14a we explore what region in the (Δ_t,Δ_s) plane the peak corresponds to. We notice that the peak is centered in the expected ARP^3 region. We can also add the assumptions that the first anti-symmetric vector after the conserved current has a dimension larger than 3, i.e. assume that $\Delta_{J'}$ takes a value somewhere in the raised plateau in figure 2.6. This assumptions restricts the island

[18]Possibly something special happens at $\Delta_s = \Delta_t$. For example, the decomposition of the contribution to $\langle vvvv \rangle$ from the traceless symmetric T^2 of $O(\bar{N})$ with $\bar{N} \neq \frac{n(n+1)-2}{2}$ will appear to have an additional singlet with $\Delta_s = \Delta_{T^2}$ when viewed from the $O(N)$ traceless symmetric bootstrap. So only when $\Delta_t = \Delta_{T^2} = \Delta_s$ could such a $O(N')$ theory appear to have exactly one relevant singlet.

further and is compatible with the expected ARP^3 region, see figure 2.14b.

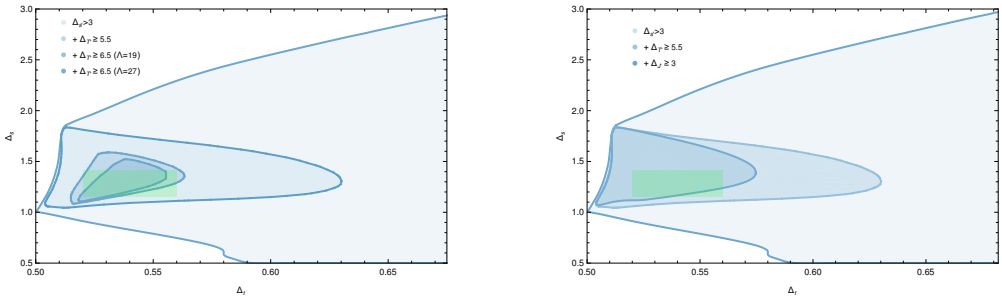

(a) (b)

Figure 2.14: On the left: Allowed region in the (Δ_t, Δ_s) plane assuming the existence of exactly one relevant singlet and $\Delta_{T'} > 5.5, 6.5$. The peak is clearly centered around the expected ARP^3 region. The bounds have been obtained at $\Lambda = 19, 27$ as indicated in the legend. On the right: Allowed region in the (Δ_t, Δ_s) plane assuming the existence of exactly one relevant singlet and the gaps $\Delta_{T'} > 5.5$ and $\Delta_{J'} > 3$. Allowed regions under the lesser assumptions of one relevant singlet and the gap $\Delta_{T'} > 5.5$ are included for reference as described in the legend.

For the sake of completion we can investigate the existence of an island where the external t is given by a Z_2 even operator where t itself is exchanged in the $t \times t$ OPE. Such a solution to the crossing equation is less likely to be a fake solution to crossing but it is also less likely to correspond to the ARP^3 CFT since t is expected to be $\mathbb{Z}_2$-odd. In order to impose the exchange of t we impose that the dimension of the first traceless symmetric operator after t has a dimension $\Delta_{t'}$ greater than would be allowed without the exchange of t itself, i.e. above the blue line shown in figure 2.8. This imposes the exchange of $t \times t$ but, this assumption also disallows theories exchanging Δ_t and an additional operator with $\Delta_{t'}$ both below the bound shown in figure 2.8. The resulting island is shown in 2.15. The persistence of the island means that we cannot exclude it corresponding to a theory where t is Z_2 even.

We saw that assumptions on the gaps $\Delta_{T'}$ and $\Delta_{J'}$ could be valuable to single out physical theories. However, for our search for the ARP^3 model we also have to exclude the influence of the O(9) model and the free theory with O(9) symmetry. For this it is useful to put assume a small gap on the fist Hook vector dimension Δ_h. Due to the identification $\phi^a = t^{ij}$ and the resulting reorganization of operators these theories effectively have $\Delta_h = \Delta_J = 2$. Thus even a small gap above the unitarity bound can exclude these. Furthermore, no theory where the symmetry group really is $O(4)$ is expected to have a conserved Hook vector. Thus, this assumptions should be safe to make. If we assume, for example, that $\Delta_h > 2.03$ the peninsula clearly detaches from

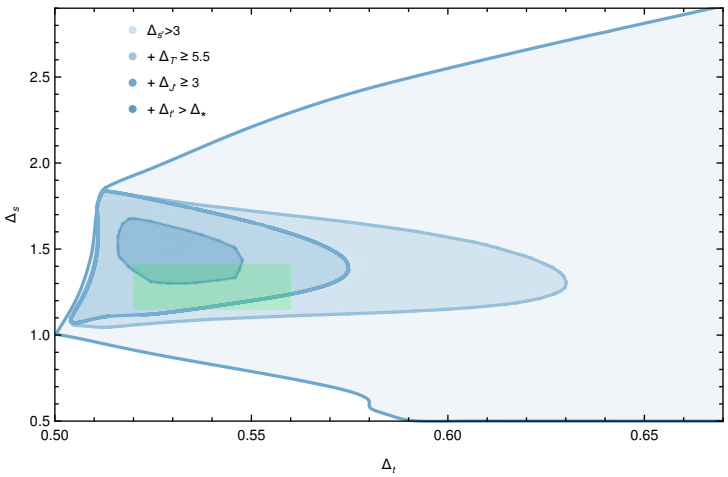

Figure 2.15: Allowed region in the (Δ_t, Δ_s) plane assuming the existence of exactly one relevant singlet and successively more constraining assumptions as described in the legend. The assumptions $\Delta_{t'} > \Delta_*$ means that we allow the exchange of t itself but assume a gap $\Delta_{t'} > \Delta_*(\Delta_t)$ where $\Delta_*(\Delta_t)$ is the value of the upper bound found on $\Delta_{t'}$ without any additional assumptions(see figure 2.8). This assumption excludes all theories where t itself is not exchanged (and hence should exclude the ARP^3 model. The green region shows the prediction for the ARP^3 model from lattice computations. The bounds have been obtained at $\Lambda = 19$. .

those theories with O(9) symmetry, as can be seen in figure 2.16. Adding the same gap to the $\Delta_{T'} > 5.5$ and $\Delta_{J'} > 3$ constraints gives a predictable intersection of the allowed regions under those two sets of assumptions as is shown in 2.17.

Finally, we should investigate the influence of assumptions on the box operator on the one relevant singlet island. Assumptions just on the Box operator do not greatly affect the island, but combined with the assumptions $\Delta_{T'} > 5.5$, $\Delta_{J'} > 3$ the island shrinks significantly [19]. This is shown in figure 2.18.

A one relevant Box scalar Island

A key feature found in the bisection bounds of the previous section were two kinks in the allowed gap in the dimension of the first Box scalar. This motivates us to investigate the existence of a theory with one relevant box operator and to isolate an island in the $(\Delta_t, \Delta_\mathrm{b})$ plane.

[19] It is really the combination of the gap $\Delta_{J'} > 3$ and $\Delta_\mathrm{b} > 1$ that is more selective. The island found under the assumptions $\Delta_{T'} > 5.5$ and $\Delta_\mathrm{b} > 1$ is the same as the one found using only $\Delta_{T'} > 5.5$.

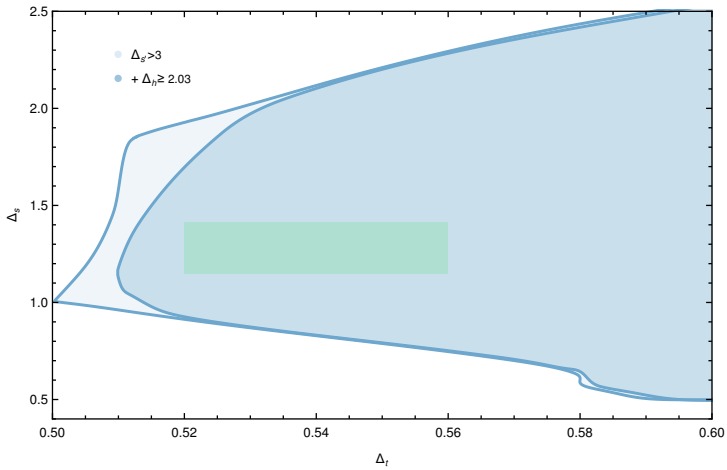

Figure 2.16: Allowed region in the (Δ_t, Δ_s) plane assuming the existence of exactly one relevant singlet and $\Delta_h > 2.03$. The green region shows the prediction for the ARP^3 model from lattice computations. The bounds have been obtained at $\Lambda = 19$.

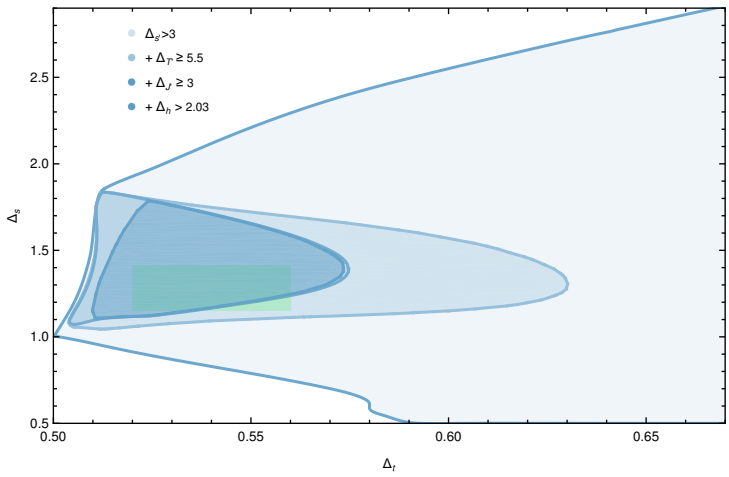

Figure 2.17: Allowed region in the (Δ_t, Δ_s) plane assuming the existence of exactly one relevant singlet and $\Delta_{T'} > 5.5$, $\Delta_{J'} > 3$ and $\Delta_h > 2.03$. The green region shows the prediction for the ARP^3 model from lattice computations. The bounds have been obtained at $\Lambda = 19$.

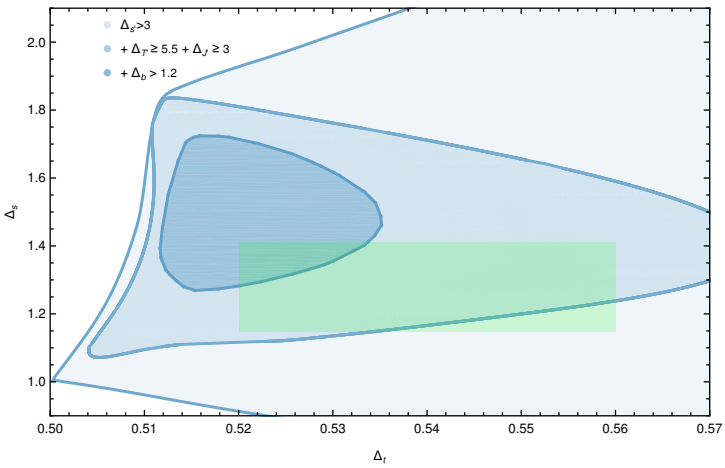

Figure 2.18: Allowed region in the (Δ_t, Δ_s) plane assuming the existence of exactly one relevant singlet and $\Delta_{T'} > 5.5$, $\Delta_{J'} > 3$ and $\Delta_{\mathrm{b}} > 1.2$. The green region shows the prediction for the ARP^3 model from lattice computations. The bounds have been obtained at $\Lambda = 19$. .

To start, assuming only the existence of exactly one relevant Box scalar we find the peninsula depicted in figure 2.19.

We can ask again what area the elevated regions of $\Delta_{T'}$ and $\Delta_{J'}$ correspond to but now in the $(\Delta_t, \Delta_{\mathrm{b}})$ plane. For example under the assumptions $\Delta_{T'} > 5.5$, $\Delta_{J'} > 3$ the one relevant Box scalar island shrinks to an island located around $\Delta_{\mathrm{b}} \approx 1$. This is shown in figure 2.20a. Since part of the shape of the resulting island is controlled by both the free theory and the O(9) theory it is useful to assume a small gap on the dimension of the Hook vector. Assuming $\Delta_h > 2.05$ results in a small island that mostly lies within the expected lattice bounds. See figure 2.20b.

However, this island is suspicious for various reasons. Firstly, the value of $\Delta_{\mathrm{b}} \approx 1$ is far from the values it takes at the kinks in figure 2.7 and is close to one, its value in the O(9) free theory. Moreover, at $\Lambda = 27$, under the same assumptions, the island gets excluded. Finally, in the next section we will see that in the mixed t-s setup such a high $\Delta_{T'}$ gap as assumed here is excluded for values of Δ_t and Δ_s close to their expected lattice value.

Thus, let us consider the allowed region in the $(\Delta_t, \Delta_{\mathrm{b}})$ plane under some more conservative assumptions. Under the assumptions $\Delta_{T'} > 4.5$, $\Delta_{J'} > 3$, $\Delta_h > 2.05$ and $\Delta_{b'} > 3$ the peninsula splits into an upper and a lower part. As we increase Λ an isolated island separates from the upper peninsula. This is shown in figure 2.21a. Moreover, the tip of the lower peninsula is the area where the highest gap $\Delta_{T'}$ is allowed while the isolated island corresponds to a second slightly lower peak in $\Delta_{T'}$. This can be seen from the

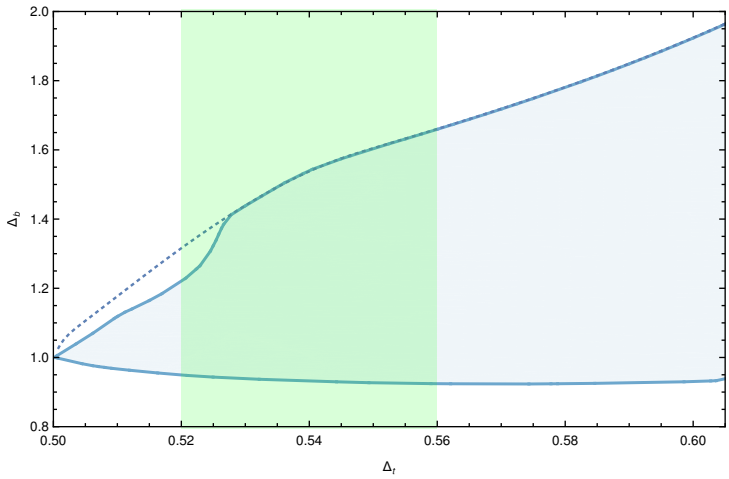

Figure 2.19: Allowed region in the $(\Delta_t, \Delta_\mathrm{b})$ plane assuming the existence of exactly one relevant Box scalar. The green region shows the prediction for the ARP^3 model from lattice computations. The blue dotted lines showes the bound on the maximal allowed gap on the dimension of the first Box scalar for reference. The bounds have been obtained at $\Lambda = 19$.

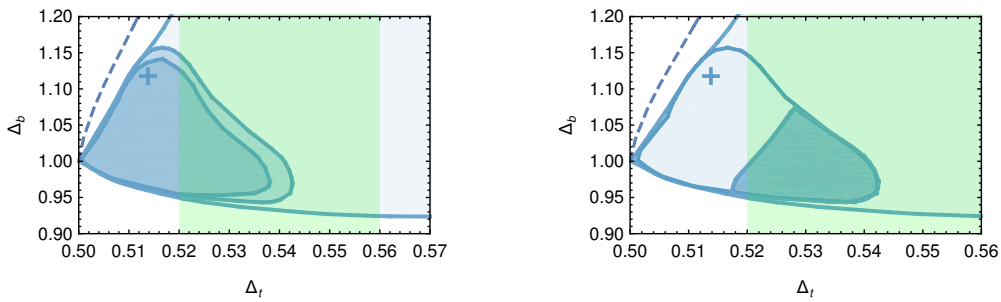

(a) (b)

Figure 2.20: On the left: Allowed region in the $(\Delta_t, \Delta_\mathrm{b})$ plane assuming the existence of exactly one relevant Box scalar and $\Delta_{T'} > 5.5$, $\Delta_{J'} > 3$. The green region shows the prediction for the ARP^3 model from lattice computations. The blue cross indicates the large N estimate of the position of the $O(9)$ model. The bounds have been obtained at $\Lambda = 19$ and $\Lambda = 27$. On the right: The same bound under the additional assumption that $\Delta_h > 2.05$ the theories with O(9) symmetry are clearly excluded by this assumption. The bound has been obtained at $\Lambda = 19$.

bounds shown in figure 2.21b where we made increasingly stronger assumptions on $\Delta_{T'}$.

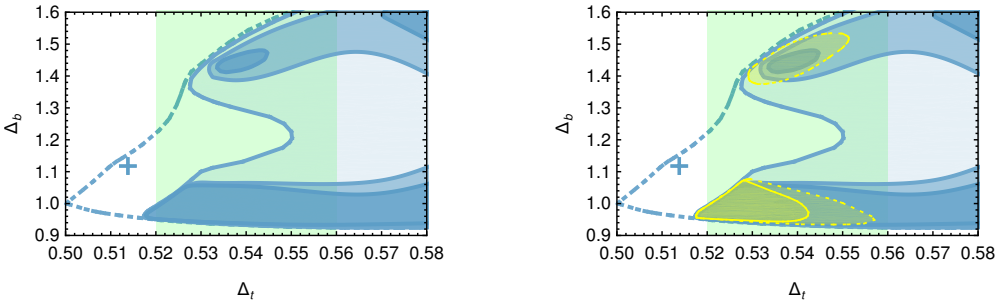

(a) (b)

Figure 2.21: On the left: Allowed region in the $(\Delta_t, \Delta_\mathrm{b})$ plane assuming the existence of exactly one relevant Box scalar and $\Delta_{T'} > 4.5$, $\Delta_{J'} > 3$ and $\Delta_h > 2.05$. The green region shows the prediction for the ARP^3 model from lattice computations. The bounds have been obtained at $\Lambda = 19, 27, 31$ (light to dark). On the right: In yellow, the same bound under the stronger assumptions that $\Delta_{T'} > 5$ (dashed) and $\Delta_{T'} > 5.5$ (solid, also shown in 2.20b). These bounds have been obtained at $\Lambda = 19$.

The island shown in figure 2.21a persists at $\Lambda = 31$ but unfortunately at $\Lambda = 35$ no primal points could be found. We suspect that one of our assumptions was again too strong. We found that if instead of $\Delta_{B'} > 3$ we demand $\Delta_{B'} > 2.8$ we find an isolated island that survives at $\Lambda = 35$. This island is shown in figure 2.22a. We can then ask what island in the (Δ_t, Δ_s) plane this island corresponds too. In order to avoid an expensive 3 dimensional scan we simply search for the allowed region under the constraints $\Delta_{T'} > 4.5$, $\Delta_{J'} > 3$, $\Delta_h > 2.05$ and $\Delta_b > 1.3$. The resulting island is shown in figure 2.22b.

2.5 Results mixed t-s bootstrap

In the mixed t-s bootstrap we always have to scan over both Δ_t and Δ_s. In order to find more than the sum of the parts it is useful to enforce mixing through the assumption of the existence of exactly one relevant singlet (equal to the dimension Δ_s of the external operator). One advantage of this setup is that it allows us to easily exclude the free theory since $\langle ssss \rangle$ exchanges multiple relevant singlets (this does not exclude the O(9) model where only one singlet is exchanged in $\langle ssss \rangle$). Making only this assumption we already find a sizeable reduction in the allowed (Δ_t, Δ_s) plane, while leaving the expected ARP^3 region intact.

Additional mixing can be enforced by explicitly contracting the external vector with a vector $\{\lambda_{tts}, \lambda_{sss}\}$. Positivity of the resulting contraction is all that is required for

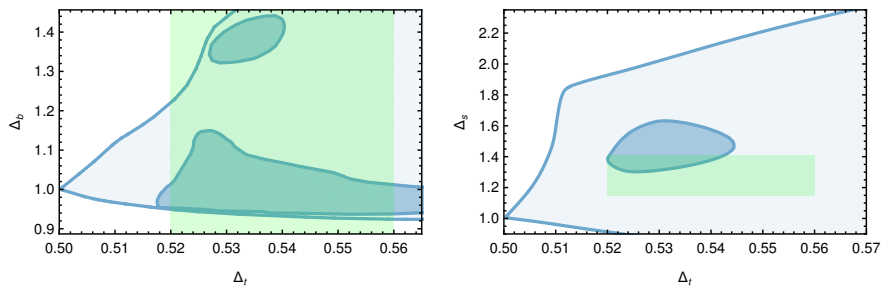

(a) (b)

Figure 2.22: On the right: Allowed region in the $(\Delta_t, \Delta_\mathrm{b})$ plane assuming $\Delta_{T'} > 4.5$, $\Delta_{J'} > 3$, $\Delta_h > 2.05$ and $\Delta_{B'} > 2.8$. The green region shows the prediction for the ARP^3 model from lattice computations. On the right: Corresponding allowed region in the (Δ_t, Δ_s) plane (assuming $\Delta_b > 1.3$ instead of $\Delta_{b'} > 2.8$ to avoid scanning over a 3 dimensional parameter space). The bounds have been obtained at $\Lambda = 35$.

the consistency of the CFT and this is a lesser requirement on the functional then semi-definite positiveness of the initial matrix. Thus, this allows us to exclude more at the cost of scanning over an additional parameter. This OPE scan was performed using the OPE scanning algorithm of Simpleboot [73]. Simpleboot efficiently takes advantage of the occurrences of both dual and primal jumps and the ability to hotstart SDPB from related points as well as the ability to exclude additional regions in the OPE space by solving a quadratic equation for the roots of the functional applied to the external vector contracted with generic ope coefficients, i.e. solving $\alpha(\{1, x\} \cdot V_\mathrm{ext} \cdot \{1, x\}) > 0$ for x.[20]

The assumption of the existence of exactly one relevant singlet is firmly backed up by the lattice data so this already rigorously shows the minor constraint that $\Delta_s > 1.052$ for the ARP^3 model.

Unfortunately additional assumptions will now have to be made. Further, mixing can be enforced by assuming a gap $\Delta_{T'}$ above the stress tensor. The ward identity $\lambda_{OOT} = \frac{\Delta_O}{\sqrt{C_T}}$ then enforces the $\langle tttt \rangle$ and $\langle ssss \rangle$ to mix. This is very effective, greatly improving the equivalent single correlator bounds. Bounds corresponding to various assumptions on the gap $\Delta_{T'}$ are shown in figure 2.24. We find that the peak in $\Delta_{T'}$ that we found earlier (see figure 2.14a) was given by a fake solution since it disappeared by the addition of additional bootstrap equations (without making any additional assumptions). The new peak is no longer located in the expected ARP^3 region and is instead located at a much higher value of Δ_s and lies closer to the O(9) model. Notably, the assumption $\Delta_{T'} > 5.5$

[20] We assumed $\lambda_{sss} \in \{-5000\lambda_{tts}, 5000\lambda_{tts}\}$. For example for the free theory $\lambda_{tts} = \lambda_{sss}$ in our normalization. Primal ratio's $\frac{\lambda_{tts}}{\lambda_{sss}}$ that we encountered were generally of order O(1).

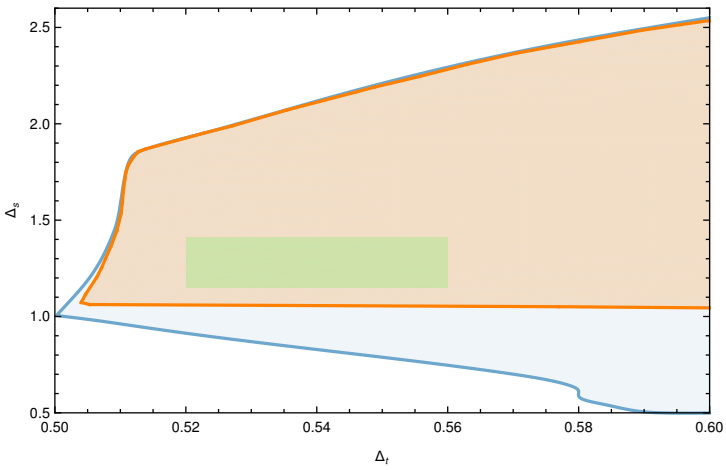

Figure 2.23: The allowed region in the (Δ_t, Δ_s) plane assuming the existence of exactly one relevant singlet scalar with dimension Δ_s is shown in orange. For reference the equivalent single correlator bound is shown in blue. The bounds have been obtained at $\Lambda = 19$.

that we often used in the previous sections is excluded for all Δ_s close to the lattice bounds. This suggests more caution is required when interpreting peaks and plateaus as evidence for a theory living high within that peak. Even so the "fake" peaks location is very suggestive and might still correspond to the location of true ARP^3 model.

As can be seen in figure 2.24, the peak in $\Delta_{T'}$ is no longer located near the expected ARP^3 region. The global peak has dropped significantly and is now located at a much higher value of Δ_s, close the O(9) theory. Assuming $\Delta_{T'} > 6$ no primal points can be found anymore (at $\Lambda = 19$). So either $\Delta_{T'}$ takes a value much closer to the base of the peak in figure 2.5 or no ARP^3 CFT corresponding to the values found by lattice computations exists.

Finally, the mixed setup also allows us to constrain the new channel of Z_2-odd traceless symmetric operators appearing in the $t \times s$ OPE. If we assume the exchange of t-itself and only one additional relevant scalar t'_O we find $\Delta_{t'_O} = 2 \pm 0.25$ for the region of interest, see figure 2.25. For large Δ_s and Δ_t all values for $\Delta_{t'_O}$ are allowed. In the same figure we also indicate the smaller allowed island corresponding to the island shown in figure 2.22b. As a side effect the OPE scan gives us an estimate for the external OPE ratio: $\frac{\lambda_{sss}}{\lambda_{tts}} \in (0.025, 2.5)$.

Surprisingly, in turn fixing $\Delta_{t'_O} = 2$ and assuming $\Delta_{t''_O} > 3$ does not seem to constrain the other parameter spaces significantly. For example it hardly effects the allowed one-relevant-singlet island we found. In general, while the mixed $t - s$ setup is significantly

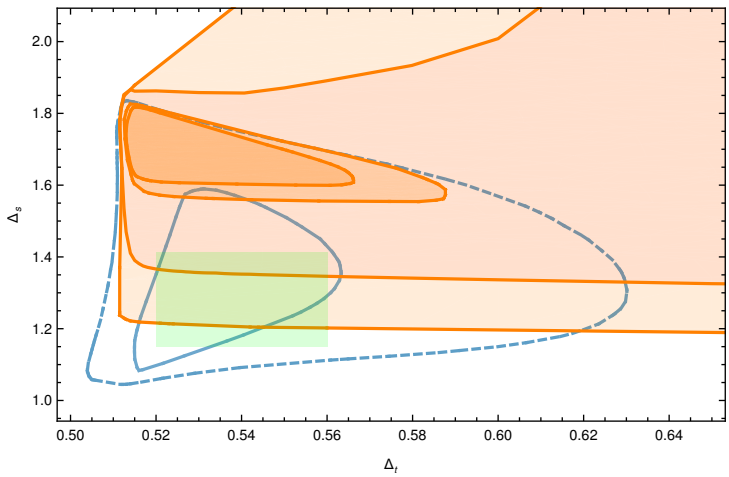

Figure 2.24: Allowed region in the (Δ_t, Δ_s) plane assuming the existence of exactly one relevant singlet scalar and the gaps $\Delta_{T'} = 4.5, 5, 5.5, 5.6$ (light to dark). For reference the single correlator bounds under the assumptions $\Delta_{T'} > 5.5$ (dashed line) and $\Delta_{T'} > 6.5$ (solid line) are indicated in blue. In the mixed setup no primal points can be found for $\Delta_{T'} \geq 6$. The bounds have been obtained at $\Lambda = 19$.

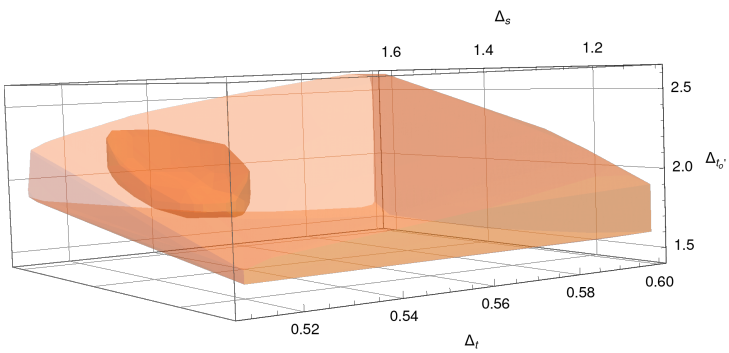

Figure 2.25: Allowed values for $\Delta_{t'_O}$ given $\{\Delta_t, \Delta_s\}$ in the expected ARP^3 region assuming the existence of exactly one relevant singlet and exactly one additional relevant $\mathbb{Z}_2$-odd operator besides t-itself. Darker: the same bounds under the additional assumptions: $\Delta_{T'} > 4.5$, $\Delta_{J'} > 3$, $\Delta_h > 2.05$ and $\Delta_b > 1.3$. The bounds have been obtained at $\Lambda = 19$.

more constraining than the single correlator for certain types of bounds, overall its power seems to be a bit underwhelming. For example, even when using the OPE scan the results for the one relevant singlet island shown in 2.22b do not show any significant improvement.

2.6 A systematic study of general N

Here we present a systematic study of bounds on the dimension of the first operator in all representations for general N. Specifically we examine $N = 4, 5, 10, 20, 100$ and occasionally $N = 1000$ to study the asymptotics of certain kinks at large N. The bounds on the singlet operators s and T are identical to the bounds found in the $SO(2N)$-vector bootstrap[21] while the other bounds are stronger then the related $SO(2N)$ bounds on $\Delta_S, \Delta_T, \Delta_A$.

The bound on the dimension of the first singlet scalar Δ_S shows a clear kink corresponding to the $O(N')$ model under the identification $\phi^a \to \phi^{ij}$. In addition there is a second set of (dull) kinks in the region $0.52 < \Delta_t < 0.58$ whose exact location becomes less and less clear as N increase. An additional kink is visible around $\Delta_t \approx 1.1$ for $N = 4$. These bounds are shown in figure 2.26.

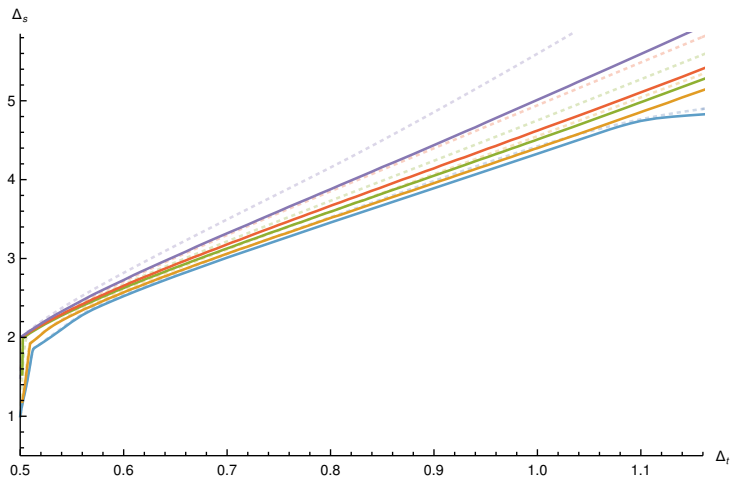

Figure 2.26: Bound on the dimension of the first singlet scalar. The blue, orange, green, red and purple lines correspond to respectively $N = 4, 5, 10, 20, 100$. These bounds have been obtained at $\Lambda = 27$. The dotted lines indicate the same bound at $\Lambda = 19$ and are included to illustrate the convergence. All bounds show a clear kink corresponding to the $O(N')$ model. An additional more dull kink is visible in the region $0.52 < \Delta_t < 0.58$. This kink gets less sharp and precisely located at larger N. For $N = 4$ an additional kink is visible around $\Delta_t = 1.1$. The bounds get strictly weaker for larger N.

Next let us turn to the bound on the dimension of the first spin-2 singlet after the stress tensor. For small N this bound shows a clear peak in the region $0.52 < \Delta_t < 0.58$. For larger N the peak fades and the most discernible feature becomes a kink around $\Delta_t \approx 0.7$. However it seems that especially for larger N the bounds are far from converged even at

[21] (as proven in section 2.3.3)

$\Lambda = 27$. These bounds are shown in figure 2.27.

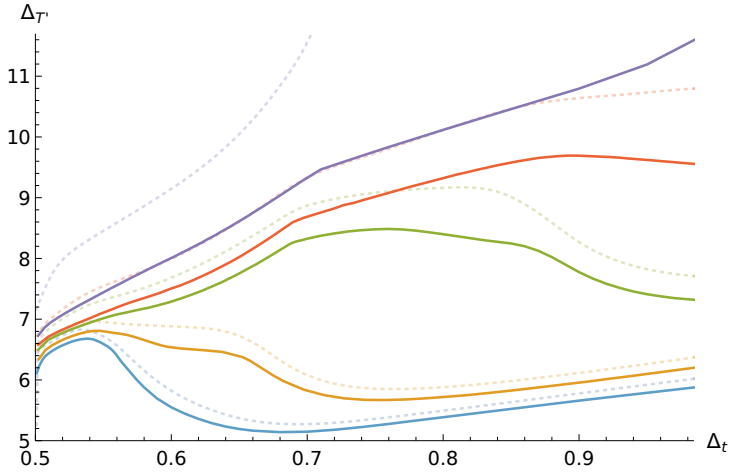

Figure 2.27: Bound on the dimension of the first spin-2 singlet after the stress tensor. The blue, orange, green, red and purple lines correspond to respectively $N = 4, 5, 10, 20, 100$. These bounds have been obtained at $\Lambda = 27$. The dotted lines indicate the same bound at $\Lambda = 19$ and are included to illustrate the convergence. For small N a peak is visible. For larger N the peak fades and the most discernible feature becomes a kink around $\Delta_t \approx 0.7$. The bounds get strictly weaker for larger N.

More interesting features are visible in the bound on the first spin-1 antisymmetric vector after the conserved current. This is the first instance where the bounds are neither strictly weaker nor stronger for increasing N. At large Δ_t we see the behavior usual found for singlet operators, i.e. the bounds get weaker for larger N. Near the unitarity bound we see the usual behavior for non-singlet, i.e. the bounds get stronger for larger N. In between there is a transition between these two regimes.

Next we examine the bound on the dimension of the first scalar Box operator, see figure 2.29a. For small N there are clear kinks in the region $0.54 < \Delta_t > 0.6$. Additionally there is a family of very sharp kinks for all N moving to the right towards $\Delta_t = 1$ as N increases. However, at $\Lambda = 27$ the location of the kink does not seem to converge to 1 in the $N \to \infty$ limit. Since the location of the kink does not change much when changing from $\Lambda = 19$ to $\Lambda = 27$ it seems unlikely the location of the kink would converge to $\Delta_t = 1$ in the $\Lambda \to \infty, N \to \infty$ limit.

A similar family of kinks can be seen in the bound on the dimension of the first spin-1 Hook vector as is shown in figure 2.29b. However, the location of the kink, i.e. the value of Δ_t of the kink, does not precisely match the location of the kinks in the bound on the first scalar Box operator. Again, at $\Lambda = 27$ the location of the kink does not converge to 1 in the $N \to \infty$ limit. In fact in this case the location of the kink seems to have

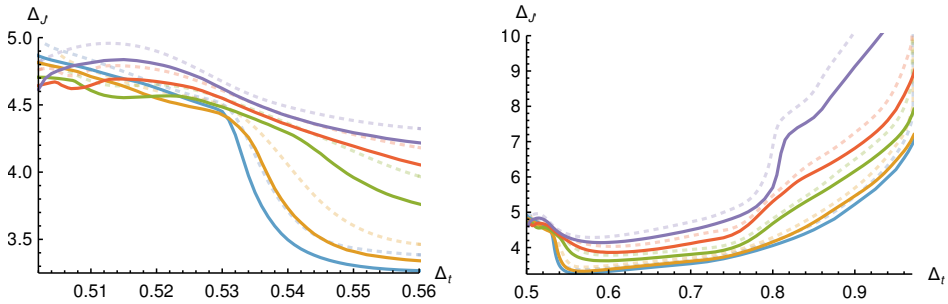

(a) (b)

Figure 2.28: Both figures: Bound on the dimension of the first spin-1 anti-symmetric vector after the conserved current. The bounds have been obtained at $\Lambda = 27$. On the left: A zoom of the region $0.5 < \Delta_t < 0.58$. Near the unitarity bound the bounds get strictly stronger for larger N. On the right: Overview of the same bound on $0.5 < \Delta_t < 1$. A second kink appears for $N = 10, 20, 100$ around $\Delta_t = 0.8$. At large Δ_t the bounds get strictly weaker for larger N. The bound diverge near $\Delta_t = 1$.

converged already at $N = 1000$.[22] However, in this case the bounds seem further from convergence in Λ at $\Lambda = 27$. It is possible that in the $\Lambda \to \infty, N \to \infty$ limit the bounds would converge to 1.

Moreover, we find strong evidence for a theory with a Z_2-even t at large N. In figure 2.30 the bound on $\Delta_{t'}$ is shown both under the assumptions that $t \times t$ exchanges itself and without it. When we assume the exchange of t itself in the $t \times t$ OPE a sharp kink appears for large N. The kink gets sharper as N increases.

Finally, the bounds on the four-index-symmetric tensor are shown in figure 2.31. For small N the only feature is the kink corresponding to the $O(N')$ model. For large N a second kink emerges, for example at $N = 100$ a kink located around $\Delta_t \approx 0.82$.

[22]Moreover, neither the Hook nor the Box bound moves substantially when changing $N = 1000$ to $N = 10^{16}$ (this bound is not included in the figures).

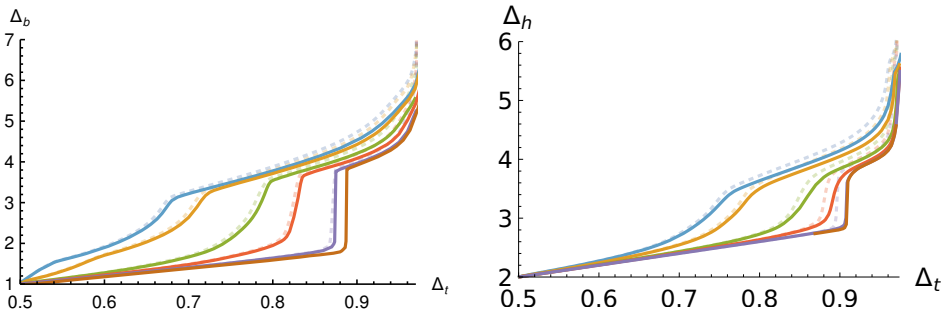

(a) (b)

Figure 2.29: Bounds on the dimension of the first Box scalar (left) and the first hook vector (right). The blue, orange, green, red, purple and brown lines correspond to respectively $N = 4, 5, 10, 20, 100, 1000$. On the left: For $N = 4, 5$ there are kinks at $\Delta_t = 0.54$ and $\Delta_t = 0.60$ respectively. For larger N this kink disappears. A family of sharp kinks is visible for all N. On the right: Again a family of sharp kinks is visible for all N, unlike the figure at the left the the location of the kinks seems to have converged to $\Delta_t \approx 0.91$. The locations of the kinks does not coincide with the family of kinks shown in the figure on the left. Neither figure seems to assymptote to $\Delta_{t'} = 1$. All bounds get strictly stronger for larger N and have been obtained at $\Lambda = 27$. The dotted lines indicate the same bound at $\Lambda = 19$ and are included to illustrate the convergence.

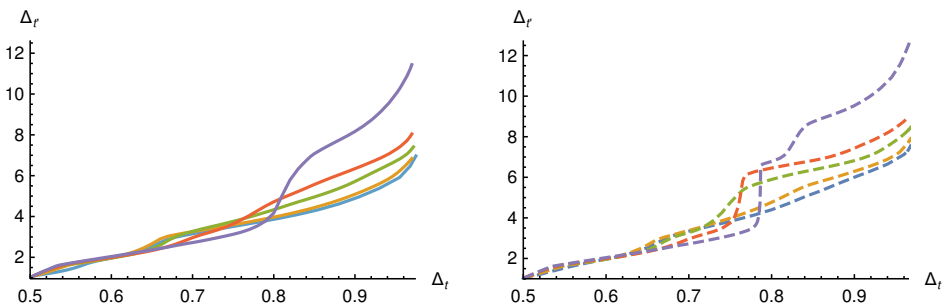

(a) (b)

Figure 2.30: Bound on the dimension of the first traceless symmetric operator. The blue, orange, green, red and purple lines correspond to respectively $N = 4, 5, 10, 20, 100$. On the left: No additional assumptions. Various families of kinks are visible: One corresponding to the $O(N')$ model, one in the region $0.55 < \Delta_{t'} < 0.6$, one in the region $0.6 < \Delta_{t'} < 0.75$ (this one disappears at $N = 100$), and a last one in the region $0.75 < \Delta_{t'} < 1$. On the right: The same bound assuming that $t \times t$ exchanges t itself. The last family of kinks becomes much sharper and more pronounced under this assumption especially for $N = 20, 100$. This is strong evidence that the kink corresponds to a theory with a Z_2 even traceless symmetric operator. All bounds have been obtained at $\Lambda = 27$.

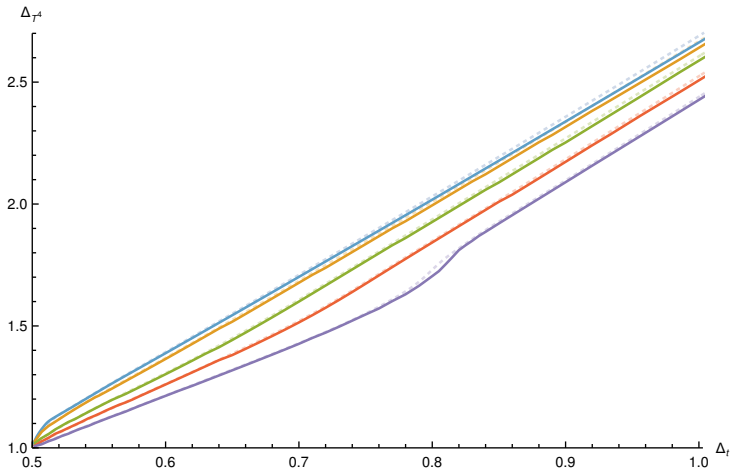

Figure 2.31: Bound on the dimension of the first four-index-symmetric scalar. The blue, orange, green, red and purple lines correspond to respectively $N = 4, 5, 10, 20, 100$. Apart from a kink at the location of the $O(N')$ model few features are visible. At $N = 100$ an additional kink becomes visible. These bounds have been obtained at $\Lambda = 27$. The dotted lines indicate the same bound at $\Lambda = 19$ and are included to illustrate the convergence. The bounds get strictly weaker for larger N.

2.7 Conclusions

By isolating a candidate island for the ARP^3 model this study gives a partial answer to the discrepancy between its effective Landau-Wilson-Ginzburg description and lattice simulations [69]. The former predicts that no stable fixed points exist for $N > 3.6$ while the lattice simulations show a clear second order phase transition. Indeed this work finds evidence for the existence of a CFT compatible with the critical exponents extracted by the lattice simulations. Possibly the perturbative estimate of N_c is wrong despite it having a stable Padé-Borel approximation.

In agreement with the lattice data the allowed island lives deep within the one-relevant-singlet peninsula. By finding an isolated island in the (Δ_t, Δ_s) plane as well as in other parameter spaces we show that such interior CFTs can still be isolated. However, we fail to determine dimensions such as (Δ_t, Δ_s) to any high precision. The mixed $t-s$ bootstrap equations did not greatly improve the bounds. Possibly the inclusion of a greater number of the relevant scalars is required to obtain precision islands (see the efficacy of including more relevant scalars in [67]). One could for example add the crossing equations involving the parity even traceless symmetric operator t_E or the first b operator. However, either of these options results in a big set of bootstrap equations and is therefore numerically quite heavy. Alternatively a mixed bootstrap involving a spinning operator such as the conserved current J might offer significant improvement.

Finally, in our systematic study of all the operators of lowest dimension for general N we also found various new and unexplained kinks. Most notably, two families of sharp kinks appear for all $N > 4$ in the bound on the first Box scalar and the first Hook vector. Additionally, we found various kinks in the bound on the dimension of the first traceless symmetric operator. Some of these kinks become much sharper when it is assumed that the $t \times t$ OPE exchanges t itself. This is strong evidence in favor of these kinks corresponding to a CFT where t is Z_2-even. We leave the investigation of these kinks (as well as some others described in the main text) to future research.

Conclusion and Outlook

In this thesis we extended the conventional numerical conformal bootstrap by performing the first bootstrap of a mixed system involving scalars and spinning operators. By extending the bootstrap of the conserved current to the mixed system of the current and the scalar operator charged under it we opened the way to a new method of studying systems with continuous symmetries. We assessed that this extension has the potential to greatly improve numerical bounds and allow new and important quantities to be bounded and extracted. Among others we found important OPE coefficients related to the OPE between two currents and the stress tensor and the OPE coefficient of two currents with the first singlet operator. Comparison of this OPE data to Monte Carlo data allowed for the prediction of the thermal one-point function of the stress tensor. Multiple extensions of this work come to mind. We saw that access to the external correlators involving the singlet operator turned out be crucial for isolating the $O(2)$ model. While we did find a way around this by isolating the theory using the assumptions of a gap $\Delta_{T'}$ in the dimension of the first spin-2 singlet after the stress tensor, a better solution would be to also include the correlators involving the singlet and do the $\phi - s - J$ bootstrap. This would of course be computationally heavier but with the new scanning algorithms of [67] it might be possible. An alternative is to consider the singlet operator instead of the charged scalar. Another interesting extension is the application of the mixed current-scalar bootstrap to non-abelian continuous symmetry groups.

We also managed to isolate a candidate island for the ARP^3 model despite the fact that it lives deep within the bounds on the first singlet dimension. However, non-trivial assumptions had to be made and we still did not achieve high precision islands. Again considering a bigger bootstrap setup might be the solution. Possible candidates for additional correlators to consider are those involving a Z_2-even traceless symmetric operator, those involving the Box operator, which seemed to play a crucial role in isolating an island in our study, or those involving the spinning conserved current operator.

Recent advances in making use of both dual and primal jumps, hot-starting and better more efficient OPE scanning algorithms [76, 67, 73] enable us to consider bigger bootstrap

setups offering an interesting direction for future research, but it also reminds us to always keep our eye out for ways of improving our basic bootstrapping methods themselves.

A Appendices to chapter 1

A.1 Conductivity in terms of CFT data

We begin by defining the two point function of the $U(1)$ current:

$$\langle J(x_1)J(x_2)\rangle \equiv \langle J(x_1,z_1)J(x_2,z_2)\rangle = \frac{C_J}{(4\pi)^2}\frac{1}{x_{12}^4}\left[z_1\cdot z_2 - 2\frac{(x_{12}\cdot z_1)(x_{12}\cdot z_2)}{|x_{12}|^2}\right]. \quad \text{(A.1)}$$

In the above expression all polarizations z_i and ccordinates are three dimensional and, as usual $x_{12}^\mu = (x_1 - x_2)^\mu$. With this normalization the current J^μ satisfies the global symmetry Ward identity and in the case of a free scalar field $C_J^{\text{free}} = 2$.

We are interested in the leading terms in the OPE expansion of $J^\mu \times J^\nu$, with a particular interest in the contribution of the smallest dimension scalar operator, let us call it S, which is normalized according to

$$\langle S(x)S(0)\rangle = \frac{A}{|x|^{2\Delta_S}}\,. \quad \text{(A.2)}$$

This can be obtained by matching with the leading term in the $x_1 \to x_2$ expansion of the three-point function [18]:

$$\langle J(x_1)J(x_2)S(x_3)\rangle = \frac{C_J\sqrt{A}}{(4\pi)^2}\,\hat{\lambda}_{JJS}\,\frac{(\Delta_S-2)\hat{H}_{12}+\Delta_S\hat{V}_{1,23}\hat{V}_{2,31}}{|x_{12}|^{4-\Delta_S}|x_{13}|^{\Delta_S}|x_{23}|^{\Delta_S}}\,, \quad \text{(A.3)}$$

where as usual we are working in three dimensions. The prefactor $C_J\sqrt{A}/(4\pi)^2$ has been added so that the three-point function coefficient $\hat{\lambda}_{JJS}$ is defined for unit-normalized current and scalar. The three point function coefficient is related to the one used in the

main text and appendix A.2 simply by

$$\hat{\lambda}_{JJS} = -\Delta_S \lambda_{JJS} \,. \tag{A.4}$$

The structures $\hat{H}$ and $\hat{V}$ —which correspond to the physical space projection of the H and V of (1.9)— are written as follows,

$$\begin{aligned} \hat{H}_{12} &= z_1 \cdot z_2 - 2\tfrac{(x_{12}\cdot z_1)(x_{12}\cdot z_2)}{|x_{12}|^2} \,, \\ \hat{V}_{1,23} &= \tfrac{(x_{12}\cdot z_1)|x_{13}|}{|x_{12}||x_{23}|} - \tfrac{(x_{13}\cdot z_1)|x_{12}|}{|x_{13}||x_{23}|} \,, \\ \hat{V}_{2,31} &= \tfrac{(x_{23}\cdot z_2)|x_{12}|}{|x_{23}||x_{13}|} + \tfrac{(x_{12}\cdot z_2)|x_{23}|}{|x_{12}||x_{13}|} \,. \end{aligned} \tag{A.5}$$

By matching with the OPE expansion we get:

$$\begin{aligned} J(x_1) \times J(x_2) \sim \frac{C_J}{(4\pi)^2} \Bigg[& \hat{H}_{12}\mathbf{1} + \frac{\hat{\lambda}_{JJS}}{|x_{12}|^{4-\Delta_S}} \times \\ & \times \left((\Delta_S - 2)(z_1 \cdot z_2) - (\Delta_S - 4)\frac{(x_{12}\cdot z_1)(x_{12}\cdot z_2)}{|x_{12}|^2} \right) \frac{S(x_2)}{\sqrt{A}} + \dots \Bigg] . \end{aligned} \tag{A.6}$$

Next, let us consider the contribution to the OPE of the stress tensor $T_{\mu\nu}$. Following [18], we can write this term as

$$J(x_1) \times J(x_2) \sim \frac{C_J}{(4\pi)^2} \frac{3}{32\pi} \frac{(4\pi)^2}{C_T} \left(t_1(x_{12}, z_1, z_2)^{\alpha\beta} + 12\,\gamma\, t_2(x_{12}, z_1, z_2)^{\alpha\beta} \right) T_{\alpha\beta}(x_2) \,, \tag{A.7}$$

where

$$\begin{aligned} t_1(x_{12}, z_1, z_2)^{\alpha'\beta'}(x) = \quad & z_1^\mu z_2^\nu P^{\alpha'\beta'}_{\alpha\beta} (6\hat{x}_{(\mu}\delta^\alpha_{\nu)}\hat{x}^\beta + 2\delta^\alpha_\mu\delta^\beta_\nu + 3\hat{x}_\mu\hat{x}_\nu\hat{x}^\alpha\hat{x}^\beta - 5\delta_{\mu\nu}\hat{x}^\alpha\hat{x}^\beta) \,, \\ t_2(x_{12}, z_1, z_2)^{\alpha'\beta'}(x) = \quad & z_1^\mu z_2^\nu P^{\alpha'\beta'}_{\alpha\beta} (2\hat{x}_{(\mu}\delta^\alpha_{\nu)}\hat{x}^\beta - 2\delta^\alpha_\mu\delta^\beta_\nu - 3\hat{x}_\mu\hat{x}_\nu\hat{x}^\alpha\hat{x}^\beta - 3\delta_{\mu\nu}\hat{x}^\alpha\hat{x}^\beta) \,, \end{aligned} \tag{A.8}$$

and we explicitly introduced the projector on traceless symmetric indices

$$P^{\alpha'\beta'}_{\alpha\beta} = \frac{1}{2}\left(\delta^{\alpha'}_\alpha \delta^{\beta'}_\beta + \delta^{\alpha'}_\beta \delta^{\beta'}_\alpha - \frac{2}{3}\eta_{\alpha\beta}\eta^{\alpha'\beta'} \right) . \tag{A.9}$$

In order to compute the conductivity we need to take the Fourier transform at point $x_{1,2}$ of the expressions (A.6) and (A.7). Using standard formulas, see for instance appendix B

of [77], we obtain:

$$\int d^3x_1 d^3x_2 e^{ip_1\cdot x_1} e^{ip_2\cdot x_2} J(x_1,z_1)\times J(x_2,z_2) \sim$$
$$\sim \left(z_1^\mu \widetilde{I}_{\mu\nu}(p_1) z_2^\nu\right)\left(-|p_1|\frac{\pi^3 C_J}{4}\delta^3(p_1+p_2) - \frac{\lambda_{JJS}}{4\pi|p_1|^{\Delta_S-1}}\frac{\Gamma(\Delta_S+1)\sin\left(\frac{\pi\Delta_S}{2}\right)}{2-\Delta_S}\frac{\widetilde{S}(p_2)}{\sqrt{A}}\right) +$$
$$+\frac{C_J}{C_T}\frac{1}{|p|}\left(\widetilde{t}_1(p_1,z_1,z_2)_{\alpha\beta} + 12\gamma\widetilde{t}_2(p_1,z_1,z_2)_{\alpha\beta}\right)\widetilde{T}^{\alpha\beta}(p_1+p_2) + \dots\,, \tag{A.10}$$

where

$$\begin{aligned}\widetilde{t}_1(p_1,z_1,z_2)_{\alpha\beta} &= 3z_1^\mu z_2^\nu\left(\eta_{\alpha\nu}\eta_{\beta\mu} + \eta_{\alpha\mu}\eta_{\beta\nu} - \eta_{\alpha\beta}\eta_{\mu\nu} + \hat{p}_\mu\hat{p}_\nu\eta_{\alpha\beta} - \hat{p}_\beta\hat{p}_\nu\eta_{\alpha\mu}\right.\\ &\quad \left. -\hat{p}_\alpha\hat{p}_\nu\eta_{\beta\mu} - \hat{p}_\beta\hat{p}_\mu\eta_{\alpha\nu} - \hat{p}_\alpha\hat{p}_\mu\eta_{\beta\nu} + \hat{p}_\alpha\hat{p}_\beta\eta_{\mu\nu} + \hat{p}_\alpha\hat{p}_\beta\hat{p}_\mu\hat{p}_\nu\right)\,, \\ \widetilde{t}_2(p,z_1,z_2)_{\alpha\beta} &= \left(z_1^\mu\widetilde{I}_{\mu\nu}(p)z_2^\nu\right)\left(\eta_{\alpha\beta} - 3\hat{p}_\alpha\hat{p}_\beta\right)\,,\end{aligned} \tag{A.11}$$

with $\widetilde{I}_{\mu\nu}(p) = (\eta_{\mu\nu} - \hat{p}_\mu\hat{p}_\nu)$ and $\hat{p}_\mu = p_\mu/|p|$. By choosing the polarizations along the 2nd direction $z_i = (0,1,0)$, the momenta

$$p_1 = w\,, \qquad p_2 = -w + p\,, \qquad w = (\Omega, 0, 0)\,, \tag{A.12}$$

and taking the expectation value of the previous expression at finite temperature, we obtain:

$$\begin{aligned}\langle J_2(-w)J_2(w+p)\rangle_T \sim (2\pi^3)\delta^3(p)|\Omega|\times \\ \Big(-\frac{C_J}{32} - \frac{C_J\lambda_{JJS}}{4\pi}\frac{\Gamma(\Delta_S+1)\sin\left(\frac{\pi\Delta_S}{2}\right)}{2-\Delta_S}\Upsilon^{-1}\left(\frac{T}{|\Omega|}\right)^{\Delta_S} \\ - 72\frac{C_J\gamma}{C_T}\frac{\Omega^2}{|\Omega|^2}H_{xx}\left(\frac{T}{|\Omega|}\right)^3 + \dots\Big)\,,\end{aligned} \tag{A.13}$$

where we defined

$$\langle S(0)\rangle_T = BT^{\Delta_S}\,, \qquad \Upsilon = \frac{\sqrt{A}}{B}\,, \qquad \langle T_{22}(0)\rangle_T = \langle T_{33}(0)\rangle_T = -\frac{1}{2}\langle T_{11}(0)\rangle_T = H_{xx}T^3\,. \tag{A.14}$$

Finally, given the relation [52],

$$\frac{\sigma(iw)}{\sigma_Q}(2\pi)^3\delta^3(p) = -\frac{1}{|w|}\langle J_2(-w)J_2(w+p)\rangle_T\,, \tag{A.15}$$

we obtain equation (1.6) shown in the main text.

A.2 Three point functions

A.2.1 Scalar-scalar OPE

We start by normalizing the OPE of two scalars $\mathcal{O}_1 \times \mathcal{O}_2$ such that

$$\mathcal{O}(x,z)\mathcal{O}_1(0) \sim \lambda_{12\mathcal{O}} \frac{(-x\cdot z)^\ell}{(x^2)^{\frac{\Delta+\Delta_{12}+\ell}{2}}} \mathcal{O}_2(0)\,, \tag{A.16}$$

where z_μ is a null polarization vector. The operator $\mathcal{O}$ is a parity even operator of spin ℓ and λ is the OPE coefficient. The symbol $\sim$ means that we consider only one primary operator exchange, in this case $\mathcal{O}_2$. We are therefore omitting the contribution of all the other primaries and all the descendants in the OPE of $\mathcal{O}\times\mathcal{O}_1$. We use this normalization for both the cases $\mathcal{O}_1 = \mathcal{O}_2 = \phi$ and $\mathcal{O}_1 = \phi, \mathcal{O}_2 = \bar{\phi}$. Notice however that for $\phi\times\phi$, the equality of the operators forces ℓ to be even.

A.2.2 Current-scalar OPE

We normalize the scalar current OPE $J\times\phi$ as

$$\begin{aligned}
\mathcal{O}_{\ell,+}(x,z)J(0,z_1) &\sim \frac{1}{\sqrt{a_\ell}}\frac{\phi(0)}{(x^2)^\alpha}\lambda_{J\phi\mathcal{O}_+}\ \textstyle\sum_{p=1}^2 \omega_p\, t_+^{(p)}(x,z,z_1)\ ,\\
\mathcal{O}_{\ell,-}(x,z)J(0,z_1) &\sim \frac{1}{\sqrt{b_\ell}}\frac{\phi(0)}{(x^2)^\alpha}\lambda_{J\phi\mathcal{O}_-}\ t_-(x,z,z_1)\ ,
\end{aligned} \tag{A.17}$$

where $\mathcal{O}_{\ell,\pm}$ is a parity even/odd operator of spin ℓ and charge one, and λ are OPE coefficients and $\alpha \equiv \frac{\Delta+\Delta_J-\Delta_\phi+\ell+1}{2}$. The coefficients a_ℓ and b_ℓ are defined to match the conventions of [26],

$$a_\ell \equiv \frac{(-2)^{\ell-1}(d/2)_{\ell-1}}{\ell^2(d-1)_{\ell-1}}\,, \qquad b_\ell \equiv \frac{a_\ell}{-2\ell(d+\ell-3)}\,. \tag{A.18}$$

The leading OPE tensor structures are defined as follows

$$\begin{aligned}
t_+^{(1)}(x,z,z_1) &= (x\cdot z)^\ell (x\cdot z_1)\ ,\\
t_+^{(2)}(x,z,z_1) &= (x\cdot z)^{\ell-1}x^2(z\cdot z_1)\ ,\\
t_-(x,z,z_1) &= |x|(x\cdot z)^{\ell-1}\epsilon(x,z_1,z)\ .
\end{aligned} \tag{A.19}$$

When $\ell = 0$ only $t_+^{(1)}$ survives. In (A.17) a single combination of $t_+^{(p)}$ is used. This is written in terms of the vector $\omega = \{2(\alpha-1), -2\alpha+d+\ell\}/\ell$, determined by imposing

conservation of J. Finally we set $d = 3$ in all formulae above.

A.2.3 Current-current OPE

The normalization of the current-current OPE is as follows

$$\mathcal{O}^{\pm}(x,z)J_1(0,z_1) \sim \frac{J_2(0,\partial_{z_2})}{(x^2)^{\alpha_\pm}} \sum_q c^{(q)}_{12\mathcal{O}^\pm}\, t^{[JJ]\,(q)}_{\pm}(x,z,z_1,z_2)\ , \tag{A.20}$$

where $\alpha_+ \equiv \frac{1}{2} + \alpha_- \equiv \frac{\Delta+\Delta_1-\Delta_2+\ell+2}{2}$. In (A.20) q runs from one to five for parity even operators. The correspondent OPE structures take the form

$$\begin{aligned}
t^{[JJ]\,(1)}_{\ell+}(x,z,z_1,z_2) &\equiv (x\cdot z)^{\ell}(z_1\cdot z_2)x^2\ ,\\
t^{[JJ]\,(2)}_{\ell+}(x,z,z_1,z_2) &\equiv (x\cdot z)^{\ell}(x\cdot z_1)(x\cdot z_2)\ ,\\
t^{[JJ]\,(3)}_{\ell+}(x,z,z_1,z_2) &\equiv (x\cdot z)^{\ell-1}(z\cdot z_1)(x\cdot z_2)x^2\ ,\\
t^{[JJ]\,(4)}_{\ell+}(x,z,z_1,z_2) &\equiv (x\cdot z)^{\ell-1}(z\cdot z_2)(x\cdot z_1)x^2\ ,\\
t^{[JJ]\,(5)}_{\ell+}(x,z,z_1,z_2) &\equiv (x\cdot z)^{\ell-2}(z\cdot z_1)(z\cdot z_2)x^4\ .
\end{aligned} \tag{A.21}$$

By imposing equality and conservation of the currents J_i we find only two linearly independent structures

$$\sum_{p=1}^{5}(m_+)_{\tilde{p}p}\ t^{[JJ]\,(p)}_{\ell+}(x,z,z_1,z_2)\ , \qquad (\tilde{p}=1,2)\ , \tag{A.22}$$

where

$$m_+ = \begin{pmatrix} (2-\Delta)(\ell+\Delta) & (\Delta-\ell)(\ell+\Delta) & 2\ell(\Delta-2) & 0 & -\ell(\Delta-2) \\ \ell-\Delta+2 & 0 & -\ell+\Delta-2 & \Delta-\ell & \ell-\Delta+1 \end{pmatrix}\ . \tag{A.23}$$

For parity odd operators there are four possible tensor structures

$$\begin{aligned}
t^{[JJ]\,(1)}_{\ell-} &= \epsilon(x,z_1,z_2)(x\cdot z)^{\ell}\\
t^{[JJ]\,(2)}_{\ell-} &= \epsilon(x,z,z_1)(x\cdot z_2)(x\cdot z)^{\ell-1}\\
t^{[JJ]\,(3)}_{\ell-} &= \epsilon(x,z,z_2)(x\cdot z_1)(x\cdot z)^{\ell-1}\\
t^{[JJ]\,(4)}_{\ell-} &= [\epsilon(x,z,z_1)(z\cdot z_2)+\epsilon(x,z,z_2)(z\cdot z_1)](x\cdot z)^{\ell-2}x^2\ .
\end{aligned} \tag{A.24}$$

For conserved equal currents we obtain just one structure which takes a different form

for ℓ even or odd,

$$\sum_p (m_-)_p \, t_{\ell-}^{[JJ]\,(p)}(x, z, z_1, z_2) \ , \tag{A.25}$$

with

$$m_- = \begin{cases} (\Delta - 3, \ell, \ell, 0) & \ell \text{ even}, \\ (0, \Delta - \ell - 3, \Delta + \ell + 1, 1 - \Delta) & \ell > 1, \text{ odd}. \end{cases} \tag{A.26}$$

When $\ell = 1$ there are no allowed tensor structures, while for $\ell = 0$ there is one.

A.3 Conformal Blocks

A.3.1 $JJ\phi\bar{\phi}$

The blocks for $JJ\phi\bar{\phi}$ are computed using the recurrence relation (1.38). We first consider correlators of two vectors V_1, V_2 and two scalars ϕ_1, ϕ_2, we finally restrict to the equal, conserved case. In order to use (1.38), we have to compute the coefficients R_A and the functions h_∞.

As described in [6], R_A are obtained as the product of three terms,

$$(R_A)_{pp'} = (M_A^{(L)})_{pp'}\, Q_A\, M_A^{(R)}\,, \tag{A.27}$$

where Q_A and M_A are respectively related to the two- and three-point functions with primary-descendants operators. For our case the three terms in (A.27) were already computed in the literature. Indeed Q_A and $M_A^{(R)}$ are the same as for the scalar blocks of [6], while $(M_A^{(L)})_{pp'}$ are the same of [18]. Thus, the only missing computation is that of $h^{(p)}_{\infty\,\ell,s}$. These functions are obtained by solving the Casimir differential equation at leading order in large Δ [35, 6]. The Casimir equation mixes the five structures resulting in a system of 5 coupled differential equations. We introduce the ansatz

$$h_s^{(s')}(r,\eta) \equiv \mathcal{A}(r,\eta) P_s^{(s')}(r,\eta)\,, \qquad \mathcal{A}(r,\eta) \equiv \frac{\left(1-r^2\right)^{1-h}}{\sqrt{r^2-2\eta r+1}\,\left(r^2+2\eta r+1\right)^{3/2}}\,. \tag{A.28}$$

The resulting differential equations for $P_s^{(s')}(r,\eta)$ are then easily solved using Mathematica. The solution is given by

$$P = \begin{pmatrix} \left(r^2-1\right)^2(2r\eta+A_3) & 0 & 0 & 0 & 0 \\ 0 & A_1A_3^2 & -2r^2\eta A_1A_3 & -2r^2\eta A_1A_3 & 4r^4\eta^2A_1 \\ 0 & -2rA_1A_3 & -A_1A_2A_3 & 4r^3\eta A_1 & 2r^2\eta A_1A_2 \\ 0 & -2rA_1A_3 & 4r^3\eta A_1 & -A_1A_2A_3 & 2r^2\eta A_1A_2 \\ 0 & 4r^2A_1 & 2rA_1A_2 & 2rA_1A_2 & A_1A_2^2 \end{pmatrix}, \tag{A.29}$$

with $A_1 = (1+r^2-2r\eta), A_2 = (-1+r^2-2r\eta), A_3 = (1+r^2)$. Hence the functions h_∞ can be written as a linear combination of the five $h_s^{(s')}$ as follows

$$h^{(p)}_{\infty\ell+,s}(r,\eta) = \sum_{s'}^{5} h_s^{(s')}(r,\eta) f^{(p)}_{\ell+,s'}(\eta)\,, \tag{A.30}$$

where the functions f are constants of integration that can be fixed by imposing the correct initial conditions $f^{(p)}_{\ell+,s}(\eta) = h^{(p)}_{\infty\ell+,s}(0,\eta)$. We then determine these constants by

studying the OPE limit $x_2 \to x_1$, $x_4 \to x_3$ of the four point function [6],

$$\lim_{\substack{x_2\to x_1\\ x_4\to x_3}} \sum_{s=1}^{43} f^{(p)}_{\ell\pm,s}(\eta) Q_s = \frac{t^{(p)}_{\ell+}(\hat{x}_{12}, I(x_{24})\cdot D_z, I(x_{12})\cdot z_1, z_2)(-x_{34}\cdot z)^\ell}{\ell!(h-1)_\ell} \ . \tag{A.31}$$

Here $(-x_{34}\cdot z)^\ell$ comes from the scalar OPE (A.16) and $t^{(p)}_{\ell+}$ are the OPE structures defined in (A.21). Here we also introduced the differential operator $D^\mu_z \equiv (d/2-1+z\cdot\partial_z)\,\partial^\mu_z - \frac{1}{2}z^\mu\partial^2_z$ and the reflection matrix $I(x)^{\mu\nu} = \delta^{\mu\nu} - 2x^\mu x^\nu/x^2$. Finally, the conserved blocks for $JJ\phi\bar{\phi}$ are obtained from the contraction $(m_+)_{pq}h^{(q)}$, where m_+ is defined in (A.23).

A.3.2 $J\phi J\bar{\phi}$

As we mention in section 1.2.3, we compute the conformal blocks of $J\phi J\bar{\phi}$ by using the an improved version of the ancillary file of [26]. The code produces a single block for the parity-odd exchanges and four blocks $g^{(p',q')}_{\Delta\ell+,s}$ (for $p,q=1,2$) for the parity-even exchanges. To be consistent with the OPE basis defined in appendix A.2.2, we write the parity-even conserved block as follows,

$$g_{\Delta\,\ell+,s} = \sum_{p',q'=1}^{2} (\tilde{\omega}^{(L)})_{p'}(\tilde{\omega}^{(R)})_{q'} g^{(p',q')}_{\Delta\,\ell+,s}\,, \tag{A.32}$$

where

$$\tilde{\omega}^{(L)} = \{\ell(\ell+1), \Delta-\Delta_\phi\}\ , \qquad \tilde{\omega}^{(R)} = \{-\ell(\ell+1), \Delta-\Delta_\phi\}\ . \tag{A.33}$$

A.3.3 $\phi JJ\bar{\phi}$

The conformal blocks for the $\phi JJ\bar{\phi}$ can be obtained from the ones of $J\phi J\bar{\phi}$ by using crossing symmetry $1 \leftrightarrow 2$. Indeed it is easy to see that the functions $\hat{h}_s$ of (1.26) are related to the $\hat{f}_s$ as follows,

$$\begin{aligned}
\hat{h}_1(u,v) &= -v^{\Delta_\phi+\Delta_J+\frac{1}{2}}\left[\hat{f}_2\left(\tfrac{u}{v},\tfrac{1}{v}\right) + \sqrt{u}\left(\hat{f}_1\left(\tfrac{u}{v},\tfrac{1}{v}\right) + \hat{f}_3\left(\tfrac{u}{v},\tfrac{1}{v}\right)\right)\right]\ ,\\
\hat{h}_2(u,v) &= \tfrac{1}{2}v^{\Delta_\phi+\Delta_J}\left[(u+v+1)\hat{f}_1\left(\tfrac{u}{v},\tfrac{1}{v}\right) + 2\sqrt{u}\hat{f}_2\left(\tfrac{u}{v},\tfrac{1}{v}\right) + (u+v-1)\hat{f}_3\left(\tfrac{u}{v},\tfrac{1}{v}\right)\right]\ ,\\
\hat{h}_3(u,v) &= \tfrac{1}{2}v^{\Delta_\phi+\Delta_J}\left[(-u+v-1)\hat{f}_1\left(\tfrac{u}{v},\tfrac{1}{v}\right) - 2\sqrt{u}\hat{f}_2\left(\tfrac{u}{v},\tfrac{1}{v}\right) + (-u+v+1)\hat{f}_3\left(\tfrac{u}{v},\tfrac{1}{v}\right)\right]\ ,\\
\hat{h}_4(u,v) &= v^{\Delta_\phi+\Delta_J}\hat{f}_4\left(\tfrac{u}{v},\tfrac{1}{v}\right)\ ,\\
\hat{h}_5(u,v) &= -v^{\Delta_\phi+\Delta_J+\frac{1}{2}}\hat{f}_5\left(\tfrac{u}{v},\tfrac{1}{v}\right)\ .
\end{aligned} \tag{A.34}$$

In terms of radial coordinates the equations above relate $\hat{h}_s(r,\eta)$ to $\hat{f}_s(r,-\eta)$. Therefore, by means of (A.34), we can reconstruct $\hat{h}_s(r,\eta)$ to some order $O(r^n)$ by knowing $\hat{f}_s(r,-\eta)$ to the same order. In particular, since $\hat{f}_s$ is evaluated at $-\eta$, its complete dependence in η has to be known at that order. This would require extra computations. Indeed, we only need some derivatives at $\eta = 1$ of the $J\phi J\bar{\phi}$ blocks and their full dependence in η was not computed. For this reason, instead of using (A.34), we built the $\phi JJ\bar{\phi}$ blocks using the differential operators of [24]. The final conserved blocks are then put in a basis compatible with (A.34). This allows to have the same definition for the OPE coefficients that multiply the $JsJs$ and the $sJJs$ blocks.

A.3.4 Conformal block decomposition

As an example, let us compute the conformal blocks decomposition of $\phi JJ\bar{\phi}$ and $J\phi J\bar{\phi}$ for the theory of a free complex boson. We use the unit normalized current $J^\mu \equiv \frac{-i}{\sqrt{2}}(\phi\partial^\mu\bar{\phi} - \bar{\phi}\partial^\mu\phi)$ and compute the correlators by Wick contractions,

$$f_s(u,v) = \left\{\frac{1}{2}u^{3/4}\left(\sqrt{u}\left(\frac{1}{\sqrt{v}}+2\right)+1\right), 0, \frac{1}{2}\sqrt[4]{u}\sqrt{v}, \frac{u^{7/4}}{2v}, 0\right\}, \tag{A.35}$$

$$h_s(u,v) = \left\{\frac{u^{3/4}\left(\sqrt{u}\left(\sqrt{v}+2\right)+\sqrt{v}\right)}{2v^2}, -\frac{u^{3/4}}{2v}, \frac{\sqrt[4]{u}}{2\sqrt{v}}, \frac{u^{5/4}+u^{7/4}}{2v^{3/2}}, -\frac{u^{3/4}}{2v}\right\}. \tag{A.36}$$

Here the functions f_s and h_s are the ones defined in (1.21) and (1.23). Because of the normalization explained in appendix A.3.3, the conformal block decomposition of the functions f_s and h_s give the same OPE coefficients $p_{\mathcal{O}}$. These are exemplified in the tables below for $\mathcal{O}$ being either a parity even or odd operator.

Δ,ℓ	$\frac{1}{2},0$	$\frac{5}{2},1$	$\frac{7}{2},2$	$\frac{9}{2},3$	$\frac{11}{2},4$	$\frac{13}{2},5$	$\frac{15}{2},6$	$\frac{17}{2},7$	$\frac{19}{2},8$
$p_{\Delta\ell+}$	$\frac{1}{2}$	$\frac{3}{8}$	$-\frac{1}{42}$	$\frac{1}{1056}$	$-\frac{12}{25025}$	$\frac{137}{4534920}$	$-\frac{367}{24025386}$	$\frac{4859}{3893984640}$	$-\frac{5669}{9546570900}$

Table A.1: OPE coefficients for parity even operators in the conformal block decomposition of $J\phi J\bar{\phi}$ and $\phi JJ\bar{\phi}$.

Δ,ℓ	$\frac{9}{2},2$	$\frac{11}{2},3$	$\frac{13}{2},4$	$\frac{15}{2},5$	$\frac{17}{2},6$	$\frac{19}{2},7$	$\frac{21}{2},8$	$\frac{23}{2},9$
$p_{\Delta\ell+}$	$\frac{1}{15}$	$-\frac{1}{182}$	$\frac{1}{510}$	$-\frac{107}{373065}$	$\frac{17}{198835}$	$-\frac{193}{12606300}$	$\frac{2969}{695987820}$	$-\frac{1319}{1564192575}$

Table A.2: OPE coefficients for parity odd operators in the conformal block decomposition of $J\phi J\bar{\phi}$ and $\phi JJ\bar{\phi}$.

A.4 Vectors for the bootstrap equations

In this appendix we detail the form of the 23-dimensional vectors in (1.51). The vector $V^{Q=0}_{\Delta,\ell,+}$ takes a different form for $\ell = 0$ and $\ell > 0$ (even),

$$
\begin{aligned}
\left(V^{Q=0}_{\substack{\Delta,\ell,+\\ \ell\text{ even}}}\right)_1 &= F^{[-]\phi\bar{\phi}\phi\bar{\phi}}_{\mathcal{O}_+}(u,v)\begin{pmatrix}1&0&0\\0&0&0\\0&0&0\end{pmatrix},\\
\left(V^{Q=0}_{\substack{\Delta,\ell,+\\ \ell\text{ even}}}\right)_2 &= F^{[+]\bar{\phi}\phi\phi\bar{\phi}}_{\mathcal{O}_+}(u,v)\begin{pmatrix}1&0&0\\0&0&0\\0&0&0\end{pmatrix},\\
\left(V^{Q=0}_{\substack{\Delta,\ell,+\\ \ell\text{ even}}}\right)_3 &= F^{[-]\bar{\phi}\phi\phi\bar{\phi}}_{\mathcal{O}_+}(u,v)\begin{pmatrix}1&0&0\\0&0&0\\0&0&0\end{pmatrix},\\
\left(V^{Q=0}_{\substack{\Delta,\ell,+\\ \ell\text{ even}}}\right)_7 &= \mathcal{S}^+_1(u,v)\,,\\
\left(V^{Q=0}_{\substack{\Delta,\ell,+\\ \ell\text{ even}}}\right)_8 &= \mathcal{S}^-_1(u,v)\,,\\
\left(V^{Q=0}_{\substack{\Delta,\ell,+\\ \ell\text{ even}}}\right)_9 &= \mathcal{S}^+_2(u,v)\,,\\
\left(V^{Q=0}_{\substack{\Delta,\ell,+\\ \ell\text{ even}}}\right)_{10} &= \mathcal{S}^-_2(u,v)\,,\\
\left(V^{Q=0}_{\substack{\Delta,\ell,+\\ \ell\text{ even}}}\right)_{11} &= \mathcal{S}^+_3(u,u)\,,\\
\left(V^{Q=0}_{\substack{\Delta,\ell,+\\ \ell\text{ even}}}\right)_{12} &= \mathcal{S}^+_4(u,u)\,,\\
\left(V^{Q=0}_{\substack{\Delta,\ell,+\\ \ell\text{ even}}}\right)_{13} &= \mathcal{R}^-_{13}(u,v)\,,\\
\left(V^{Q=0}_{\substack{\Delta,\ell,+\\ \ell\text{ even}}}\right)_{14} &= \mathcal{R}^-_{15}(u,v)\,,\\
\left(V^{Q=0}_{\substack{\Delta,\ell,+\\ \ell\text{ even}}}\right)_{15} &= \mathcal{R}^-_{16}(u,v)\,,\\
\left(V^{Q=0}_{\substack{\Delta,\ell,+\\ \ell\text{ even}}}\right)_{16} &= \mathcal{R}^-_{17}(u,v)\,,\\
\left(V^{Q=0}_{\substack{\Delta,\ell,+\\ \ell\text{ even}}}\right)_{17} &= \mathcal{R}^+_7(u,v)\,,\\
\left(V^{Q=0}_{\substack{\Delta,\ell,+\\ \ell\text{ even}}}\right)_{18} &= \mathcal{R}^+_1(u,u)\,,\\
\left(V^{Q=0}_{\substack{\Delta,\ell,+\\ \ell\text{ even}}}\right)_{19} &= \mathcal{R}^+_2(u,u)\,,\\
\left(V^{Q=0}_{\substack{\Delta,\ell,+\\ \ell\text{ even}}}\right)_{20} &= \mathcal{R}^+_4(u,u)\,,\\
\left(V^{Q=0}_{\substack{\Delta,\ell,+\\ \ell\text{ even}}}\right)_{21} &= \mathcal{R}^+_5(u,u)\,,\\
\left(V^{Q=0}_{\substack{\Delta,\ell,+\\ \ell\text{ even}}}\right)_{22} &= \mathcal{R}^+_6(u,u)\,,\\
\left(V^{Q=0}_{\substack{\Delta,\ell,+\\ \ell\text{ even}}}\right)_{23} &= \mathcal{R}^+_3(\tfrac{1}{4},\tfrac{1}{4})\,,\\
\left(V^{Q=0}_{\substack{\Delta,\ell,+\\ \ell\text{ even}}}\right)_{i} &= 0\,, \qquad \text{i=4,5,6,}
\end{aligned}
$$

$$
\begin{aligned}
\left(V^{Q=0}_{\Delta,0,+}\right)_1 &= F^{[-]\phi\bar{\phi}\phi\bar{\phi}}_{\mathcal{O}_+}(u,v)\begin{pmatrix}1&0\\0&0\end{pmatrix},\\
\left(V^{Q=0}_{\Delta,0,+}\right)_2 &= F^{[+]\bar{\phi}\phi\phi\bar{\phi}}_{\mathcal{O}_+}(u,v)\begin{pmatrix}1&0\\0&0\end{pmatrix},\\
\left(V^{Q=0}_{\Delta,0,+}\right)_3 &= F^{[-]\bar{\phi}\phi\phi\bar{\phi}}_{\mathcal{O}_+}(u,v)\begin{pmatrix}1&0\\0&0\end{pmatrix},\\
\left(V^{Q=0}_{\Delta,0,+}\right)_7 &= S^+_1(u,v)\,,\\
\left(V^{Q=0}_{\Delta,0,+}\right)_8 &= S^-_1(u,v)\,,\\
\left(V^{Q=0}_{\Delta,0,+}\right)_9 &= S^+_2(u,v)\,,\\
\left(V^{Q=0}_{\Delta,0,+}\right)_{10} &= S^-_2(u,v)\,,\\
\left(V^{Q=0}_{\Delta,0,+}\right)_{11} &= S^+_3(u,u)\,,\\
\left(V^{Q=0}_{\Delta,0,+}\right)_{12} &= S^+_4(u,u)\,,\\
\left(V^{Q=0}_{\Delta,0,+}\right)_{13} &= R^-_{13}(u,v)\,,\\
\left(V^{Q=0}_{\Delta,0,+}\right)_{14} &= R^-_{15}(u,v)\,,\\
\left(V^{Q=0}_{\Delta,0,+}\right)_{15} &= R^-_{16}(u,v)\,,\\
\left(V^{Q=0}_{\Delta,0,+}\right)_{16} &= R^-_{17}(u,v)\,,\\
\left(V^{Q=0}_{\Delta,0,+}\right)_{17} &= R^+_7(u,v)\,,\\
\left(V^{Q=0}_{\Delta,0,+}\right)_{18} &= R^+_1(u,u)\,,\\
\left(V^{Q=0}_{\Delta,0,+}\right)_{19} &= R^+_2(u,u)\,,\\
\left(V^{Q=0}_{\Delta,0,+}\right)_{20} &= R^+_4(u,u)\,,\\
\left(V^{Q=0}_{\Delta,0,+}\right)_{21} &= R^+_5(u,u)\,,\\
\left(V^{Q=0}_{\Delta,0,+}\right)_{22} &= R^+_6(u,u)\,,\\
\left(V^{Q=0}_{\Delta,0,+}\right)_{23} &= R^+_3(\tfrac{1}{4},\tfrac{1}{4})\,,\\
\left(V^{Q=0}_{\Delta,0,+}\right)_{i} &= 0\,, \qquad \text{i=4,5,6.}
\end{aligned}
\tag{A.37}
$$

The matrices $\mathcal{R}$ and $\mathcal{S}$ are 3×3 and they can be written in terms of the functions F as follows,

$$\mathcal{R}_s^{\pm}(u,v) \equiv \begin{pmatrix} 0 & 0 & 0 \\ 0 & F_{\mathcal{O}_+,s}^{[\pm](1,1)JJJJ}(u,v) & F_{\mathcal{O}_+,s}^{[\pm](1,2)JJJJ}(u,v) \\ 0 & F_{\mathcal{O}_+,s}^{[\pm](2,1)JJJJ}(u,v) & F_{\mathcal{O}_+,s}^{[\pm](2,2)JJJJ}(u,v) \end{pmatrix}, \tag{A.38}$$

$$\mathcal{S}_s^{\pm}(u,v) \equiv \frac{1}{2}\begin{pmatrix} 0 & F_{\mathcal{O}_+,s}^{[\pm](1)JJ\phi\bar{\phi}}(u,v) & F_{\mathcal{O}_+,s}^{[\pm](2)JJ\phi\bar{\phi}}(u,v) \\ F_{\mathcal{O}_+,s}^{[\pm](1)JJ\phi\bar{\phi}}(u,v) & 0 & 0 \\ F_{\mathcal{O}_+,s}^{[\pm](2)JJ\phi\bar{\phi}}(u,v) & 0 & 0 \end{pmatrix}. \tag{A.39}$$

The matrices R and S are their 2×2 counterparts,

$$R_s^{\pm}(u,v) \equiv \begin{pmatrix} 0 & 0 \\ 0 & F_{\mathcal{O}_+,s}^{[\pm](1,1)JJJJ}(u,v) \end{pmatrix}, \qquad S_s^{\pm}(u,v) \equiv \frac{1}{2}F_{\mathcal{O}_+,s}^{[\pm](1)JJ\phi\bar{\phi}}(u,v)\begin{pmatrix} 0 & 1 \\ 1 & 0 \end{pmatrix}. \tag{A.40}$$

All the other vectors do not have any matrix structure,

$$\begin{aligned} \left(V^{Q=0}_{\substack{\Delta,\ell,+\\ \ell\text{ odd}}}\right)_1 &= -F_{\mathcal{O}_+}^{[-]\phi\bar{\phi}\phi\bar{\phi}}(u,v)\,, \\ \left(V^{Q=0}_{\substack{\Delta,\ell,+\\ \ell\text{ odd}}}\right)_2 &= F_{\mathcal{O}_+}^{[+]\bar{\phi}\phi\phi\bar{\phi}}(u,v)\,, \\ \left(V^{Q=0}_{\substack{\Delta,\ell,+\\ \ell\text{ odd}}}\right)_3 &= F_{\mathcal{O}_+}^{[-]\bar{\phi}\phi\phi\bar{\phi}}(u,v)\,, \\ \left(V^{Q=0}_{\substack{\Delta,\ell,+\\ \ell\text{ odd}}}\right)_i &= 0\,, \quad (i\neq 1,2,3) \end{aligned} \qquad \begin{aligned} \left(V^{Q=2}_{\Delta,\ell,+}\right)_2 &= -F_{\mathcal{O}}^{[+]\phi\phi\bar{\phi}\bar{\phi}}(u,v)\,, \\ \left(V^{Q=2}_{\Delta,\ell,+}\right)_3 &= F_{\mathcal{O}}^{[-]\phi\phi\bar{\phi}\bar{\phi}}(u,v)\,, \\ \left(V^{Q=2}_{\Delta,\ell,+}\right)_i &= 0\,, \quad (i\neq 2,3)\,. \end{aligned} \tag{A.41}$$

$$
\begin{aligned}
\left(V^{Q=0}_{\Delta,\ell,-}\right)_{13} &= F^{[-](1,1)JJJJ}_{\mathcal{O}_-,13}(u,v)\,, \\
\left(V^{Q=0}_{\Delta,\ell,-}\right)_{14} &= F^{[-](1,1)JJJJ}_{\mathcal{O}_-,15}(u,v)\,, \\
\left(V^{Q=0}_{\Delta,\ell,-}\right)_{15} &= F^{[-](1,1)JJJJ}_{\mathcal{O}_-,16}(u,v)\,, \\
\left(V^{Q=0}_{\Delta,\ell,-}\right)_{16} &= F^{[-](1,1)JJJJ}_{\mathcal{O}_-,17}(u,v)\,, \\
\left(V^{Q=0}_{\Delta,\ell,-}\right)_{17} &= F^{[+](1,1)JJJJ}_{\mathcal{O}_-,7}(u,v)\,, \\
\left(V^{Q=0}_{\Delta,\ell,-}\right)_{18} &= F^{[+](1,1)JJJJ}_{\mathcal{O}_-,1}(u,u)\,, \\
\left(V^{Q=0}_{\Delta,\ell,-}\right)_{19} &= F^{[+](1,1)JJJJ}_{\mathcal{O}_-,2}(u,u)\,, \\
\left(V^{Q=0}_{\Delta,\ell,-}\right)_{20} &= F^{[+](1,1)JJJJ}_{\mathcal{O}_-,4}(u,u)\,, \\
\left(V^{Q=0}_{\Delta,\ell,-}\right)_{21} &= F^{[+](1,1)JJJJ}_{\mathcal{O}_-,5}(u,u)\,, \\
\left(V^{Q=0}_{\Delta,\ell,-}\right)_{22} &= F^{[+](1,1)JJJJ}_{\mathcal{O}_-,6}(u,u)\,, \\
\left(V^{Q=0}_{\Delta,\ell,-}\right)_{23} &= F^{[+](1,1)JJJJ}_{\mathcal{O}_-,3}(1/4,1/4)\,, \\
\left(V^{Q=0}_{\Delta,\ell,-}\right)_{i} &= 0\,, \qquad \text{otherwise}\,,
\end{aligned}
\qquad
\begin{aligned}
\left(V^{Q=1}_{\Delta,\ell,\pm}\right)_{4} &= \sigma_{\mathcal{O}} F^{[-]J\bar{\phi}J\phi}_{\mathcal{O}_\pm,1}(u,v)\,, \\
\left(V^{Q=1}_{\Delta,\ell,\pm}\right)_{5} &= \sigma_{\mathcal{O}} F^{[-]J\bar{\phi}J\phi}_{\mathcal{O}_\pm,2}(u,v)\,, \\
\left(V^{Q=1}_{\Delta,\ell,\pm}\right)_{6} &= \sigma_{\mathcal{O}} F^{[+]J\bar{\phi}J\phi}_{\mathcal{O}_\pm,3}(u,u)\,, \\
\left(V^{Q=1}_{\Delta,\ell,\pm}\right)_{7} &= -\sigma_{\mathcal{O}} F^{[+]\bar{\phi}JJ\phi}_{\mathcal{O}_\pm,1}(u,v)\,, \\
\left(V^{Q=1}_{\Delta,\ell,\pm}\right)_{8} &= \sigma_{\mathcal{O}} F^{[-]\bar{\phi}JJ\phi}_{\mathcal{O}_\pm,1}(u,v)\,, \\
\left(V^{Q=1}_{\Delta,\ell,\pm}\right)_{9} &= -\sigma_{\mathcal{O}} F^{[+]\bar{\phi}JJ\phi}_{\mathcal{O}_\pm,2}(u,v)\,, \\
\left(V^{Q=1}_{\Delta,\ell,\pm}\right)_{10} &= \sigma_{\mathcal{O}} F^{[-]\bar{\phi}JJ\phi}_{\mathcal{O}_\pm,2}(u,v)\,, \\
\left(V^{Q=1}_{\Delta,\ell,\pm}\right)_{11} &= -\sigma_{\mathcal{O}} F^{[+]\bar{\phi}JJ\phi}_{\mathcal{O}_\pm,3}(u,u)\,, \\
\left(V^{Q=1}_{\Delta,\ell,\pm}\right)_{12} &= -\sigma_{\mathcal{O}} F^{[+]\bar{\phi}JJ\phi}_{\mathcal{O}_\pm,4}(u,u)\,, \\
\left(V^{Q=1}_{\Delta,\ell,\pm}\right)_{i} &= 0\,, \qquad \text{otherwise.}
\end{aligned}
\tag{A.42}
$$

Recall that the sign sigma is defined in (1.48).

B Appendices to chapter 2

B.1 Spectra at maximal OPE values

It is interesting to examine the spectrum of the lowest operators at the maximal values of λ_{ttT}, λ_{ttJ} and λ_{ttt}. It is expected that real theories often live close to the maximal value of the OPE coefficient. This follows from the same logic that holds for operator dimensions. It is often physical solutions to crossing that prevent the bound from coming down further. A kink in this maximum or a sudden rearrangement in the spectrum gives evidence for the presence of a genuine CFT. Indeed we observe that close to the location of the kink in λ_{ttJ} the spectrum indeed rearranges itself. Below we show once more the bounds on all operator dimension but this time we include also the spectrum of the corresponding lowest operator in the various extremal spectra[1].

[1] We exclude from the spectrum any crossing through 0 of the extremal functional from negative to positive values within machine precision of the unitarity bound. Otherwise the plot looks more erratic because sometimes we do accurately detect this operator and sometimes we do not. As a consequence the "lowest" dimensional operator is allowed to exceed the bound since in those cases another operator exactly at the unitarity bound was already included.

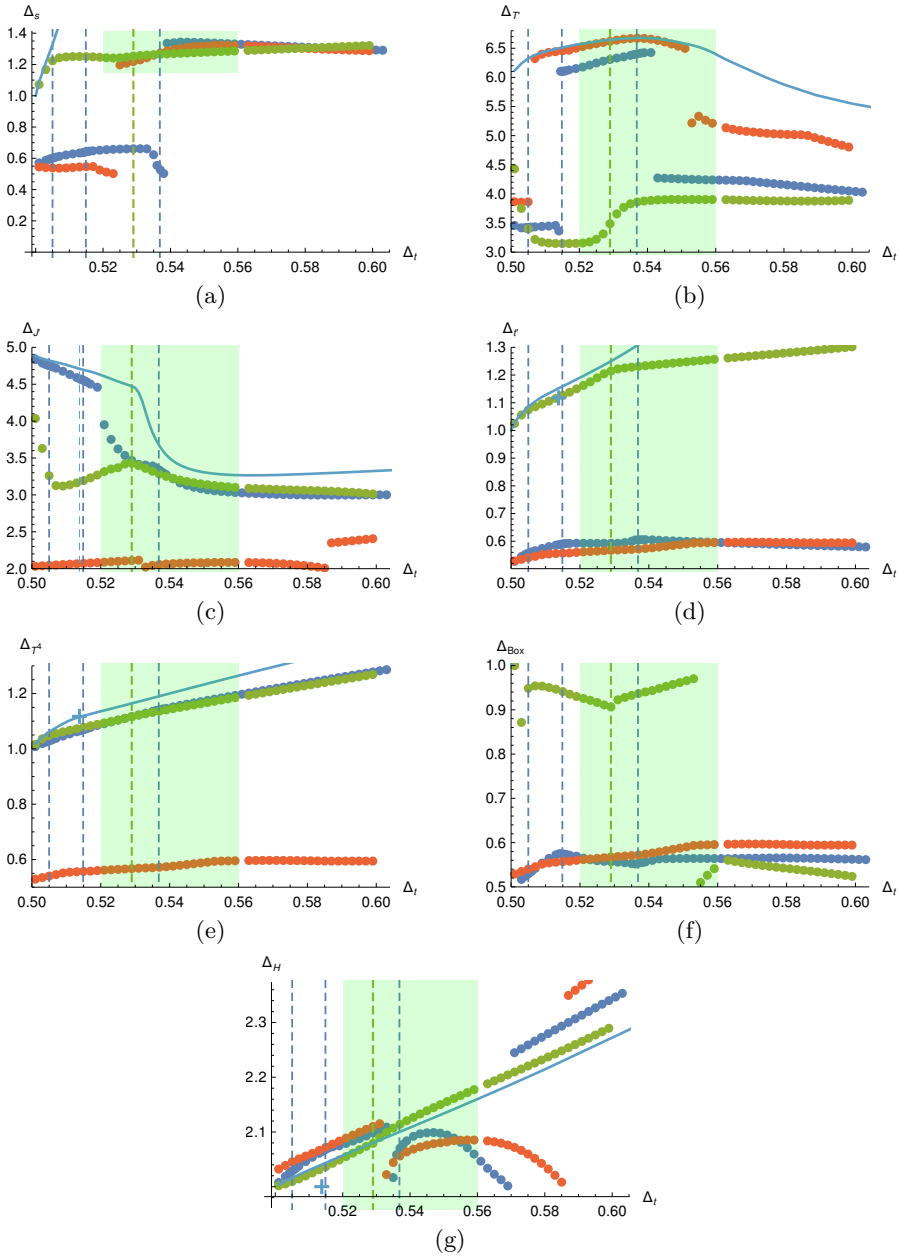

Figure B.1: The lowest dimensional operator in the extremal spectra found when maximizing the OPE coefficients λ_{ttT}, λ_{ttJ} and λ_{ttt}. The blue line show to the upperbound on the lowest dimensional operator. The green, orange and red lines shows the lowest dimensional operator found in the extremal functional at respectively the maximal value of λ_{ttT}, λ_{ttJ} and λ_{ttt}. The dashed orange lines indicate the location of kinks in the upper bound on λ_{ttJ} while the dashed red line indicates the location of a kink in the upper bound on λ_{ttt}.

Bibliography

[1] M. Reehorst, E. Trevisani, and A. Vichi, "Mixed Scalar-Current bootstrap in three dimensions," `arXiv:1911.05747 [hep-th]`.

[2] M. Reehorst, M. Refinetti, and A. Vichi, "Bootstrapping the ARP^3 model using traceless symmetric $O(N)$ scalars," `arXiv:20xx.xxxxx [hep-th]`.

[3] Y. Nakayama, "Scale invariance vs conformal invariance," *Phys. Rept.* **569** (2015) 1–93, `arXiv:1302.0884 [hep-th]`.

[4] M. Hogervorst and S. Rychkov, "Radial Coordinates for Conformal Blocks," *Phys.Rev.* **D87** no. 10, (2013) 106004, `arXiv:1303.1111 [hep-th]`.

[5] F. Kos, D. Poland, and D. Simmons-Duffin, "Bootstrapping Mixed Correlators in the 3D Ising Model," *JHEP* **1411** (2014) 109, `arXiv:1406.4858 [hep-th]`.

[6] J. a. Penedones, E. Trevisani, and M. Yamazaki, "Recursion Relations for Conformal Blocks," *JHEP* **09** (2016) 070, `arXiv:1509.00428 [hep-th]`.

[7] R. Rattazzi, V. S. Rychkov, E. Tonni, and A. Vichi, "Bounding scalar operator dimensions in 4D CFT," *JHEP* **12** (2008) 031, `arXiv:0807.0004 [hep-th]`.

[8] V. S. Rychkov and A. Vichi, "Universal Constraints on Conformal Operator Dimensions," *Phys. Rev.* **D80** (2009) 045006, `arXiv:0905.2211 [hep-th]`.

[9] R. Rattazzi, S. Rychkov, and A. Vichi, "Central Charge Bounds in 4D Conformal Field Theory," *Phys. Rev.* **D83** (2011) 046011, `arXiv:1009.2725 [hep-th]`.

[10] R. Rattazzi, S. Rychkov, and A. Vichi, "Bounds in 4D Conformal Field Theories with Global Symmetry," *J. Phys.* **A44** (2011) 035402, `arXiv:1009.5985 [hep-th]`.

[11] D. Poland and D. Simmons-Duffin, "Bounds on 4D Conformal and Superconformal Field Theories," *JHEP* **1105** (2011) 017, `arXiv:1009.2087 [hep-th]`.

[12] D. Poland, D. Simmons-Duffin, and A. Vichi, "Carving Out the Space of 4D CFTs," *JHEP* **1205** (2012) 110, `arXiv:1109.5176 [hep-th]`.

[13] D. Simmons-Duffin, "A Semidefinite Program Solver for the Conformal Bootstrap," *JHEP* **06** (2015) 174, `arXiv:1502.02033 [hep-th]`.

[14] W. Landry and D. Simmons-Duffin, "Scaling the semidefinite program solver sdpb," 2019.

[15] F. Kos, D. Poland, D. Simmons-Duffin, and A. Vichi, "Precision Islands in the Ising and $O(N)$ Models," *JHEP* **08** (2016) 036, `arXiv:1603.04436 [hep-th]`.

[16] L. Iliesiu, F. Kos, D. Poland, S. S. Pufu, D. Simmons-Duffin, and R. Yacoby, "Bootstrapping 3D Fermions," *JHEP* **03** (2016) 120, `arXiv:1508.00012 [hep-th]`.

[17] L. Iliesiu, F. Kos, D. Poland, S. S. Pufu, and D. Simmons-Duffin, "Bootstrapping 3D Fermions with Global Symmetries," *JHEP* **01** (2018) 036, `arXiv:1705.03484 [hep-th]`.

[18] A. Dymarsky, J. Penedones, E. Trevisani, and A. Vichi, "Charting the space of 3D CFTs with a continuous global symmetry," `arXiv:1705.04278 [hep-th]`.

[19] A. Dymarsky, F. Kos, P. Kravchuk, D. Poland, and D. Simmons-Duffin, "The 3d Stress-Tensor Bootstrap," *JHEP* **02** (2018) 164, `arXiv:1708.05718 [hep-th]`.

[20] D. Karateev, P. Kravchuk, M. Serone, and A. Vichi, "Fermion Conformal Bootstrap in 4d," *JHEP* **06** (2019) 088, `arXiv:1902.05969 [hep-th]`.

[21] D. Simmons-Duffin, "Tasi lectures on the conformal bootstrap," 2016.

[22] S. Rychkov, "Epfl lectures on conformal field theory in d $\geq$ 3 dimensions," *SpringerBriefs in Physics* (2017) . http://dx.doi.org/10.1007/978-3-319-43626-5.

[23] D. Poland and D. Simmons-Duffin, "The conformal bootstrap," *Nature Phys.* **12** no. 6, (2016) 535–539.

[24] M. S. Costa, J. Penedones, D. Poland, and S. Rychkov, "Spinning Conformal Blocks," *JHEP* **1111** (2011) 154, `arXiv:1109.6321 [hep-th]`.

[25] M. S. Costa, J. Penedones, D. Poland, and S. Rychkov, "Spinning Conformal Correlators," *JHEP* **1111** (2011) 071, `arXiv:1107.3554 [hep-th]`.

[26] M. S. Costa, T. Hansen, J. Penedones, and E. Trevisani, "Radial expansion for spinning conformal blocks," *JHEP* **07** (2016) 057, `arXiv:1603.05552 [hep-th]`.

[27] P. Kravchuk, "Casimir recursion relations for general conformal blocks," *Journal of High Energy Physics* **2018** no. 2, (Feb, 2018) . http://dx.doi.org/10.1007/JHEP02(2018)011.

[28] J. L. Cardy, *Scaling and renormalization in statistical physics.* Cambridge lecture notes in physics: 3. Cambridge, UK: Univ. Pr., 1996. 238 p.

[29] S. El-Showk, M. F. Paulos, D. Poland, S. Rychkov, D. Simmons-Duffin, and A. Vichi, "Solving the 3d Ising Model with the Conformal Bootstrap II. c-Minimization and Precise Critical Exponents," *J.Stat.Phys.* **157** (June, 2014) 869, `arXiv:1403.4545 [hep-th]`.

[30] F. Kos, D. Poland, D. Simmons-Duffin, and A. Vichi, "Bootstrapping the O(N) Archipelago," *JHEP* **11** (2015) 106, `arXiv:1504.07997 [hep-th]`.

[31] D. Simmons-Duffin, "The Lightcone Bootstrap and the Spectrum of the 3d Ising CFT," *JHEP* **03** (2017) 086, `arXiv:1612.08471 [hep-th]`.

[32] J. Rong and N. Su, "Bootstrapping minimal $\mathcal{N} = 1$ superconformal field theory in three dimensions," `arXiv:1807.04434 [hep-th]`.

[33] S. R. Kousvos and A. Stergiou, "Bootstrapping Mixed Correlators in Three-Dimensional Cubic Theories," *SciPost Phys.* **6** no. 3, (2019) 035, `arXiv:1810.10015 [hep-th]`.

[34] A. Stergiou, "Bootstrapping MN and Tetragonal CFTs in Three Dimensions," *SciPost Phys.* **7** (2019) 010, `arXiv:1904.00017 [hep-th]`.

[35] F. Kos, D. Poland, and D. Simmons-Duffin, "Bootstrapping the $O(N)$ vector models," *JHEP* **1406** (2014) 091, `arXiv:1307.6856`.

[36] S. M. Chester, S. S. Pufu, and R. Yacoby, "Bootstrapping $O(N)$ vector models in $4 < d < 6$," *Phys. Rev.* **D91** no. 8, (2015) 086014, `arXiv:1412.7746 [hep-th]`.

[37] S. M. Chester, J. Lee, S. S. Pufu, and R. Yacoby, "The $\mathcal{N} = 8$ superconformal bootstrap in three dimensions," *JHEP* **1409** (2014) 143, `arXiv:1406.4814 [hep-th]`.

[38] S. M. Chester, L. V. Iliesiu, S. S. Pufu, and R. Yacoby, "Bootstrapping $O(N)$ Vector Models with Four Supercharges in $3 \leq d \leq 4$," *JHEP* **05** (2016) 103, `arXiv:1511.07552 [hep-th]`.

[39] S. M. Chester and S. S. Pufu, "Towards bootstrapping QED_3," *JHEP* **08** (2016) 019, `arXiv:1601.03476 [hep-th]`.

[40] S. M. Chester, L. V. Iliesiu, M. Mezei, and S. S. Pufu, "Monopole Operators in $U(1)$ Chern-Simons-Matter Theories," `arXiv:1710.00654 [hep-th]`.

[41] M. Baggio, N. Bobev, S. M. Chester, E. Lauria, and S. S. Pufu, "Decoding a Three-Dimensional Conformal Manifold," *JHEP* **02** (2018) 062, `arXiv:1712.02698 [hep-th]`.

[42] Z. Li and N. Su, "3D CFT Archipelago from Single Correlator Bootstrap," `arXiv:1706.06960 [hep-th]`.

[43] C. Behan, "Bootstrapping the long-range Ising model in three dimensions," *J. Phys.* **A52** no. 7, (2019) 075401, `arXiv:1810.07199 [hep-th]`.

[44] N. B. Agmon, S. M. Chester, and S. S. Pufu, "The M-theory Archipelago," `arXiv:1907.13222 [hep-th]`.

[45] S. R. Kousvos and A. Stergiou, "Bootstrapping Mixed Correlators in Three-Dimensional Cubic Theories II," `arXiv:1911.00522 [hep-th]`.

[46] J. Rong and N. Su, "Bootstrapping the $\mathcal{N} = 1$ Wess-Zumino models in three dimensions," `arXiv:1910.08578 [hep-th]`.

[47] D. Poland, S. Rychkov, and A. Vichi, "The Conformal Bootstrap: Theory, Numerical Techniques, and Applications," *Rev. Mod. Phys.* **91** (2019) 015002, `arXiv:1805.04405 [hep-th]`.

[48] S. M. Chester, "Weizmann Lectures on the Numerical Conformal Bootstrap," `arXiv:1907.05147 [hep-th]`.

[49] D. M. Hofman and J. Maldacena, "Conformal collider physics: Energy and charge correlations," *JHEP* **05** (2008) 012, `arXiv:0803.1467 [hep-th]`.

[50] A. Buchel, J. Escobedo, R. C. Myers, M. F. Paulos, A. Sinha, and M. Smolkin, "Holographic GB gravity in arbitrary dimensions," *JHEP* **03** (2010) 111, `arXiv:0911.4257 [hep-th]`.

[51] S. Chester, W. Landry, J. Liu, D. Poland, D. Simmons-Duffin, and A. Su, Ning Vichi, "to appear,".

[52] E. Katz, S. Sachdev, E. S. Sørensen, and W. Witczak-Krempa, "Conformal field theories at nonzero temperature: Operator product expansions, Monte Carlo, and holography," *Phys. Rev.* **B90** no. 24, (2014) 245109, `arXiv:1409.3841 [cond-mat.str-el]`.

[53] A. Lucas, S. Gazit, D. Podolsky, and W. Witczak-Krempa, "Dynamical response near quantum critical points," *Phys. Rev. Lett.* **118** no. 5, (2017) 056601, `arXiv:1608.02586 [cond-mat.str-el]`.

[54] W. Witczak-Krempa, E. Sorensen, and S. Sachdev, "The dynamics of quantum criticality via Quantum Monte Carlo and holography," *Nature Phys.* **10** (2014) 361, `arXiv:1309.2941 [cond-mat.str-el]`.

[55] L. Iliesiu, M. Koloğlu, R. Mahajan, E. Perlmutter, and D. Simmons-Duffin, "The Conformal Bootstrap at Finite Temperature," `arXiv:1802.10266 [hep-th]`.

[56] L. Iliesiu, M. Kolo?lu, and D. Simmons-Duffin, "Bootstrapping the 3d Ising model at finite temperature," `arXiv:1811.05451 [hep-th]`.

[57] A. Manenti, "Thermal CFTs in momentum space," `arXiv:1905.01355 [hep-th]`.

[58] M. S. Costa, T. Hansen, J. Penedones, and E. Trevisani, "Projectors and seed conformal blocks for traceless mixed-symmetry tensors," *JHEP* **07** (2016) 018, `arXiv:1603.05551 [hep-th]`.

[59] R. S. Erramilli, L. V. Iliesiu, and P. Kravchuk, "Recursion relation for general 3d blocks," `arXiv:1907.11247 [hep-th]`.

[60] E. Dyer, M. Mezei, and S. S. Pufu, "Monopole Taxonomy in Three-Dimensional Conformal Field Theories," `arXiv:1309.1160 [hep-th]`.

[61] E. Dyer, M. Mezei, S. S. Pufu, and S. Sachdev, "Scaling dimensions of monopole operators in the $\mathbb{CP}^{N_b-1}$ theory in $2+1$ dimensions," *JHEP* **06** (2015) 037, `arXiv:1504.00368 [hep-th]`. [Erratum: JHEP03,111(2016)].

[62] M. S. Block, R. G. Melko, and R. K. Kaul, "Fate of cp$n-1$ fixed points with q-monopoles," *Physical Review Letters* **111** no. 13, (Sep, 2013) . http://dx.doi.org/10.1103/PhysRevLett.111.137202.

[63] D. Li, D. Meltzer, and A. Stergiou, "Bootstrapping mixed correlators in 4D $\mathcal{N}=1$ SCFTs," *JHEP* **07** (2017) 029, `arXiv:1702.00404 [hep-th]`.

[64] Y. Nakayama and T. Ohtsuki, "Five dimensional $O(N)$-symmetric CFTs from conformal bootstrap," *Phys. Lett.* **B734** (2014) 193–197, `arXiv:1404.5201 [hep-th]`.

[65] S. Giombi, G. Tarnopolsky, and I. R. Klebanov, "On C_J and C_T in Conformal QED," *JHEP* **08** (2016) 156, `arXiv:1602.01076 [hep-th]`.

[66] Y. Liu, K. Sun, and Z. Y. Meng, "Designer monte carlo simulation for gross-neveu transition," `arXiv:1910.07430 [cond-mat.stat-mech]`.

[67] S. M. Chester, W. Landry, J. Liu, D. Poland, D. Simmons-Duffin, N. Su, and A. Vichi, "Carving out ope space and precise o(2) model critical exponents," *Journal of High Energy Physics* **2020** no. 6, (Jun, 2020) . http://dx.doi.org/10.1007/JHEP06(2020)142.

[68] J. Henriksson, S. R. Kousvos, and A. Stergiou, "Analytic and numerical bootstrap of cfts with $o(m) \times o(n)$ global symmetry in 3d," 2020.

[69] A. Pelissetto, A. Tripodo, and E. Vicari, "Landau-Ginzburg-Wilson approach to critical phenomena in the presence of gauge symmetries," *Phys. Rev.* **D96** no. 3, (2017) 034505, `arXiv:1706.04365 [hep-lat]`.

[70] Y.-C. He, J. Rong, and N. Su, "Non-wilson-fisher kinks of $o(n)$ numerical bootstrap: from the deconfined phase transition to a putative new family of cfts," 2020.

[71] A. Pelissetto, A. Tripodo, and E. Vicari, "Criticality of O(N) symmetric models in the presence of discrete gauge symmetries," *Phys. Rev.* **E97** no. 1, (2018) 012123, `arXiv:1711.04567 [cond-mat.stat-mech]`.

[72] F. Delfino, A. Pelissetto, and E. Vicari, "Three-dimensional antiferromagnetic CP^{N-1} models," *Phys. Rev.* **E91** no. 5, (2015) 052109, `arXiv:1502.07599 [cond-mat.stat-mech]`.

[73] N. Su. https://gitlab.com/bootstrapcollaboration/simpleboot.

[74] Z. Li and D. Poland, "Searching for gauge theories with the conformal bootstrap," 2020.

[75] S. El-Showk and M. F. Paulos, "Bootstrapping Conformal Field Theories with the Extremal Functional Method," *Phys.Rev.Lett.* **111** no. 24, (2013) 241601, `arXiv:1211.2810 [hep-th]`.

[76] M. Go and Y. Tachikawa, "autoboot: A generator of bootstrap equations with global symmetry," 2019.

[77] S. Benvenuti and H. Khachatryan, "Easy-plane QED_3s in the large N_f limit," *JHEP* **05** (2019) 214, `arXiv:1902.05767 [hep-th]`.

Marten Reehorst
Curriculum Vitae

Personal Data

Name:	Marten Jan Reehorst
Born:	03 February 1993, Amsterdam, Netherlands
Nationality:	Dutch

Education

Okt 2016 - Sep 2020	**PhD in Theoretical Physics** - École polytechnique fédérale de Lausanne Specialisation: Numerical Conformal Bootstrap Thesis Advisor: Prof. Alessandro Vichi
Sep 2014 - 31 August 2016	**Master in Theoretical Physics** - University of Amsterdam GPA Courses: $8.5/10$ over 120 + 28 EC of courses[1], *Cum Laude* Specialisation: Emergent spacetime and the AdS/CFT correspondence Thesis Advisor: Prof. Erik Verlinde
28 Jul 2014	**Bachelor in Physics and Astronomy** - University of Amsterdam GPA: $8.4/10$ over 180 + 45 EC[2], *Cum Laude*, *Cum Honore* Specialization: The AdS-CFT correspondence principle Thesis Advisor: Dr. Diego Hofman
Jun 2011	**Gymnasium Diploma** - Ignatius Gymnasium GPA: $8.6/10$, STEM profile (with additional classes such as History, Latin, Art and Computer Science).

Work Experience

Okt 2016 - Sep 2020	**Teaching Assistant at EPFL for Quantum Physics III & IV** Taught by resp. Mikhail Shaposhnikov and Alessandro Vichi.
Sep 2011 - Aug 2014	**Worked on various science outreach events** such as *Natuurkunde Kermis*, *Techniek Toernooi* and *Viva Fysica*.

Publications

2019	Mixed Scalar-Current bootstrap in three dimensions. ArXiv: 1911.05747 by Marten Reehorst, Emilio Trevisani and Alessandro Vichi.

Conferences, schools and PhD Courses

2016	Solvay Amsterdam-Brussels-Geneva-Paris Doctoral School
2017	EPFL Course Conformal Field Theory by Joao Penedones
	EPFL Course Advanced Quantum Field Theory by Alessandro Vichi
	ICTP-SAIFR Bootstrap Conference and School
2018	Caltech Bootstrap Conference and School
2019	Perimeter Institute Bootstrap Conference
2019	Simons Center Workshop, Stony Brook NY
2019	New York Annual Bootstrap Meeting
2020	Boston Bootstrap Conference and School (remote)

Skills

Programming skills:	Mathematica (Advanced), Python (Beginner)
Computer skills:	Linux/Bash (Intermediate), Windows (Advanced), Git (Intermediate), LateX (Advanced), Slurm Workload Manager / High-Performance Cluster Computing (Advanced)
Languages:	Dutch (Mothertongue), English (Fluent), French (Basic Knowledge), Latin (Passive only)

[2]A standard two year Master program consists of 120 EC. I did 28 EC of extra courses.
[2]A standard three year Bachelor program consists of 180 EC. I did 45 EC of extra courses.